University of South-Eastern Norway

www.usn.no

FMH606 Master's Thesis 2021

Electrical Power Engineering

Thermal capacity and loading assessment for 24 kV XLPE-insulated cables in air

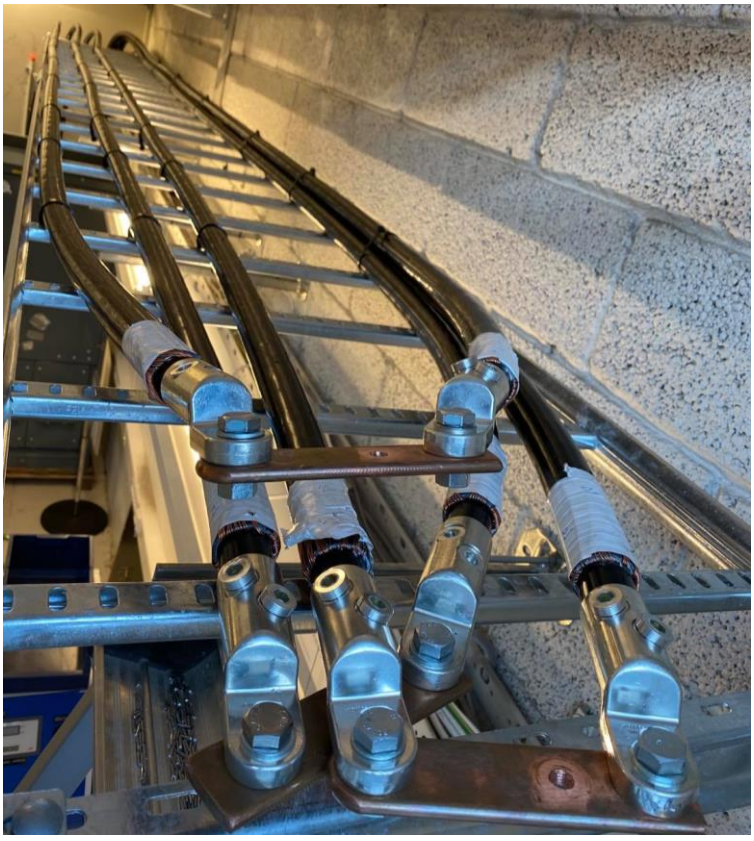

Hyeonyoung Kwak

University of South-Eastern Norway

www.usn.no

Course: FMH606 Master's Thesis, 2021

Title: Thermal capacity and loading assessment for 24 kV XLPE-insulated cables in air

Number of pages: 144

Keywords: XLPE-insulated cable, thermal model, loading profiles.

Student: Hyeonyoung Kwak

Supervisor: Elin Fjeld

External partner: Lede

Summary:

Charging large battery packs requires high currents, especially for short-term charging of electric vehicles. The ohmic losses heats up power cables and is the limiting factor for the current capacity. However, the power cables may be overloaded for short periods because of the thermal inertia. Therefore, there can be great advantages if one knows both the short-term and long-term current limitations for the power cables.

Color Hybrid is a hybrid ferry, and the charging station is supplied by a 12 and 24 kV XLPE 240 mm^2 Al cable. Loading and temperature data from Lede has been obtained, and a laboratory setup with a set of XLPE 24 kV cables in air will be constructed at the USN High Current Laboratory. The lab setup should be able to recreate the obtained data. The laboratory setup will have two cable formations, namely flat and trefoil, where temperature measurements are taken from the cable surface, and the cable conductor surface. Thermal response for long-term and short-term charging is used to calculate thermal properties.

A simplified thermal model is created using the calculated thermal properties. The model makes a good long-term temperature prediction but fails to provide accurate data for short-term loading. Therefore, the model parameters were optimized to minimize the simulation error for both long- and short-term charging. The resulting thermal model estimates 15 ℃ higher conductor temperature for trefoil formation compared to measurements.

The thermal model is able to emulate temperature responses from cyclic charging profiles with two loading periods and a resting time between the loadings. From this, illustrations and are made to show the correlations between the loading currents, the loading duration, and the resting time. These illustrations may be used for optimization of the charging schedule for one or more electric/hybrid ferries.

Preface

One of the mandatory courses in MSc Electrical Power Engineering has three laboratory exercises in the High Current Laboratory at University of South-Eastern Norway (USN). The three laboratory exercises are resistance measurements and temperature rise test of MV switchgear and de-rating of LV fused switchgear. USN have a goal to make more and diverse laboratory exercises for thesis work and laboratory exercises in courses. I am thankful for helping expand the laboratory, and to increase the learning activities present at USN.

This thesis has given me the opportunity to investigate the thermal rating of XLPE power cable, together with practical laboratory work. I have been fortunate to receive a thesis topic that is working towards the electrification of vehicles and I hope that this type of work can be expanded into similar applications.

I want to thank my supervisor Elin Fjeld for allowing me to work with a practical laboratory project. I also want to thank her for effective and supportive dialog, useful advice, structural guidance, and for motivating me to work towards the thesis goals. I am thankful to Thea Øverli from Lede for her time to give appropriate information about the cables that supplies Color Hybrid, and to supply necessary data of it. Thanks to Nexans for supplying a length of XLPE 24kV cable to be used in laboratory at the USN.

I would like to express my sincere gratitude to my family, in particular my mother Jiyeon and my father Chung-Guen. I am so lucky to be the daughter of my mother, who supports me endlessly and is so devoted to put her family first no matter what. I am grateful for my father who is an electrical power engineer for sincerity motivating and impressing me to be an engineer. Thank you to my little sister Dowon and little brother Aron for the support and understanding.

And finally, I would like to express my heartfelt gratitude to my sweetheart and partner Emil Melfald, for his support and to keep me motivated in tough times during this thesis. He has been involved in building the laboratory setup, advising me with his expertise in Python, and held many informative discussions. Thank you for sharing your knowledge and insights, and for pushing me towards becoming a better engineer.

Porsgrunn, 17th May 2021

Hyeonyoung Kwak

Contents

List of Figures

List of Tables

Nomenclature

Acronyms

A	Ampere
AC	Alternating current
ACSR	Aluminum cable steel reinforced
BEM	Boundary element method
CENELEC	European Committee for Electrotechnical Standardization
CCS	Carbon Capture Storage
CSP	Sulphonated polyethylene
DC	Direct current
EPR	Ethylene propylene rubber
FDM	Finite difference method
FEM	Finite element method
GSW	Galvanized steel wire
HV	High voltage
IEC	International Electrotechnical Commission
IEEE	Institute of Electrical and Electronics Engineers
MV	Medium voltage
NEC	National Electrical Code
NR	Natural rubber
SR	Silicone rubber
V	Volt
PCP	polychloroprene

PE	Polyethylene
PP	Polypropylene
PVC	Polyvinyl chloride
SINTEF	SINTEF is an independent research institute and has developed solutions and innovation (Norwegian: Stiftelsen for industriell og teknisk forskning)
SWA	Single-wire armour
TRP	Thermoplastic rubber
TPE	Thermoplastic elastomers
USN	University of South-Eastern Norway
W	Watt
XLPE	Cross-linked polyethylene

Symbols used in Laboratory Work and Data Simulation

A_{inner}	Aluminum conductor surface area
A_{outer}	Cable outer surface area
c_p^{Al}	Heat capacity of the aluminum conductor
c_p^{XLPE}	Heat capacity of the XLPE insulation
d_{inner}	Diameter of the aluminum conductor
d_{outer}	Diameter of the XLPE cable
h_{inner}	Heat transfer coefficients between conductor and insulation
h_{outer}	Heat transfer coefficients between insulation and surrounding air
hA_{inner}	Thermal conductivity between conductor and insulation
hA_{outer}	Thermal conductivity between insulation and surrounding air
I_1	First charging current for the periodic loading
I_2	Second charging current for the periodic loading
I_{max}	Maximum allowed current for the periodic loading
I_{test}	Testing current in the laboratory
m_{Al}	Mass of aluminum conductor
m_{XLPE}	Mass of XLPE insulation
n	Number of data points
P_{in}^{Al}	Power generated in aluminum conductor
P_{out}^{Al}	Power dissipated from the aluminum conductor
P_{out}^{XLPE}	Power dissipated from the cable surface
R_{cold}	Cold resistance of the cable
$T_{inner,-}$	Conductor surface temperature for flat formation
$T_{inner,\Delta}$	Conductor surface temperature for trefoil formation

Nomenclature

T_{on}	Charging time
$T_{outer,-}$	Cable surface temperature for flat formation
$T_{outer,\Delta}$	Cable surface temperature for trefoil formation
T_{off}	Resting time
$T_{off,test}$	Tested resting time
T_{room}	Room temperature at High Current Laboratory
V_{Al}	Volume of aluminum conductor
V_{XLPE}	Volume of XLPE insulation
y_i	Simulated values
$\hat{y}_i$	Measured values
α	Temperature coefficients
$\hat{c}_p^{Al}$	Specific heat capacity of aluminum
$\hat{c}_p^{XLPE}$	Specific heat capacity of XLPE insulation
κ_{inner}	Adjustment factors for trefoil area between conductor and insulation
κ_{outer}	Adjustment factors for trefoil area between insulation and surrounding air
ρ_{Al}	Density of aluminum
ρ_{XLPE}	Density of XLPE

1 Introduction

1.1 Background

To tackle climate change, and to reduce greenhouse gas emissions and its negative impacts, both science and engineering solutions are needed for significant progress. Transportation in Norway is the largest source of greenhouse gas emissions, counting 31 % of total emissions, where shipping and fishing counts for 2.98 %. The emissions from transport increased by 19 % from 1990 to 2019 and was reduced by 4.5 % from 2018 to 2019. This may be due to many electric or hybrid cars and ferries that have been introduced in the society. One example of this electrification is "Future of the Fjords" which have been in operation in the Norwegian fjords since 2018. [1]

As the demand for renewable and sustainable electrical energy continues to increase, infrastructure and grid must be built to utilize the available renewable resources. Researchers expect more electrical transport such as cars, ships, and airplanes by using the renewable sources in the future. The electrification will however place a large demand for reliable and flexible grids.

There are many quays in Grenland and examples of ferries, ships and cruises are:

- Telemark Canal travels from Skien to Dalen [2].
- Fully electric and autonomous container ship, Yara Birkeland, which travels from Herøya to Brevik or Larvik [3].
- The Longship project that comprises of capture, transport, and storage of CO_2 called Norcem Brevik [4].
- Fjord Line, with daily departures from Langesund to Hirtshals in Denmark with conventional ferries [5].

Moreover, there are many small ferries traveling in the Grenland area which can be electric in the future.

Color Line have a vision of reducing greenhouse gas emissions from their ferry, in line with the zero-emission goal of Norway. In August 2019, Color Line launched the world's largest plug-in hybrid ferry, Color Hybrid. The hybrid ferry has both conventional diesel engines and a 4.7 MWh lithium-ion battery pack. The battery pack is quick charged several times a day at Sandefjord and is used for peak shaving which results lower fuel consumption and emissions. The shore-based power supply is delivered via XLPE 12 kV and 24 kV cables from Lede's power system. The Color Hybrid regularly travels between Sandefjord and Strömstad with a traveling time of 2.5 hours and can carry up to 2000 passengers and 500 cars. [6]

The charging time of ferries are typically short during the day, with high currents for short time spans. Thus, making a thermal model of the power cable can easily help charge ferries optimally. Underground cables have a lower stationary loadability compared to cables in air with the same conductor cross-section. However, underground cables heat up slower than cables in air. This means that cables in air may be the limiting factor for short-term, high current charging. Knowing the limits of the short-term charging and the resting time between charges may be a key part in optimizing the ferry charging for Color Line and other electrical charging stations.

1.2 Previous work

The growing demand for electrical energy has forced suppliers of high voltage (HV) cables to specify the loadability of their component in both steady-state and short-term loading. The cable capacity is limited by the long-term enduring conductor temperature that affects insulating material's ability. There are many case studies of conductor temperature calculations, with proposed thermal models of underground XLPE-insulated power cables such as [7], [8], and [9]. There have also been studies of cables laying in trench [10], cables in conduits [11], and thermal analysis of power cables in free air as in [12] and [13].

The research institute SINTEF have researched physical difficulties regarding HV-cables and any restrictions on temperature development. REN is developing standardization of materials and working methods in Norwegian grid companies. Together, REN and SINTEF designed a tool for cable trenches. This tool is called "Grøft" (REN Trench) where thermal simulations are essential [14].

SINTEF has assessed the thermal conditions around the Color Line cable that supplies shore power to the Color Hybrid. Lede has placed temperature sensors on the surface of the Color Line cable. The conductor temperature of a cable in service is difficult to measure directly. However, conductor temperature has been obtained by calculations since temperature on the surface of the cable is measured. SINTEF have examined maximum stationary temperature development of two cross-sections of the Color Line cable path. The first cross-section is a culvert near the substation. The other is a crossroad with 11 power cables by using REN Trench. According to the results from SINTEF the Color Line cable has sufficient load capacity to be able to supply the desired load current without exceeding the temperature limit in the culvert near the substation during long-term charging. [15]

1.3 Objectives and scope of work

This thesis will focus on temperature development of an XLPE 24 kV cable similar to the Color Line cable, laid in air. The conductor temperature and cable surface temperature of an experiment cable will be measured during different loading profiles. Short-term charging responses is compared with temperature data from the Color Line cable during charging of the Color Hybrid.

Further, the thesis focuses on the thermal dimensioning and to make a simplified thermal model for the XLPE cables in air to predict the conductor and surface temperatures. Attention is paid to the ampacity and temperature development of the XLPE cable in two different cable formations, namely flat and trefoil.

Color Line may need to charge several hybrid/electric ferries many times a day. Therefore, the thermal dimensioning of the Color Line cable can play an important role in planning the different charging cycles. With a representative model, one can start to figure out important aspects of the short-term charging, such as how much time must pass from the end of one charging to the start of next. It is also interesting to know how the current values affect the temperatures of the conductor over time, and how Color Line can achieve the optimal charging pattern.

The validity of the thermal model will be tested in experiments by comparing the result from simulations in Python to measurements made from tests in the laboratory setup of the cable. The model parameters will then be adjusted to best represent the simulated data with measurements. The objectives for working towards this goal are listed below and the task description for this thesis is shown in Appendix A.

- Do a survey on thermal dimensioning of cables.
- Search the literature for similar studies and gather relevant data.
- Build a test set-up in the High Current Laboratory for loadability of cables in air, in both flat and trefoil formation.
- Measuring the conductor and cable surface temperature.
- Run steady state temperature rise tests to determine the time constants, total heat transfer coefficient, heat capacity and cable resistance.
- Simulate and test different dynamic load profiles of the cables.
- Compare temperatures measured in the laboratory with temperature data gathered from the field during charging of the Color Hybrid in Sandefjord.
- Make a simplified thermal model for the cables in air.
- Adjust model parameter of the thermal model to best fit the experiment data done in the laboratory.

1.3.1 Methods and data

To begin with the practical arrangement, a test set-up will be built in the High Current Laboratory at USN. The experiment cable is an XLPE 24 kV 240 mm^2 cable provided by Nexans, which were laid on a cable tray in flat and trefoil formation. Temperature sensors and a high current injection transformer is available in the laboratory. Cable temperatures are measured by a data logger and collected in the software Agilent BenchLink Data Logger 3 during the different loading profiles.

Excel (Microsoft office 365) will be used for plotting and graphically representing data. Python 3.8 will be used to implement the thermal model of the cable and do calculations and analysis of the temperature data from the laboratory. Several important modules in Python will be used, such as Numpy, Scipy, Pandas, Numba and Matplotlib. Numpy is data processing and calculation, Scipy is used for optimizing model parameters, Pandas is used for working with data tables, Numba is a Python compiler for speeding up code, and Matplotlib is used for graphically presenting data and results.

General information about the Color Line cable such as properties, length, cable formation, and cable environment are provided by Lede with several documents, mails, and digital meetings. The temperature data and loading profiles is also provided by Lede.

1.3.2 Scope and limitation of work

This thesis does not focus on economical solutions and the regulations on delivery quality.

During the project, campus Porsgrunn was closed by the Norwegian government to students due to spreading of global pandemic COVID-19 in Porsgrunn from 20th March to 6th April 2021. Restrictions resulting from the pandemic led to the project experiencing difficulties with the schedule for laboratory tests during this time.

1.3.3 Thesis overview

The overview of this thesis is listed below.

Chapter 2 contains the basic theory to understand the results and the discussion from the experiments and simulations. General theories around power cables components, thermal dimensioning of power cable, XLPE cable and heat generation in power cables is presented.

Chapter 3 is about the Color Line cable including the loading profile of the Color Hybrid battery pack, the installed temperature sensor, and thermal condition analysis done by SINTEF.

Chapter 4 covers the laboratory setup at USN and thermal properties of the laboratory cable. Tests are done for both long-term and short-term charging currents.

Chapter 5 deals with the data simulations and compares the simulation results with measured data from the laboratory. In addition, model parameter optimization is done based on measurement data. The thermal model is then tested and compared with different loading profiles and is then used to determine optimal charging patterns.

Chapter 6 discusses the obtained results from the experiments and the simulations.

Chapter 7 concludes about the results and gives recommendations for future work.

2 Thermal aspects of power cables

The conceptual evaluation of the current ratings in power cables has been considered for over a century with theories based on thermal and heat transfer properties of the cable installed in each material. Nowadays, the development of the computational methods and technologies is powerful, and studies like steady state and dynamic rating is more available.

In this chapter, an overview of some important thermal aspects of power cables will be presented.

2.1 MV/HV Cable design

As long as there has been electricity, there have been cables to supply the electric current to the customers and consumers. Electric power cables are used for the transmission and distribution of electric energy. The demand for electric energy requires the support of increasingly higher voltage and power levels. Power cables comes in a variety of types, size, conductor materials, insulation, and sheathing materials. The construction of power cables is determined by three main factors:

- Current-carrying capacity – cross-sectional area of the conductor
- Voltage – thickness of the insulation
- Environmental conditions – determine the sheathing materials considering temperature, water, oil, sunlight, chemical exposure, fire, mechanical impact etc.

2.1.1 Conductor

The conductor provides the conducting path for the current and the cross-sectional area of the conductor determines the maximum current carrying capacity of the cable. The materials of the conductor are copper or aluminum which has high electrical conductivity and may be either a solid type or a stranded type. The solid type has only one solid wire, while the stranded type consists of several twisting wires together. The wires are arranged around a center wire and the standard number of strands in a conductor may be 7, 19, 37, 61, etc. as shown in Figure 2.1. [2]

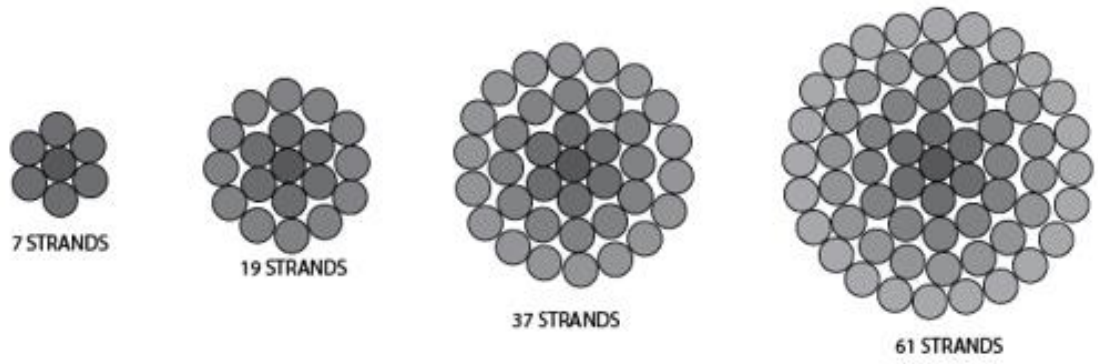

Figure 2.1: The typical number of strands in a stranded conductor. [2, edited]

The dc resistance of different conductor size for copper and aluminum is shown in Table 2.1. Aluminum have only 61 % of the conductivity of copper and for equal conductance, an aluminum conductor required 1.6 times larger area than that of copper. The low density of aluminum results in the actual weight of a comparable conductor being only half that required with copper. [17]

Table 2.1: Maximum dc resistance for copper and aluminum. [17]

Conductor size [mm^2]	**Maximum dc resistance at 20 ℃ [Ω/km]**	
	Copper	**Aluminum**
4	4.61	7.41
6	3.08	4.61
16	1.15	1.91
25	0.727	1.20
50	0.378	0.641
120	0.153	0.253
150	0.124	0.206
240	0.0754	0.125
500	0.0366	0.0605
630	0.0283	0.0469
800	0.0221	0.0367
1000	0.0176	0.0291

2.1.2 Insulation

The insulation isolates the conductor such that the electric charges do not flow away from the conducting path and can be viewed as the exact opposite of conductors. The insulating materal properties can be categorized into the categories; physical, mechanical, electrical, and chemical. Physical properties are related to density, moisture absorption, thermal effects, ageing, and characteristic such as viscosity, moisture content, uniformity of thickness, and porosity. Mechanical properties are related to tensile strength, cross-breaking strength, shearing strength and compressive strength. The essential electrical property of a dielectric is that it shall insulate and is related to resistivity, electric strength, surface breakdown, flashover, tracking, permittivity, and dielectric loss. The chemical properties of insulating materials are associated with resistance to external chemical effects, effects on the other materials, and chemical changes of its insulating material. The dielectric strength of an insulation material is the voltage that the insulation material can withstand before breakdown occurs. [18] [17]

Development of electric cables for high current, 100 V DC application started in 1880. The first cables were single-conductor cables insulated with thermoplastic latex produced from the sap of the tree [19]. In the 1890's the mass-impregnated paper insulated cables were used on MV that consists of paper impregnated with highly viscous oil and is still in-service in some countries and used in long distance dc transmission [20]. In 1920, the oil-insulated cable was invented by Emanueli where oil was pressurized to manage the changes in pressure and volume

resulting from load variation and ambient temperature [17]. An advantage of this cable is high reliability with regards to electric withstand capability while a disadvantage is the pressurized oil tanks requires maintenance and environmental risk.

The plastic-insulated cables were developed consistently to replace the paper- and oil-insulated cable due to a simple manufacturing and little maintenance [20]. In general, the insulation used for power cables are either thermoplastic or elastomeric materials. Examples of thermoplastic materials are polyethylene (PE), polypropylene (PP), and polyvinyl chloride (PVC,. Figure 2.2 shows the construction of a PE insulated cable.

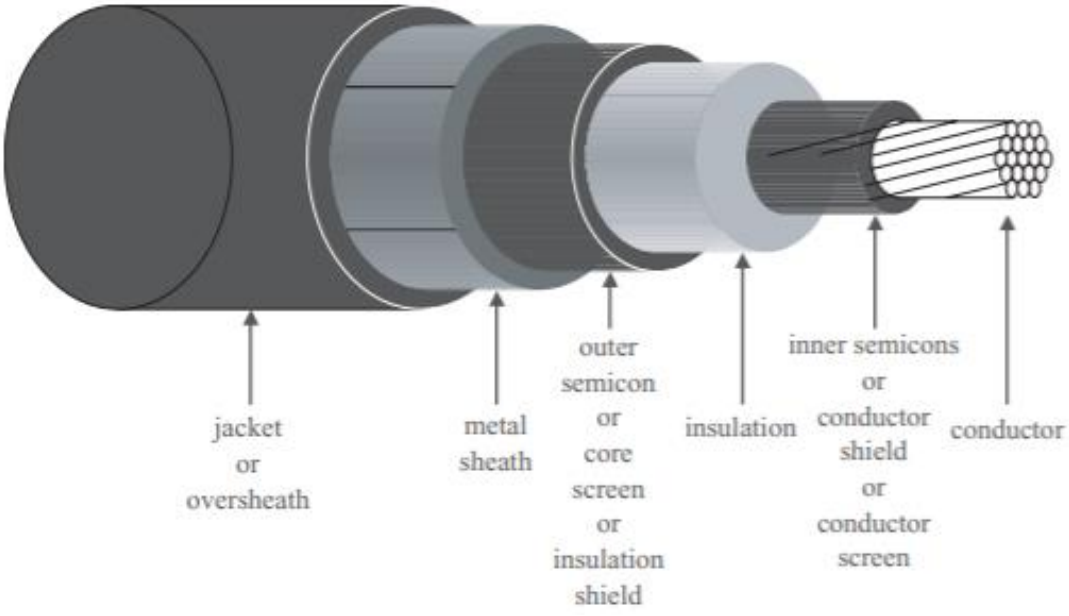

Figure 2.2: Cut-away section of PE cable for 12 or 24 kV. [14]

By the 1930's the first trials with PVC cables were developed in Germany, and during world war II the insulation of cables were applied with synthetic rubber and polyethylene [19]. PVC was the most common insulating material due to its uncomplex processability and good general-purpose performance. Examples of elastomeric materials are chlorosulphonated polyethylene (CSP), ethylene propylene rubber (EPR), natural rubber (NR), polychloroprene (PCP), and silicone rubber (SR), and cross-linked polyethylene (XLPE). Table 2.2 shows the advantage and disadvantage of different insulation materials with maximum operating temperature. EPR and XLPE are the most common and recommended polymeric insulation materials today since the electrical properties of natural rubber with a higher continuous operating temperature limit (90 ℃). [17]

Table 2.2: Comparison of different HV cable insulations. [17]

Material	Advantage	Disadvantage	Maximum operating temperature
PVC	• Cheap • Durable • Widely available	• Highest dielectric losses • Melts at high temperature • Contains halogens	70 °C for general purpose 85 °C for heat resisting purpose
PE	• Lowest dielectric losses • High initial dielectric strength	• Highly sensitive to water treeing • Material breaks down at high temperatures	
XLPE	• Very low dielectric losses • Improved material properties at high temperatures • Acceptable fire performance • No risk of oil leakage	• Does not melt but thermal expansion occurs • Medium sensitivity to water treeing	90 °C
EPR	• Increased flexibility • Reduced thermal expansion • Acceptable fire performance • Low sensitivity to water treeing • No risk of oil leakage	• Medium-high dielectric losses • Requires inorganic filler/additive • High dielectric losses	90 °C
Paper/oil insulated	• Low-medium dielectric losses • Low conductor losses • Not harmed by DC testing • Known history of reliability	• High weight and cost • Requires hydraulic pressure/pumps for insulating fluid • Difficult to repair • Degrades with moisture	70 °C

Solid dielectric extruded cables have been dominating the distribution market since 1960. The plastic-insulated cables have smaller dielectric losses, maintenance free, lower capacitive load, lower weight, lower cost, easy to install, and more environmentally friendly than the paper- and oil-insulated cables. The disadvantage of the plastic-insulated cable can be electric trees, water trees and possible defects. The plastic-insulated cable can be exposed to gradual degradation due to electrical and mechanical stress, temperature and pollution, water etc. [20]

In general, the most important requirements for power cable are long service life, high operating temperature, short installation time, and high reliability. The essential requirements of high voltage dielectrics are high impulse strength since the design stress determines dimensions. Cable has low permittivity to decrease both the electrical losses and charging currents. Furthermore, ease of bending is important during installation to avoid sustained damage that could affect service life. Research and development of new cable insulation technologies are still going on towards the withstand of extreme hot and cold temperatures, high tolerance to abrasion, and to handle higher rated voltages with thinner insulation. [17]

2.1.3 Semiconductors

Semiconductors are not good conductors nor good insulators and have electrical properties somewhere in the middle between conductor and insulator. Materials of semiconductors are silicon (Si), germanium (Ge), and gallium arsenide (GaAs) [21].

The surface of a conductor is not uniform, and concentration of electric filed will occur. Inner semiconductor, also called conductor shield, completely covers the conductor to improve the distribution of the electric field on the conductor surface and to avoid partial discharge between the conductor and the insulator. There is also a semiconductor between insulation and sheath, called outer semiconductor or insulation shield. It covers the insulation to avoid partial discharge between the insulation and the sheath. In other words, semiconductors have a function to prevent air-filled cavities so that little electric discharge cannot arise and endanger the insulation material. Figure 2.3 shows the structure of the three-single core XLPE insulated power cable where inner semiconductor is between conductor and XLPE insulation while outer semiconductor is between XLPE insulation and metal screen [22].

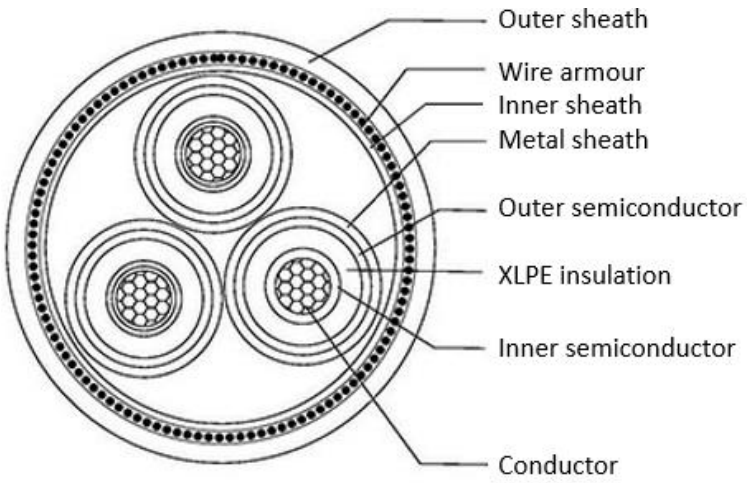

Figure 2.3: Structure of three-single core medium voltage XLPE insulated power cable. [14, edited]

2.1.4 Sheath

The sheath protects the conductor from all external influences and comes in a variety of types and purposes. The function of the sheath is that it covers around the outside of the power cable to hold the conductors inside. If there are multiple wires inside a power cable, the sheath helps bundle the conductors together.

Medium voltage cables have a metal sheath in contact with the outer semiconductor. The main materials of metal sheath were lead or lead alloys for years since the low melting temperature allows those materials to be extruded at around 200 ℃ over the polymeric cable. The high density (11 400 kg/m^3) of lead causes a heavy product and creep under cyclic temperature loadings which can cause the sheath to rupture. Nowadays, extruded aluminum, aluminum and copper foil, and welded copper and stainless steel is used instead of lead. The metal sheath is uniformly covering the whole perimeter of the cable. [16]

All armored cables have a separation cover between the metal screen and the armor. Inner sheath is used for protecting the power cable from contact with water and air and to protect against mechanical damage. The material of the inner sheath should be nonmagnetic. [18]

A power cable in hazardous environments and not installed in conduits requires armor. The armored cable is a protective layer between inner sheath and outer sheath which can withstand higher tension and improve the protection of the cable against external aggressions. For that reason, the armored cable is often used in areas where there is high risk of mechanical aggression such as high traffic. The most common armor is provided by galvanized steel wire (GSW) and single-wire armor (SWA) where most distribution power cables is provided by SWA. The power cable with the armored cable does not receive damage from mechanical external forces and demonstrate excellent crush, heat, and chemical resistance. The armoring is normally connected to earth, and the fault current flows through the armoring if there is insulation failure. [17], [24]

Outer sheath protects the cable from external stresses and overall mechanical and chemical aggressions such as corrosion, water, dust, oil etc. In another word, it gives the mechanical strength to the power cables. The properties of oversheath are good abrasion and stress crack resistance, good barrier, and good processing. The best composite performance of oversheath is based on polyethylene and most common cables are dry design type that includes metal barrier. The metal barrier carries fault and loss currents and prevent water from the construction. It affects how a cable system may be installed in practice. The metal layer is protected by a polymeric oversheath. [23]

Power cables must be grounded for safety and reliable operation, and outer sheath, metal sheath and armor need to be connected to ground. Without grounding, the outer sheath will operate at a potential above ground, dangerous to touch and can cause rapid degradation of the jacket. The metal sheath provides a return path for a current fault event and permit rapid operation of the protection devices. [25]

There are two grounding methods, single point grounding and multiple point grounding. Single point grounding connects the cable sheath to ground only at one point while multiple point grounding connects the cable sheath to ground at multiple readily accessible locations with minimum of two connections. Advantage of single point grounding is that it is an open circuit and therefore induced shield currents cannot flow. However, small eddy currents will still circulate within the shield and the voltage across the open circuit portion of the shield with maximum voltage appearing at the end that is farthest away from the grounded point.

Advantage of multiple point grounding is that shield is connected to ground at both ends, hence no shield voltage exists and increases safety. The circulating shield current is induced in the shield which has a closed circuit, and it will vary with the loading on the power cable and results in additional cable heating. [26]

2.1.5 Laying method

The three-single core cables in a three-phase circuit can be placed in different formations and typical formations are trefoil (triangular) and flat formations, see Figure 2.4.

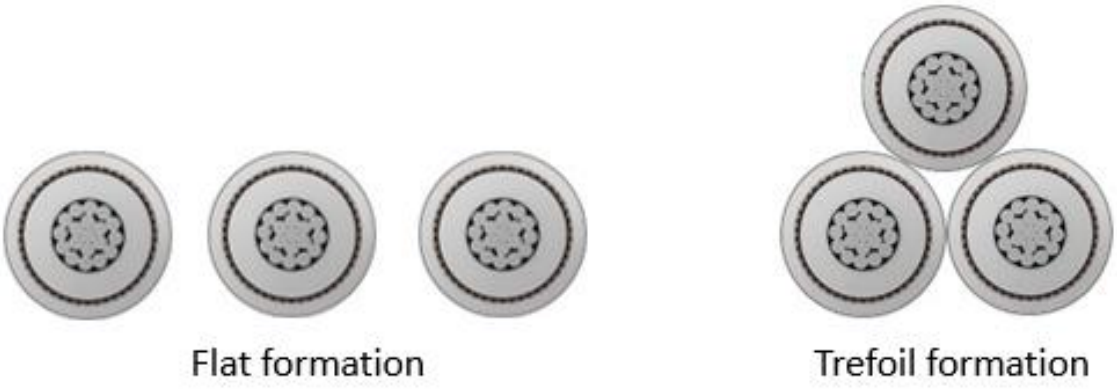

Figure 2.4. Typical formations of three-single core cables in three-phase.

The flat formation is the most common laying method for cables since it is appropriate for heat dissipation and has a better current rating than trefoil. However, the flat formation is dependent on factors such as conductor area and available space for installation. The center phase of this formation is adversely affected by the magnetic fields around the neighboring phases which results higher temperature and subsequent voltage imbalance. [25]

In the trefoil formation, the three individual conductors are placed near each other such that the net inductance decreases as the magnetic field of the currents are cancelled by each other. This formation is used to minimize the magnetic field around the conductor under short circuit conditions and to avoid eddy-current heating, see chapter 2.2. This reduces the circulating currents in sheath that is induced by the magnetic flux linking the cable conductors and metal sheath or copper wire screens. However, the trefoil formation has poor heat dissipation since there is mutual heating effect of the three power cables. Due to the cumulated heat in the power cables, the current carrying capacity reduces and increasing the cable ageing. [25]

2.1.6 Cable denotation

The denotation codes for plastic-insulated power cables are maintained by list the symbols in Table 2.3. The is “N” types according to German Institute for Standardization (DIN) and Association of Electrical Engineering (VDE) in the arrangement of their composition, starting from the conductor, and copper conductors are not identified in the type of designation. [19]

Table 2.3: The identification codes for power cables. [27]

A	Aluminum conductor
Y	Insulation of thermoplastic polyvinyl chloride (PVC)
2Y	Insulation of thermoplastic polyethylene (PE)
2X	Insulation of cross-linked polyethylene (XLPE)
HX	Insulation of cross-linked halogen-free polymer
C	Concentric copper conductor
CW	Concentric copper conductor, meander-shaped applied
S	Copper screen
SE	Copper screen, applied over each core of three-core cables
(F)	Screen area longitudinally watertight
Y	Protective PVC inner sheath
F	Armoring of galvanized flat steel wire
R	Armoring of galvanized round steel wire
G	Counter tape or binder of galvanized steel strip
Y	PVC outer sheath
2Y	PE outer sheath
H	Outer sheath of thermoplastic halogen-free polymer
HX	Outer sheath of cross-linked halogen-free polymer
-FE	Insulation maintained in case of fire

2.2 Heat generation in power cables

When the power cable transfers a load current, it will heat up the cable. The temperature of the cable will be higher as the load current increases. The temperature rise of a power cable depends on the current rating of the cables, type of conductor in a cable, types of current flow in the conductor, the production of heat within the external periphery and proximity of the cable, the nature of the load whether continuous or intermittent, insulation type, joints, manufacturing technology etc.

2.2.1 Conductor loss

Conductor loss, also called electrical resistance, Joule heating or ohmic heating occurs when an electric current through a conductor produces power losses. This is normally the dominating heat sources of power cables. The fundamental formula for Joule heating is defined as [21]

$$P = R\, I_{rms}^2 \tag{2.1}$$

where

- P is power converted from electrical energy to thermal energy
- R is the resistance of a conductor
- I_{rms}^2 is the root mean square current through a conductor

Electrical resistance comes from the moving free electrons in the conductor, which collide with the atoms of the conductor and resists the free motion of electrons, generating heat in the process. This causes resistance and reduces the electric current flow through the conductor. The ohmic resistance of a conductor is defined as [21]

$$R = \frac{P}{I^2} = \frac{\ell \cdot \rho}{A} = \frac{\ell}{A \cdot \chi} \tag{2.2}$$

where

- ℓ is total length of the cable
- ρ is electrical resistivity (specific electric resistance)
- A is cross-sectional area of the conductor
- χ is electrical conductivity (specific electric conductance)

The electrical resistance depends on material type where conductors tend to have low resistance and high conductivity. It also depends on the size and the shape of conductor. The specific electric resistance and conductance for typical electrical conducting materials at 20 ℃ are given in Table 2.4. The variation in resistivity with temperature of several common materials is shown in Figure 2.5.

Table 2.4: Electrical properties for different conducting materials at 20 ℃. [28]

Conductor	**resistivity** $\boldsymbol{\rho}$ **[Ωm]**	**Conductivity** $\boldsymbol{\chi}$ $[\boldsymbol{m/mm^2\Omega}]$	**Temperature coefficient** $\boldsymbol{\alpha}$ $[\boldsymbol{K^{-1}}]$	**Density** $[\boldsymbol{g/cm^3}]$
Aluminum	$2.65 \cdot 10^{-8}$	$3.77 \cdot 10^{7}$	$3.9 \cdot 10^{-3}$	2.7
Copper	$1.68 \cdot 10^{-8}$	$5.96 \cdot 10^{7}$	$4.04 \cdot 10^{-3}$	8.96
Iron	$9.7 \cdot 10^{-8}$	10^{7}	$5 \cdot 10^{-3}$	7.874
Nickel	$6.99 \cdot 10^{-8}$	$1.43 \cdot 10^{7}$	$6 \cdot 10^{-3}$	8.908
Silver	$1.59 \cdot 10^{-8}$	$6.3 \cdot 10^{7}$	$3.8 \cdot 10^{-3}$	10.49
Tungsten	$5.6 \cdot 10^{-8}$	$1.79 \cdot 10^{7}$	$4.5 \cdot 10^{-3}$	19.28

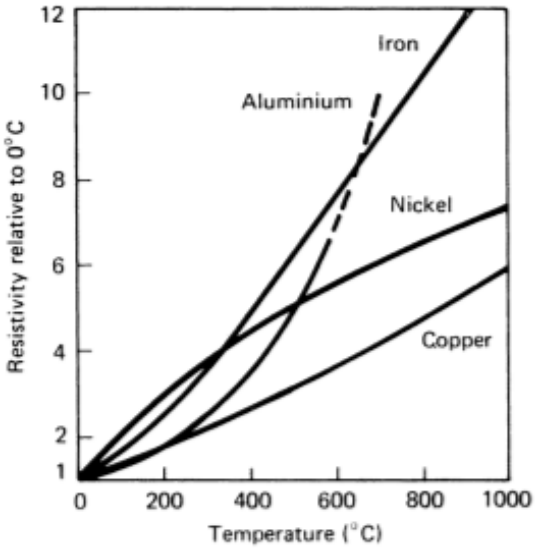

Figure 2.5: Variation of resistivity with temperature in different materials. [17]

The temperature coefficient for conductor materials given in Table 2.4 describes the rate of change in electrical resistance in a material with respect to the temperature per degree. During operation, the temperature rises due to the heat losses in the conductor. According to IEC-60277-1-1, the specific electric resistance for a temperature range between -50 ℃ to 200 ℃ can be calculated as in Equation (2.3). This is a linear equation because the resistivities are approximately linear with respect to temperature in this range, as shown in Figure 2.5. [29]

$$\rho_T = \rho_{20}[1 + \alpha(T - 20)] \tag{2.3}$$

α is the temperature coefficient and T is the temperature in which resistivity is calculated. The resistance of a conductor can be calculated similarly shown in Equation (2.4).

$$R_w = R_c\,[1 + \alpha(T_w - T_c)] \tag{2.4}$$

Where

- R_w is resistance at warm condition
- R_c is resistance at cold condition
- T_w is temperature at warm condition
- T_c is temperature at cold condition

2.2.2 Skin effect

When the direct current (DC) flows through a conductor, the current is evenly distributed throughout the cross-section of the conductor. When the alternating current (AC) flows through the conductor, the current density is largest at the conductor surface due to the skin effect. When there is an alternating current I in the conductor, as shown in Figure 2.6, the current produces a magnetic field H which changes when the intensity of current changes. The alternating magnetic field induces small eddy currents I_{ed} in the opposite direction of the main current flow I towards the center, and in the same direction in the outward direction of the conductor. [29]

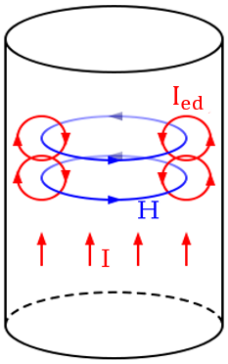

Figure 2.6: Cause of skin effect. [9, edited]

Figure 2.7 shows the cross section of the conductor where the intensity of the red color represents the intensity of the current.

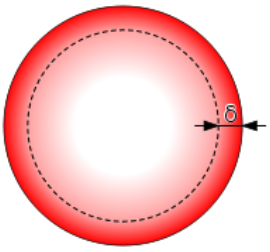

Figure 2.7: Distribution of AC current flow in a conductor. [30]

The skin depth δ is a distance where the current density decreases to $\frac{1}{e} \approx 37\ \%$ of the value at the conductor's surface. The formula for the skin depth is defined in Equation (2.5). [31]

$$\delta = \sqrt{\frac{2\rho}{\mu\omega}} = \sqrt{\frac{\rho}{\mu_r \mu_0 \pi f}} \tag{2.5}$$

where

- ρ is specific electric resistance
- μ is permeability of the conductor
- ω is the angular frequency of the current
- μ_r is relative permeability
- μ_0 is magnetic permeability in vacuum
- f is frequency of the current

Since the skin depth is depend on the frequency of the current, the higher frequency gives smaller skin depth. Skin depth is dependent on conducting materials as shown in Figure 2.8 where Mn-Zn is magnetically soft ferrite, steel 410 is magnetic stainless steel, Al is metallic aluminum, Cu is metallic copper, Fe-Si is grain-oriented electrical steel, and Fe-Ni is high-permeability permalloy (80% Ni and 20% Fe) [30]. The red vertical line indicates 50 Hz frequency. In comparison between aluminum and copper conductor with same permeability, the skin depth of aluminum is higher than copper due to the higher electric resistance of aluminum. Another comparison between iron and steel with nearly the same electric resistance, the skin depth of steel is higher than iron because iron is more magnetic and therefore have higher relative permeability.

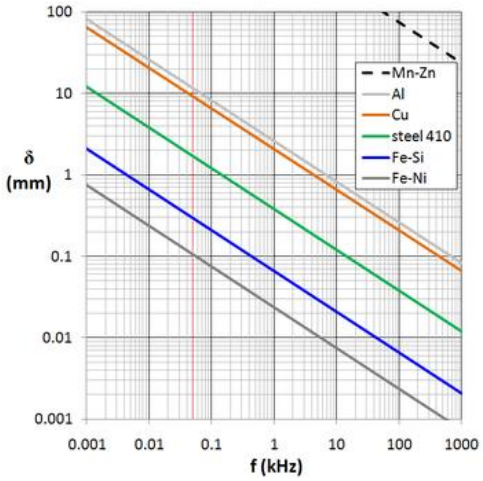

Figure 2.8: Skin depth of conductor materials for different frequencies at room temperature. [30]

In the distribution grid with low rated current, the skin effect may be negligible because the cross-section of conductors is in the same range as the skin depth. The consequence of skin depth is that only surface area of the conductor will conduct which reduces the effective cross-section of the conductor and leads to higher effective resistance. The skin depth may influence the effective cross-section of conductors for rated current around 2.5 kA and higher, and hollow conductor can be used to minimize the skin effect, see Figure 2.9. [31]

Figure 2.9: Different shapes of hollow copper conductors [32]

2.2.3 Proximity effect

The non-uniformly distribution of AC current is affected by a changing magnetic field by electromagnetic induction and creates alternating magnetic field around a conductor which induces eddy currents in adjacent conductors. The direction of eddy currents will be such that its produced magnetic field opposes the external magnetic field. [31]

When several conductors are placed near to each other, their electromagnetic field interact with each other. The current in each conductor is redistributed such that the current density is concentrated in one side due to this interaction and the produced eddy currents. The proximity effect gives a reduced effective cross-sectional area and comes in addition to the skin effect. Similar to the skin effect, the proximity effect also increases with frequency. The AC resistance of the conductor increases at higher frequencies. The proximity effect also decreases with increasing distance between the parallel conductors and is insignificant when the distance between two cables in two adjacent circuit is at least 8 times the outside diameter of the cable. [12]

The skin effect behaves differently depending on the current direction. When currents are in the opposite direction, the eddy currents increase the current on the sides facing the other conductor and canceling the current flow on the furthest side, as shown in Figure 2.10. For two adjacent conductors carrying current in the same direction, the magnetic field is cancelling current that is facing the other conductor, seen in Figure 2.11. Thus, the eddy current increases the current on the furthest side. The cross (×) means that the current direction is into the plane while a dot (•) means out of the plane of view. [31]

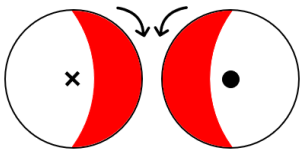

Figure 2.10: Current in the opposite direction. [12]

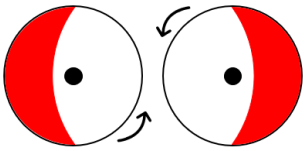

Figure 2.11: Current in the same direction. [12]

2.2.4 Contact resistance

In addition to electrical resistance or loss along the conductor, there is also contact resistance between the conductor contacts. An electrical contact is an interface between two or more conductive material that assures the continuity of the electric circuit. The conductors are called contact members where the anode is where positive current enters the contact, and the other member is the cathode. The electrical contacts are divided into two categories: stationary and moving. This chapter only focuses on the stationary contact since there is not moving part when it comes to power cable splicing. The contact members are connected rigidly to provide a permanent joint in stationary contacts. Stationary contacts are divided into two categories: welded and bolted. [31]

Welded joints (non-separable) have a high mechanical strength and is often formed within one contact member. It provides stable electrical contact with a low transition resistance and no physical interface between the conductors. The cable lugs, also called cable shoe, to a cable conductor is an example. Bolted contacts are built by joining conductors directly with bolts, screws, or clamps without damaging the joint integrity. Two massive busbars with flat contact surfaces can be jointed with the contacts. The interface between contacts is controlled by contact pressure and the ability of the material to undergo plastic deformation. [31]

The degradation of the contacting interface results in higher contact transition resistance. The contact resistance will introduce an extra resistance due to increased ohmic losses and temperature. Consequently, contact surfaces are covered with a soft and corrosion-resistant material. Cleaning techniques for both insulations and conductors are used to improve the joint connectivity. Any substances left at the interface can disrupt the electrical function of the termination and moreover cause failure [33].

Although surfaces are visibly smooth and clean, it could be microscopic roughness on the surface, contaminated with air. The effective metal-to-metal contact area R_{eff} is smaller than apparent metal-to-metal contact area R_a and therefore the conducting paths is localized for the transfer of electrical current as shown in Figure 2.12. [34]

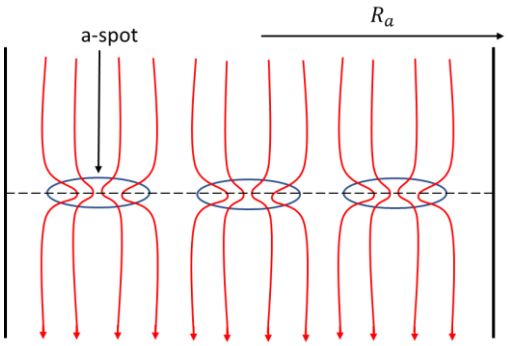

Figure 2.12: Lines of constricted current flow.

These small areas between two contacts are called a-spots where "a" stands for asperity. Several contacting a-spots are amalgamated into a single area of conducting current. Figure 2.13 shows the amalgamated a-spot combined from all the small a-spots in the left drawing. [34]

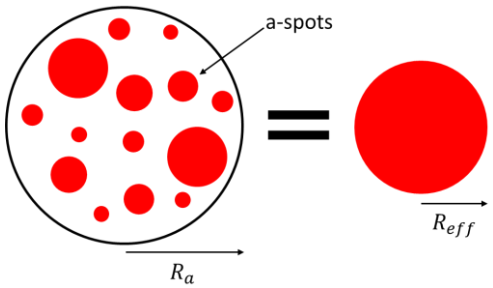

Figure 2.13: apparent radius and effective radius of a spot model.

The constriction resistance is the contact resistance due to the constricted current flow which is related to the properties of metals like hardness and electrical resistivity. Physicist Ragnar Holm came up with an expression for one contact member constriction resistance for a single a-spot can be expressed as [34]

$$R_c = \frac{\rho_1 + \rho_2}{4a} \tag{2.6}$$

where R_c is constriction resistance, ρ_1 and ρ_2 is specific resistivity of the contacting materials, and a is effective radius of a-spots.

The contact resistance is the general characteristic of all electrical contacts and is always considered when it comes to overall circuit resistance. Further, the contact resistance may differ from the changes in the contact area, resistive film non-uniformity, contact pressure variations, and other factors. The path of electric current can be affected by thin oxide, sulphide and other inorganic films which is usually covered on metal surfaces since the metals are not clean. The role of these films is negligible in practical application because the contact spots are created by the mechanical rupture of surface films. [35]

Temperature is the main factor that causes degradation of the contacts. The higher the temperature, the faster the possible degradation mechanisms e.g., oxidation. The a-spot is often the hottest area, and the contact resistance will increase if degradation takes place which can cause a run-away-effect. The oxidation process depends on the conducting materials where bare copper contact in air will be more influenced than silver plated contacts. Silver plated contact will be responsive to degradation if there are sulphureous vapors. [31]

2.2.5 Induced loss

Moreover, there is an induced loss or extra heat source alongside the losses mentioned above. When a magnetic field changes directional orientation in a ferromagnetic structure, heat is generated from hysteresis, which causes energy loss. These induced losses are called iron losses since the iron is highly ferromagnetic. Iron losses occurs in cable screens even though the screen is not iron or magnetic material but is still called iron losses because of induced eddy currents. Total iron losses can be calculated as the sum of the eddy current losses and the hysteresis losses. [31]

The power loss is proportional to the area of the eddy current loop, the strength of the magnetic field, and the rate of change of magnetic flux. The magnitude of the current is inversely proportional to the resistivity of the conductor material. According to Faraday's induction law, the induced voltage can be expressed in Equation (2.7). [21]

$$V_{ind} = -\frac{d\Phi_m}{dt} = -\frac{d(\vec{B} \cdot \vec{A})}{dt} \tag{2.7}$$

Where Φ_m is magnetic flux, B is magnetic field, and A is size of the loop. Then the induced power loss becomes [21]

$$P_{ind} = V_{ind} \cdot P_{ind} = \frac{V_{ind}^2}{R} \tag{2.8}$$

Reducing eddy current losses is difficult as it is required that the sheath is conductive. Reducing eddy currents in highly magnetic environments can be done, for instance as in transformers, where the transformer core is made out of thin laminations and will make the core have higher electrical resistance.

2.2.6 Dielectric loss

Dielectrics are materials processing high electrical. Dielectric loss is the dielectric material's inherent dissipation of heat through the movement of charges in an alternating electric field in switching polarization of field direction. It depends on frequency and the dielectric material, and the dielectric losses are zero in the ideal case. Dielectric losses are reasonably negligible for paper and XLPE cables up to about 60 kV and for PVC cables up to 6 kV. The dielectric losses are more significant for higher voltage transmission cables. [17]

Dielectric loss tends to be high in higher dielectric constant materials and is high around resonance frequencies of the polarization mechanisms as the polarization lags the applied field. Consequently, heating in interaction between the field and the dielectric's polarization occurs. The dielectric constant is a measure of the charge retention capacity of a medium or material's permittivity expressed as a ratio of relative to the vacuum permittivity. The permittivity is a quantity of the electric polarizability of dielectric materials, defined in Equation (2.9). [36]

$$\varepsilon = \varepsilon' - j\varepsilon'' \tag{2.9}$$

Where $\varepsilon' = \varepsilon_0 \varepsilon_r'$ is lossless permittivity and ε'' is imaginary component of permittivity. Dielectric loss is the loss angle δ with regards to the phasor in the complex plane where real and imaginary pairs are the resistive of the electromagnetic field. The AC current in an ideal capacitor leads the voltage by 90 º while there is a resistive component that dissipates some of energy as Joule heat in real capacitors. This reduces the lead angle δ somewhat from the dielectric losses. The loss angle is much smaller than 1 for dielectrics with small loss, then $tan\delta \approx \delta$. The loss tangent determines the ratio of the resistive response to the electromagnetic field. The loss tangent can be calculated as [36]

$$tan\delta = \frac{\omega\varepsilon'' + \sigma}{\varepsilon'} \tag{2.10}$$

where ω is the angular frequency and σ is conductivity. The dielectric constant, dielectric strength and dielectric losses for different materials are given in Table 2.5. The dielectric strength depends on the thickness of the material. [14]

Table 2.5: Dielectric properties of materials at around 27 ºC. [35], [37]

Material	**Dielectric constant at $60\ Hz$**	**Dielectric strength [kV/mm]**	**Dielectric loss tangent (tan δ)**
Air	1	3.0	
PE	2.3	20-35	10.4
Polyethylene	2.3	18.1	0.0005
Porcelain	6-7	9.8-15.7	0.003-0.002
PVC	6-8	20-35	0.1
XLPE	2.5	35-50	10.4

2.3 Thermodynamics

Many problems in electric power systems are related to the cooling of components and the rating of power cables was approached with theories made from the physical and heat transfer properties of the power cable. Thermal analysis must be able to determine how much and how long the power cables can be loaded and still be within acceptable temperature limits. Thus, thermal phenomena are at the basis of the current rating in power cables. For this purpose, the quantity of energy the equipment can store and dissipate to the surroundings must be determined. There are two different cases, dynamic and stationary, which is defined by the fundamental equations for the thermal energy balance.

Heat is energy that is transferred under the motive force of a temperature difference between systems. Heat can be transferred from a region of higher temperature to a region of lower temperature by conduction, convection, and radiation. If there is no temperature difference, there is no heat transfer. The total rate of heat transfer is defined as the sum of heat transfer by each mechanism.

2.3.1 Thermal energy balance

The fundamental equations for the thermal energy balance are conservation of energy. The law of conservation of energy states that the total energy of an isolated system remains constant. It means that the power balance or heat generated in a conductor (P_{in}) is balanced by power stored in the construction materials (P_{stored}) and power loss to the surroundings ($P_{dissipated}$). The constant power input to a conductor is the conductor losses which is the main source of losses in the power cable, and is given by [31]

$$P_{in} = R\, I^2 = \rho \frac{l}{A_{cs}} I^2 \tag{2.11}$$

where

- R is ohmic resistance
- I is current
- ρ is resistivity
- l is length of cable
- A_{cs} is cross-section of the conductor

There are two methods for specifying the current-carrying capability of a conductor and can be classified over a very short time or over a long time. Very short time spans assume adiabatic conditions, meaning no heat escapes the system, all incoming heat goes into increasing the temperature of the system. For long-term conditions (steady state) it is assumed that all incoming heat goes out to the environment, and no heat goes into heating the system. These two cases are important in classifying current ratings. The power balance in adiabatic condition becomes [31]

$$P_{in} = P_{stored} \;\rightarrow\; \rho \frac{l}{A_{cs}} I^2 = \; cM \frac{d}{dt} \Delta T = c\gamma V \frac{d}{dt} \Delta T \tag{2.12}$$

where M, V and γ is mass, volume, and density of the substance. The parameters specific heat capacity c and resistivity ρ are hard to determine since they change with temperature,

especially in the adiabatic condition. The specific heat capacity gives an indication of the materials ability to store heat which means how much energy is required to raise temperature of 1 kg of the material by 1 ℃. Those parameters are usually set at the environment temperature at first approximation.

After the adiabatic condition, it starts to dissipate heat to the surroundings by conduction, convection, and radiation. The total rate of dissipated heat to the surroundings becomes [31]

$$\mathrm{P}_{in} = \mathrm{P}_{dissipated} = \mathrm{P}_{cond} + \mathrm{P}_{conv} + \mathrm{P}_{rad} \tag{2.13}$$

where P_{cond}, P_{conv}, and P_{rad} is heat transfer by conduction, convection, and radiation, respectively. The stationary period is where the temperature has reached steady state and all heat is going into the surroundings. This means there is no more heat to be stored in the system and therefore no temperature change occurs.

The power dissipated in the stationary period is simplified due to the three heat dissipation mechanisms having different temperature dependencies. The power balance is given by [31]

$$\mathrm{P}_{in} = \mathrm{P}_{dissipated} \;\rightarrow\; \rho \frac{l}{A_{cs}} I^2 = h\, A_{surf}\, \Delta T \tag{2.14}$$

where h is heat transfer coefficient, A_{surf} is heat emitting surface, and ΔT is temperature difference. The heat transfer coefficient h gives an indication of how much energy the surface can dissipate and is difficult to determine due to the different temperature dependencies in different heat transfer mechanisms. Then the power balance in a conductor becomes [31]

$$\begin{aligned} \mathrm{P}_{in} &= \mathrm{P}_{stored} + \mathrm{P}_{dissipated} \\ \rho \frac{l}{A_{cs}} I^2 &= c\gamma V \frac{d}{dt}\Delta T + h\, A_{surf}\, \Delta T \end{aligned} \tag{2.15}$$

The power balance per unit length is often convenient for electrical power engineering where the power is supplied in cables, lines, busbars etc. The power balance per unit length is [31]

$$\frac{\rho}{A_{cs}} I^2 = c\gamma A_{cs} \frac{d}{dt}\Delta T + h\, U\, \Delta T \tag{2.16}$$

where U is circumference of the conductor.

The temperature rise can be calculated by solving the differential Equation (2.15).

$$\Delta T(t) = \Delta T_e (1 - e^{-t/\tau}) \tag{2.17}$$

Where ΔT_e is final steady state temperature difference and τ is thermal time constant. The time constant gives an indication about the time required to reach 63.2 % of steady state temperature difference between its initial and final temperature value when subjected to a step function change in input power. It determines how long the equipment can be overloaded without overheating (short-term overload), for example during daily load cycles. The time constant is also a characteristic of the lumped parameter analysis for thermal systems. In heat transfer analysis, interior temperatures of the object are assumed spatially uniform at all times during a heat transfer process. The thermal system is reduced to a number of discrete lumps and the temperature difference inside each lump is negligible. This is called a lumped parameter system. The thermal time constant is defined as [31]

$$\tau = \frac{c\gamma V}{h\, A_{surf}} = \frac{cM}{h\, A_{surf}} \tag{2.18}$$

The numerator expresses the storage capacity of the equipment and the denominator expresses the thermal dissipation capacity of the equipment. The temperature change rate (%) at n times the thermal time constant τ is shown in Figure 2.14. The temperature rise is fast in the beginning, then becomes slower until it reaches the final steady state temperature approximately within 5 times the thermal time constant. Further according to IEC, the temperature is stable enough if the temperature does not increase more than 1 ℃ per hour as defined in Equation (2.19). [31]

$$\frac{\mathrm{d}}{\mathrm{dt}}\Delta\mathrm{T} < \frac{1\ ℃}{\mathrm{hour}} \tag{2.19}$$

where $\frac{\mathrm{d}}{\mathrm{dt}}\Delta\mathrm{T}$ is change in temperature rise per unit time.

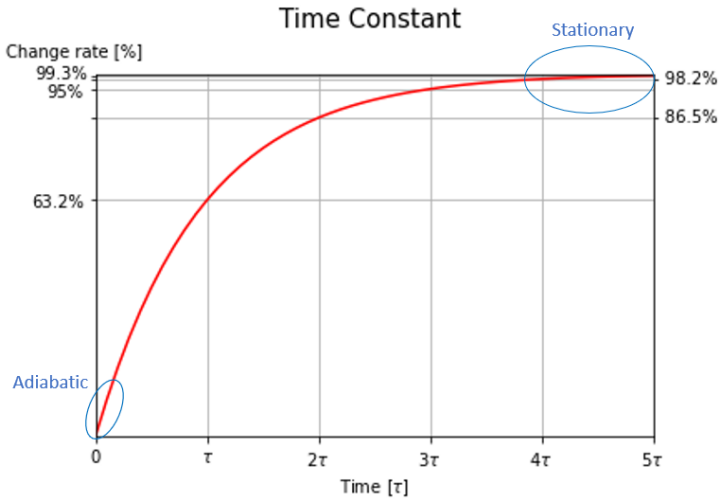

Figure 2.14: The temperature change rate over the thermal time constants

If the equipment has large heat dissipating surface compared to the mass, the time constant of this equipment will be small and cannot be as much overloaded. If the equipment has large mass compared to the heat dissipating surface, it will have a long time constant which means that it can be overloaded for hours. [31]

Underground cables have lower current ratings than comparable overhead lines with the same conductor cross-section due to restricted cooling. However, the long thermal time constant of underground cables, typically from minutes to hours, depends on cross-section of the conductor and soil which influences heat capacity and heat transfer. The relatively long thermal time constant allows underground cables to have very high emergency ratings with short duration. Thus, underground cables may be limiting under normal, stable, and long duration conditions while overhead lines are limiting during emergencies and short-term overload. [31]

The time constant of cables increases with increasing cross-section. Example of time constants for different cross-section areas (A_{cs}) of PVC copper cables laid well apart on a wall is shown in Table 2.6. [27]

Table 2.6: Thermal time constant for PVC copper cable of different cross-section area. [27]

A_{cs} $[mm^2]$	1.5	2.5	4	10	25	95	150	240
τ $[min]$	0.7	1.0	1.5	3	6	16	23	32

2.3.2 Thermal conduction

The conduction of heat is partly due to the motion of adjacent molecules and interaction. The conduction heat transfer through solids is due to molecular vibration and thermal conductivity generally does not vary with temperature in solids. A number of mobile electrons can move through the material and contribute to the redistribution of thermal energy. The large-scale motion with frequent collisions assists the conduction of heat in liquids. The thermal conductivity is often strongly influenced by temperature in liquids and gases. The conductivity is lower in gases than liquids and solids even if the mobility of individual particles is greater. This is due to the relatively long "mean free path" in gases and therefore the relatively infrequent impact between the molecules. The power conducted through a cross-sectional area is given by Fourier's law. [38]

$$P_{cond} = \lambda A_{cs} \nabla T \tag{2.20}$$

Heat conduction in one dimension is often considered for simple applications. The Fourier's law is then reduced to [38]

$$P_{cond} = \frac{\lambda}{s} A_{cs} \Delta T \tag{2.21}$$

where

- λ $[W/mK]$ is thermal conductivity of material
- A_{cs} $[m^2]$ is cross-sectional area
- ∇T is tempertarue gradient
- s is distance over the temperature difference ΔT

Thermal conductivity is a materials ability to conduct heat and is defined as the quantity of heat flowing per unit time through a volume of $1\,m^3$ when the temperature of the two surfaces differs by 1 ºC [31]. High thermal conductivity materials are used in heat sink applications while low thermal conductivity materials are used as thermal insulation. Thermal resistivity is material's capability to resist heat flow which is the reciprocal of thermal conductivity. The thermal resistivity is usually stated for different cable materials. Different thermal conductivity and resistivity, and specific heat capacity for materials is shown in Table 2.7.

Table 2.7: Thermal conductivity for different materials. [31], [39], [40], [41], [42]

Material	**Thermal conductivity λ [W/mK]**	**Thermal resistivity R_λ [mK/W]**	**Specific heat capacity $\hat{c}$ [J/kgK]**
Al	240	0.0042	900
Cu	385	0.0026	390
EPR	0.3	3.33	2800
Impregnated paper	0.167	6.0	1994*
Steel	12-16	0.083-0.0625	490
PE	0.4	2.5	1550
PEX	0.4	2.5	2300
PVC	0.19	5.26	880
XLPE	0.28	3.5	2174

*Synthetic ester at 60 ℃

2.3.3 Thermal convection

Convection is the circulation of heat exchange between fluids and solid boundaries by the motion of fluids. Convection is classified as either forced convection or free convection depending on how the fluid motion is conducted. Forced convection is causes when some external source is used to cause the motion of fluid. Free or natural convection occurs when the motion of fluid is only due to density gradients or buoyancy forces in fluid caused by the temperature variation. [38]

Newton's law of cooling is often used to simplify the complicated process of convection cooling. The power generated by convection is defined as [38]

$$P_{conv} = h_{conv} A_{surf} (T_s - T_0) \tag{2.22}$$

where

- h_{conv} [W/m^2K] is convective heat transfer coefficient
- A_{surf} is surface area
- T_s is surrounding temperature
- T_0 is ambient temperature

The convective heat transfer coefficient depends on the type (velocity, turbulent, laminar, etc.) and physical properties (thermal conductivity, dynamic viscosity, thermal capacity, density, etc.) of fluid and the physical situation. Further these properties are often combined in the

mechanism of dimensionless characteristics (Nusselt, Prandtl, Reynolds, Grasshof numbers, etc.). Table 2.8 shows the approximate convection heat transfer coefficient done by empirical examples. [31]

Table 2.8: Approximate convective heat transfer coefficient. [31]

	Materials	**Convective heat transfer coefficient h_{conv}**
Free convection	Atmospheric air	5-25
	Water	400-1000
Forced convection	Air	15-500
	Water	100-15000
	Engine oil	1000-2000

2.3.4 Thermal radiation

Thermal radiation is the thermal motion of particles in material generated by electromagnetic waves even if there is no matter between the materials and does not depend upon the existence of an intervening matter. [38]

All materials with a temperature greater than absolute zero (zero Kelvin) radiates thermal radiation and all materials absorb radiant energy surrounding objects. The intensity of the energy radiated depends upon the temperature of the surrounding objects and the nature of its surface. Equilibrium sets in when the temperature of a material is the same as that of its surroundings which means that the material radiates as much energy as it receives, thereby the net radiation is zero. The power generated by radiation is defined as [38]

$$\mathrm{P_{rad}} = \varepsilon\, \sigma_s\, \mathrm{A_{surf}}\, (T^4 - T_0^4) \tag{2.23}$$

where

- ε is emissivity of the surface, $0 \leq \varepsilon \leq 1$
- $\sigma_s = 5.67 \cdot 10^{-8}\ [W/(m^2K^4)]$ is Stefan Boltzmann's constant
- $\mathrm{A_{surf}}$ is radiating surface area
- T [K] is absoulte temperature of the surface
- $\mathrm{T_0}\ [K]$ is absolute temperature of the ambient walls

As shown in the formula, the power generated by radiation is strongly dependent of temperature. The emissivity factor ε indicates the radiation of heat from surfaces and the radiation of heat from an ideal "black body" has the perfect emissivity factor, $\varepsilon = 1$. Different emissivity factors of materials are shown in Table 2.9. It is an experimental fact that unit surface area of a black body emits more energy by radiation than unit area of any other body at the same temperature. [27]

Table 2.9: The emissivity factor for some materials below 200 ℃. [27]

Surface materials	Emissivity ε
Black body	1
Aluminum bright/oxidized	0.04/0.5
Copper bright/oxidized	0.05/0.6
Steel dull, oxidized/polished	0.8/0.06
Oil	0.82
Paper	0.85
Paints	0.8-0.95

2.4 Thermal dimensioning of cables

Heat is generated in the power cable mainly due to current flow and understanding how cables perform is a thermal problem. In this chapter, stationery and dynamic thermal dimensioning is discussed.

2.4.1 Current-carrying capacity (ampacity)

Current-carrying capacity, also called as ampacity, is defined as the maximum current a conductor of a power cable can carry continuously under the normal usage conditions without generating excessive heat. It can be regarded as ability of conductor to dissipate heat without damaging the insulation or the cable. Exceeding the conductor ampacity too long will result the insulation to degrade because of the excessive heat. [27]

The amount of conductor resistance increases as the amount of current is increased. Consequently, increases the amount of heat generated of a power cable. Thus, the ampacity can increase with increasing the diameter of the cable. The larger the diameter of the power cable, the more effectively it can dissipate the heat. The ampacity of the cable is limited by the ability of its insulation and outer sheath to withstand the generated heat. [27]

The National Electrical Code (NEC), the Institute of Electrical and Electronics Engineers (IEEE) and Insulated Cable Engineers Association (ICEA) have published tables of recognized and comprehensive ampacity ratings. Tables of ampacities cover the maximum ampacity of conductor based on the conductor material, conductor diameter, the maximum withstand temperature, and installation conditions.

The current ratings of cables are based on the way heat in the conductor is transmitted through the cable and dissipated from the cable to the outer surface. The maximum rating can be calculated by limiting the temperature rise in the cable such that conductor temperature stays below a safe limit, usually 90 ºC. [17]

The surrounding temperature normally defaults to 15 ℃ for buried cables and 25 or 30 ℃ for cables in air. At steady state, the generated heat in the cable is equal to the dissipated heat from the cable surface. That means the maximum steady state temperature is depending on the thermal resistance of the cable components and the surrounding temperatures. [17]

The internationally authorized conductor temperature limits of polymeric cables are shown in Table 2.10. Short-circuit ratings are contributed by reduction of thickness of PVC and PE by thermomechanical forces, conductor and core screens, and design of accessories. The softness of the thermoplastic insulation is higher with increasing temperature and the temperature limit is controlled by deformation. One can see that the thermosetting materials can withstand much higher temperatures without excessive deformation. [17]

Table 2.10: Conductor temperature limits of polymetric cables. [17]

Insulating compound	**Continuous temp [℃]**	**Short-circuit temp [℃]**
Polyvinyl chloride (PVC)	70	160
Polyethylene (PE)	70	130
Ethylene propylene rubber (EPR)	90	250
Cross-linked polyethylene (XLPE)	90	250

Other factors in cable ratings are conductor losses, dielectric losses, sheath and armor losses, and internal and external thermal resistances. Metallic sheath losses are more significant for large single-core conductor cables bonded and earthed at both ends. The sheath losses can be reduced by cross-bonding. [17]

A loaded cable shows logarithmic temperature rise and time relationship. It takes times to reach steady state and consequently, it can carry more than maximum continuous rating for a limited or a short time. The factor for overload depends on the amount of initial loading. The short-circuit current may be 20 or more times higher than the loading current and consequently, the thermal and electromagnetic effects produce proportional to the square of the current. If the cable insulation is only concerned, higher conductor temperatures can be allowed since the heating and cooling are very fast that the entire temperature will not be maintained for considerable time by the insulation. [17]

2.4.2 Determination of ampacity

The determination of the ampacity requires formulating a heat transfer, thermal properties of the cable materials, heat sources inside and outside of the cable, and the mechanisms of heat dissipation, etc. Depending on the cable environment, ampacity ratings may require to be adjusted because of changed thermal properties. In the transient thermal case, it is necessary to consider the thermal resistance of cable insulation and external sheath, and heat capacity of each layers [31].

There are two types of cable installation – underground cable and cables in air. Thermal resistance within the underground cable is related to the cable design, construction, and thermal resistivity and thickness of the individual materials. The external thermal resistance of the underground cable is influenced by the laying environment, thermal resistance of duct, uniformity of soil, and temperature-dependent resistivity of soil. [17]

Thermal properties of soil are significant for the overall underground power cable design since the soil is in the heat flow path between the cable and the ambient environment temperature. Current ratings of underground cables are determined by conduction) from the conductor, through the cable layers and soil to ambient ground. The soil characteristics must be surveyed to determine the ability for heat to pass through the soil. Further, ambient soil temperature, burial depth, and available space between cables, and other heat sources should be surveyed to choose the right cable conductor size, number of cables per phase, etc. Figure 2.15 shows an example of thermal curves surrounding an underground cable [31]. [44]

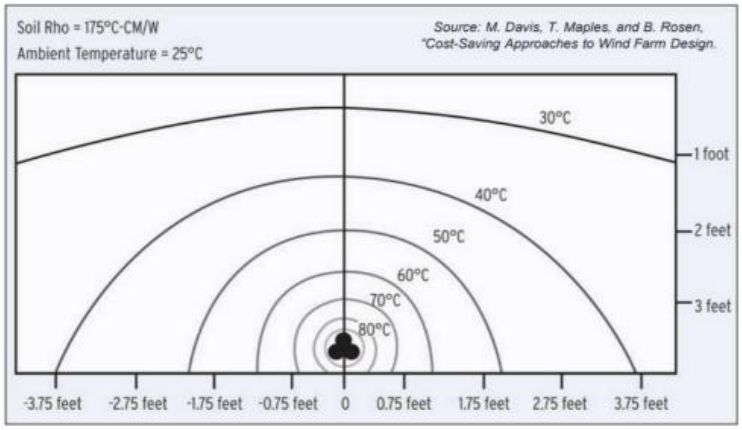

Figure 2.15: Example of thermal curves surrounding an underground cable at full load. [31]

Table 2.11 shows the thermal conductivity of different external materials of the power cable. According to the recommendation tables from the ABB Switchgear handbook the resistance varies from 0.4 to 1.4 W/mK. [27]

Table 2.11: Thermal properties of external materials and soil constituents at 20 ℃ and 1 atm. [31]

Material	**Thermal conductivity [W/mK]**	**Thermal resistivity [mK/W]**
Air	0.062	16.13
Water	0.6	1.67
Many soil minerals	2.9	0.34
Soil organic matter	0.25	4

The thermal resistivity of different types of soil is dependent on soil density and water content. Figure 2.16 shows how the soil thermal resistivity decreases with increasing density for dry materials. Organic materials are not suitable for dissipating heat from underground cables. Figure 2.17 shows the influence of water content on the thermal resistance of soils where density is around 1.6 Mg/m^3. [43]

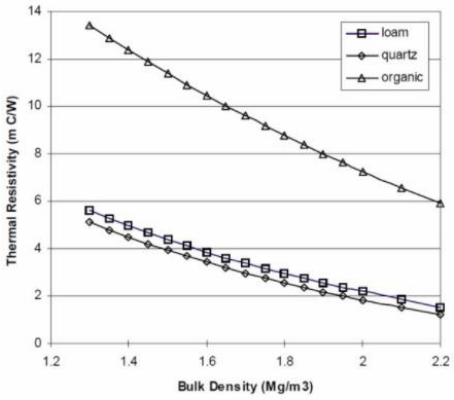

Figure 2.16: Thermal resistivity of dry soils is dependent on its density. [43]

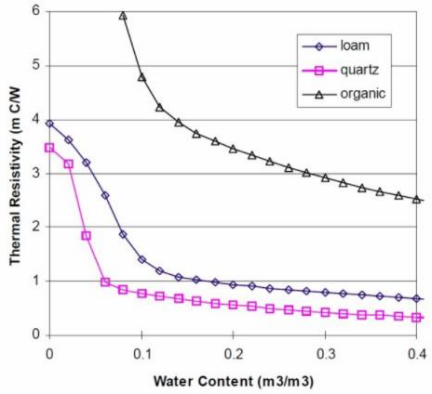

Figure 2.17: Thermal resistivity of soils is dependent on its water content. [43]

The critical water content is very significant for underground cable design since the cable heat will lead the moisture away. Consequently, drying the soil around the cable will lead to additional heating. The heat dissipation from the cable can be restricted due to heat dissipation from other nearby cables and cover plates with some air gaps as mechanical protection. [43]

Insulated power cables installed in air is within substations, power station buildings, tunnels, charging of ferries, etc. There is no adjustment for different load factor since the cables in air has shorter time constant than for the underground cables. For overhead lines or cables in air, the external thermal resistance depends on cable surface environment which is related to the degree of exposure such as solar heating and wind, and to the surface emissivity. Those external effects must be evaluated when determining ampacity for in-air cables. Published current ratings for overhead lines assume shading form the sun. If this is not provided, derating may be required. Heat generation and losses in cables are described more detail in chapter 2.2. [17]

2.4.3 Rated current

The recognized rated current of a power cable is published by different institutions. One example is by ABB, which presents the current carrying capacity of power cables laid underground and in air. Table 2.12 shows the rated current for XLPE and paper cable for copper and aluminum conductors for 12/20 kV and 18/30 kV, respectively. Assumptions regarding the cable surroundings are made since possible loading will depend on the actual cooling condition. The rated current values are for 3-phase continuous operation with a load factor of 0.7. Load factor is described in chapter 2.4.6. For underground cables, specific ground thermal resistance is assumed to be 1 Km/W, ground temperature of 20 ºC and cable laying depth of 0.7 m to 1.2 m. For cables in air, the air temperature is assumed to be 30 ºC. [27]

Table 2.12: Rated current for impregnated paper and XLPE cable with copper and aluminum conductor for V_0/V = 12/20 kV (left) and V_0/V = 18/30 kV (right). [27]

Rated current (three-phase operation) as per DIN VDE 0276-620 (XLPE cables) and DIN VDE 0276-621 (paper cable)
cable with U_0/U = 12/20 kV
laid underground and in air

1	2	3	4	5	6	7
Insulation material	Impregnated paper		XLPE			
Metal sheath	Lead					
Type designation	N(A)EKBA		N(A)2XSY, N(A)2XS2Y N(A)2X(F)2Y			
Permissible operating temperature	65 °C		90 °C			
Configuration	✪	✪	⁂	⁂	⊙⊙⊙	⊙⊙⊙
Installation	*Ground*	*Air*	*Ground*	*Air*	*Ground*	*Air*
Nominal cross-section Copper conductor mm²	Rated current in A					
25	129	111	—	—	—	—
35	155	134	189	200	213	235
50	185	161	222	239	250	282
70	229	200	271	297	303	351
95	274	243	323	361	360	426
120	314	279	367	416	407	491
150	354	317	409	470	445	549
185	402	363	461	538	498	625
240	468	426	532	634	568	731
300	530	488	599	724	633	830
400	600	560	671	829	685	923
500	674	641	754	953	760	1045
Aluminium conductor mm²						
25	100	86	—	—	—	—
35	121	104	—	—	—	—
50	144	125	172	185	195	219
70	178	156	210	231	237	273
95	213	189	251	280	282	332
120	244	218	285	323	319	384
150	275	247	319	366	352	432
185	314	284	361	420	396	494
240	367	334	417	496	455	581
300	417	384	471	569	510	663
400	478	445	535	660	564	753
500	545	516	609	766	634	866
Conversion factors						
$f_1/f^{1)}$ from tables	13-54	13-51	13-54	13-51	13-54	13-51
$f_2/f^{2)}$ from tables	13-59	13-53	13-56 13-57	13-52	13-58	13-52

1) for ground temperature/for air temperature
2) for grouping in ground/in air

Rated current (three-phase operation) as per DIN VDE 0276-620 (XLPE cables) and DIN VDE 0276-621 (paper cable)
cable with U_0/U = 18/30 kV
laid underground and in air

1	2	3	4	5	6	7
Insulation material	Impregnated paper		XLPE			
Metal sheath	Lead					
Type designation	N(A)EKEBA		N(A)2XSY, N(A)2XS2Y N(A)2XS(F)2Y			
Permissible operating temperature	60 °C		90 °C			
Configuration	✪	✪	⁂	⁂	⊙⊙⊙	⊙⊙⊙
Installation	*Ground*	*Air*	*Ground*	*Air*	*Ground*	*Air*
Nominal cross-section Copper conductor mm²	Rated current in A					
35	146	126	—	—	—	—
50	174	150	225	241	251	282
70	215	187	274	299	304	350
95	259	227	327	363	362	425
120	297	261	371	418	409	488
150	334	295	414	472	449	548
185	379	338	466	539	502	624
240	442	397	539	635	574	728
300	501	453	606	725	640	828
400	569	519	680	831	695	922
500	644	594	765	953	773	1045
Aluminium conductor mm²						
35	113	98	—	—	—	—
50	135	117	174	187	195	219
70	167	145	213	232	238	273
95	201	176	254	282	283	331
120	231	203	289	325	321	382
150	260	230	322	367	354	429
185	297	264	364	421	399	492
240	347	311	422	496	458	578
300	394	356	476	568	514	659
400	454	414	541	650	570	750
500	520	478	616	764	642	861
Conversion factors						
$f_1/f^{1)}$ from tables	13-54	13-51	13-54	13-51	13-54	13-51
$f_2/f^{2)}$ from tables	13-59	13-53	13-56 13-57	13-52	13-58	13-52

1) for ground temperature/for air temperature
2) for grouping in ground/in air

The copper conductors have current ratings approximately 30 % higher than aluminum conductors with the equal cross-sectional area. The ampacity increases when increasing cross-section and surface area for the cables in air due to the more effective cooling by convection and radiation. For XLPE-insulated cables, the cables in air have the higher current rating, regardless of the cross-section since the radiation is more important for the higher temperature.

2.4.4 Correction factors

As mentioned, the rated current values (I_{rated}) on Table 2.12 assume certain cooling conditions of the power cable. I_{rated} is different if the cooling conditions differ from the assumptions. Then the actual loading (I_{load}) is calculated as the product of I_{rated} and correction factors. The correction factor (f) depends on wheter the power cables are laid in underground or in air. [31]

Two conversion factors must be applied, one for external conditions and another for the configuration of the power cable. Therefore the acutual loading is adjusted to [27]

$$I_{load} = I_{rated} \cdot f_1 \cdot f_2 \tag{2.24}$$

For the underground cables, f_1 is conversion factor for different ground temperatures and f_2 is conversion factor for cable's laying and grouping, see Table 2.13 and Table 2.14 respectively. The resulting actual loading current will be the peak value during a 24-hour cycle. Additional conversion factors for laying underground power cables are 0.8 when laying in conduits and 0.9 when laying under mechanical protective covers with some air space. [27]

Table 2.13: Conversion factor f_1 for all underground cables (except PVC cables for 6/10kV). [27]

1	2	3					4					5					6
Permissible operating temperature	Soil temperature	Specific thermal resistance of soil K · m/W 0.7					1.0					1.5					2.5
		Load factor					Load factor					Load factor					Load factor
°C	°C	0.50	0.60	0.70	0.85	1.00	0.50	0.60	0.70	0.85	1.00	0.50	0.60	0.70	0.85	1.00	0.5 to 1.00
90	5	1.24	1.21	1.18	1.13	1.07	1.11	1.09	1.07	1.03	1.00	0.99	0.98	0.97	0.96	0.94	0.89
	10	1.23	1.19	1.16	1.11	1.05	1.09	1.07	1.05	1.01	0.98	0.97	0.96	0.95	0.93	0.91	0.86
	15	1.21	1.17	1.14	1.08	1.03	1.07	1.05	1.02	0.99	0.95	0.95	0.93	0.92	0.91	0.89	0.84
	20	1.19	1.15	1.12	1.06	1.00	1.05	1.02	1.00	0.96	0.93	0.92	0.91	0.90	0.88	0.86	0.81
	25						1.02	1.00	0.98	0.94	0.90	0.90	0.88	0.87	0.85	0.84	0.78
	30								0.95	0.91	0.88	0.87	0.86	0.84	0.83	0.81	0.75
	35													0.82	0.80	0.78	0.72
	40																0.68
80	5	1.27	1.23	1.20	1.14	1.08	1.12	1.10	1.07	1.04	1.00	0.99	0.98	0.97	0.95	0.93	0.88
	10	1.25	1.21	1.17	1.12	1.06	1.10	1.07	1.05	1.01	0.97	0.97	0.95	0.94	0.92	0.91	0.85
	15	1.23	1.19	1.15	1.09	1.03	1.07	1.05	1.03	0.99	0.95	0.94	0.93	0.92	0.90	0.88	0.82
	20	1.20	1.17	1.13	1.07	1.01	1.05	1.03	1.00	0.96	0.92	0.91	0.90	0.89	0.87	0.85	0.78
	25						1.03	1.00	0.97	0.93	0.89	0.88	0.87	0.86	0.84	0.82	0.75
	30								0.95	0.91	0.86	0.85	0.84	0.83	0.81	0.78	0.72
	35													0.80	0.77	0.75	0.68
	40																0.64
70	5	1.29	1.26	1.22	1.15	1.09	1.13	1.11	1.08	1.04	1.00	0.99	0.98	0.97	0.95	0.93	0.86
	10	1.27	1.23	1.19	1.13	1.06	1.11	1.08	1.06	1.01	0.97	0.96	0.95	0.94	0.92	0.89	0.83
	15	1.25	1.21	1.17	1.10	1.03	1.08	1.06	1.03	0.99	0.94	0.93	0.92	0.91	0.88	0.86	0.79
	20	1.23	1.18	1.14	1.08	1.01	1.06	1.03	1.00	0.96	0.91	0.90	0.89	0.87	0.85	0.83	0.76
	25						1.03	1.00	0.97	0.93	0.88	0.87	0.85	0.84	0.82	0.79	0.72
	30								0.94	0.89	0.85	0.84	0.82	0.80	0.78	0.76	0.68
	35													0.77	0.74	0.72	0.63
	40																0.59

The conversion factor f_1 must always be used with the conversion factor f_2.

Table 2.14: Conversion factor f_2 for single-core cables in three phase systems, trefoil formation with 7 cm distance between cables. [27]

1	2	3					4					5					6				
Type	Number of systems	Specific thermal resistance of soil in K · m/W 0.7					1.0					1.5					2.5				
XLPE cables 0.6/1 kV 6/10 kV 12/20 kV 18/30 kV		load factor					load factor					load factor					load factor				
		0.5	0.6	0.7	0.85	1.00	0.5	0.6	0.7	0.85	1.00	0.5	0.6	0.7	0.85	1.00	0.5	0.6	0.7	0.85	1.00
	1	1.09	1.04	0.99	0.93	0.87	1.11	1.05	1.00	0.93	0.87	1.13	1.07	1.01	0.94	0.87	1.17	1.09	1.03	0.94	0.87
	2	0.97	0.90	0.84	0.77	0.71	0.98	0.91	0.85	0.77	0.71	1.00	0.92	0.86	0.77	0.71	1.02	0.94	0.87	0.78	0.71
	3	0.88	0.80	0.74	0.67	0.61	0.89	0.82	0.75	0.67	0.61	0.90	0.82	0.76	0.68	0.61	0.92	0.83	0.76	0.68	0.61
	4	0.83	0.75	0.69	0.62	0.56	0.84	0.76	0.70	0.62	0.56	0.85	0.77	0.70	0.62	0.56	0.86	0.78	0.71	0.63	0.56
	5	0.79	0.71	0.65	0.58	0.52	0.80	0.72	0.66	0.58	0.52	0.80	0.73	0.66	0.58	0.52	0.82	0.73	0.67	0.59	0.52
	6	0.76	0.68	0.62	0.55	0.50	0.77	0.69	0.63	0.55	0.50	0.77	0.70	0.63	0.56	0.50	0.78	0.70	0.64	0.56	0.50
	8	0.72	0.64	0.58	0.51	0.46	0.72	0.65	0.59	0.52	0.46	0.73	0.65	0.59	0.52	0.46	0.74	0.66	0.59	0.52	0.46
	10	0.69	0.61	0.56	0.49	0.44	0.69	0.62	0.56	0.49	0.44	0.70	0.62	0.56	0.49	0.44	0.70	0.63	0.57	0.49	0.44
PVC cables 0.6/1 kV 3.6/6 kV 6/10 kV		load factor					load factor					load factor					load factor				
		0.5	0.6	0.7	0.85	1.00	0.5	0.6	0.7	0.85	1.00	0.5	0.6	0.7	0.85	1.00	0.5	0.6	0.7	0.85	1.00
	1	1.01	1.02	0.99	0.93	0.87	1.04	1.05	1.00	0.93	0.87	1.07	1.06	1.01	0.94	0.87	1.11	1.08	1.01	0.94	0.87
	2	0.94	0.89	0.84	0.77	0.71	0.97	0.91	0.85	0.77	0.71	0.99	0.92	0.86	0.77	0.71	1.01	0.93	0.87	0.78	0.71
	3	0.86	0.79	0.74	0.67	0.61	0.89	0.81	0.75	0.67	0.61	0.90	0.83	0.76	0.68	0.61	0.91	0.83	0.77	0.68	0.61
	4	0.82	0.75	0.69	0.62	0.56	0.84	0.76	0.70	0.62	0.56	0.85	0.77	0.71	0.62	0.56	0.86	0.78	0.71	0.63	0.56
	5	0.78	0.71	0.65	0.58	0.52	0.80	0.72	0.66	0.58	0.52	0.80	0.73	0.66	0.58	0.52	0.81	0.73	0.67	0.59	0.52
	6	0.75	0.68	0.62	0.55	0.50	0.77	0.69	0.63	0.55	0.50	0.77	0.70	0.64	0.56	0.50	0.78	0.70	0.64	0.56	0.50
	8	0.71	0.64	0.58	0.51	0.46	0.72	0.65	0.59	0.52	0.46	0.73	0.65	0.59	0.52	0.46	0.73	0.66	0.60	0.52	0.46
	10	0.68	0.61	0.55	0.49	0.44	0.69	0.62	0.56	0.49	0.44	0.69	0.62	0.56	0.49	0.44	0.70	0.63	0.57	0.49	0.44

The conversion factor f_2 must be applied only together with conversion factor f_1.

For cables in air, f_1 is conversion factor for ambinet temperatures different from 30 ºC, and f_2 is conversion factor for grouping of cables in air, see Table 2.15 and Table 2.16, resepectively.

Table 2.15: Correction factor f_1 for different ambient temperature for cables laid in air. [27]

Conversion factors for different air temperatures (as per DIN VDE 0276-1000)

1	2	3	4	5	6	7	8	9	10	11	12
Type	Permissible operating temper-ature	Permissible temper-ature rise	Conversion factors for the air temperature in °C								
			10	15	20	25	30	35	40	45	50
—	°C	K	—	—	—	—	—	—	—	—	—
XLPE cables	90	—	1.15	1.12	1.08	1.04	1.0	0.96	0.91	0.87	0.82
PVC cables	70	—	1.22	1.17	1.12	1.06	1.0	0.94	0.87	0.79	0.71
Mass-impreg. cables:											
Belted cables											
6/10 kV	65	35	1.0	1.0	1.0	1.0	1.0	0.93	0.85	0.76	0.65
Single-core, three-core single lead sheathed and H-type cables											
12/20 kV	65	35	1.0	1.0	1.0	1.0	1.0	0.93	0.85	0.76	0.65
18/30 kV	60	30	1.0	1.0	1.0	1.0	1.0	0.91	0.82	0.71	0.58

Table 2.16: Correction factor f_2 for cable grouping in air. [27]

1	2	3	4	5	6	7
Installation Spacing = cable diameter *d*	Number of troughs/ racks vertical	Number of cables horizontal[4]				
		1	2	3	4	6
Laid on the floor	1	0.97	0.96	0.94	0.93	0.90
Unperforated cable troughs[2]	1	0.97	0.96	0.94	0.93	0.90
	2	0.97	0.95	0.92	0.90	0.86
	3	0.97	0.94	0.91	0.89	0.84
	6	0.97	0.93	0.90	0.88	0.83
Perforated cable troughs[2]	1	1.00	1.00	0.98	0.95	0.91
	2	1.00	0.99	0.96	0.92	0.87
	3	1.00	0.98	0.95	0.91	0.85
	6	1.00	0.97	0.94	0.90	0.84
Cable racks[2] (cable gratings)	1	1.00	1.00	1.00	1.00	1.00
	2	1.00	0.99	0.98	0.97	0.96
	3	1.00	0.98	0.97	0.96	0.93
	6	1.00	0.97	0.96	0.94	0.91
On racks or on the wall or on perforated cable troughs in vertical configuration	Number of troughs horizontal	Number of systems vertical				
		1	2	3	4	6
	1	1.00	0.91	0.89	0.88	0.87
	2	1.00	0.91	0.88	0.87	0.85

Similar to the swtichgear manual from ABB, Nexans has been calculated correction factors for flat and trefoil formations. For flat formation, correction factor for three-phase single conductors on one cable tray is 0.88 with minimum one cable diameter distance between the cables. For trefoil formation, the correction factors are 0.95 and 0.9 for one or two group, respectively, with minimum two cable diameter distance between the groups. The distance between wall and cable should be minimum 20 mm which is the same as given in ABB. [44]

2.4.5 Steady state temperature simulations

There is several software to calculate and simulate the steady state temperature of a power cables such as integrity calculation program in MATLAB, COMSOL Multiphysics and Grøft (Trench) developed by SINTEF, etc.

The COMSOL Multiphysics software is a software where one can create physics-based models and simulate different physical scenarios. It allows for multi-physics simulations for simulations of real-world phenomena. There are several numerical methods such as finite element method (FEM), finite difference method (FDM) and the boundary element method (BEM) that are used for simulating the steady state temperatures of power cables. In research [7], the FEM simulation model for 110 kV XLPE cable was built in COMSOL Multiphysics as shown in figure above in Figure 2.18. The steady temperature distribution for two approaches was simulated as shown in figure below in Figure 2.18.

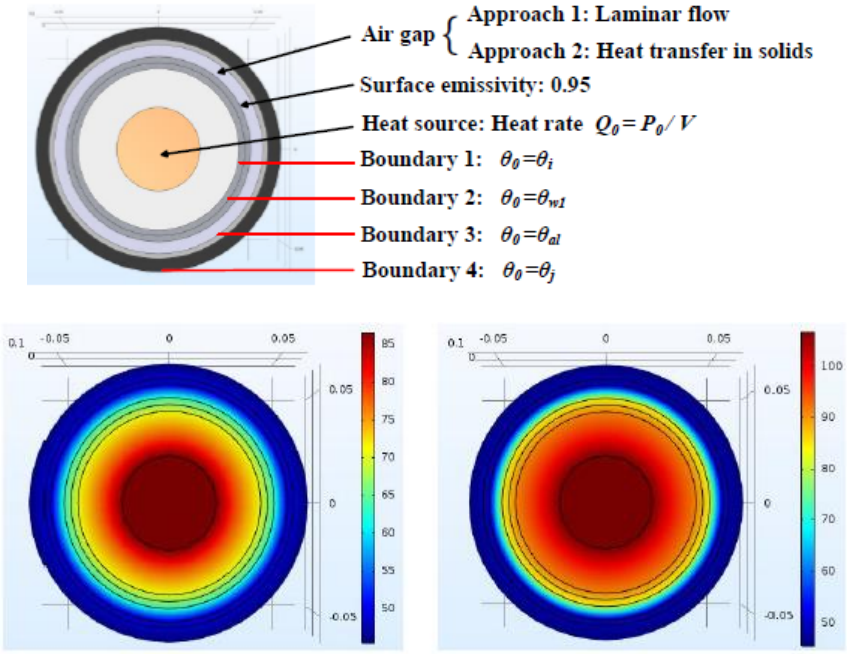

Figure 2.18: FEM simulation model in COMSOL Multiphysics (above) and simulation results of steady state temperature distribution based on flow characteristics of air gap, [7]

The research institute SINTEF have researched physical difficulties regarding the cable and any restrictions on temperature development. REN is a Norwegian company developing methods and guidelines to ensure best practice in standardizing materials, design, assembly, installation, maintenance, and operation through REN magazines in Norwegian electric grid companies. Together with SINETEF, design tool for cable trenches have been developed called Grøft (Trench) where thermal simulations are essential. In this design tool, REN Trench, one can draw advanced trench cuts, create sections with different cable configurations, visualize the trench section, make mass and quantity calculations, calculate thermal conductivity and magnetic field, etc. Further one has access to a large library of power cable type and dimensions for different voltage levels. Figure 2.19 shows an example of the use of REN Trench where the cable was designed and the temperature was simulated for the cable and the surroundings. [14]

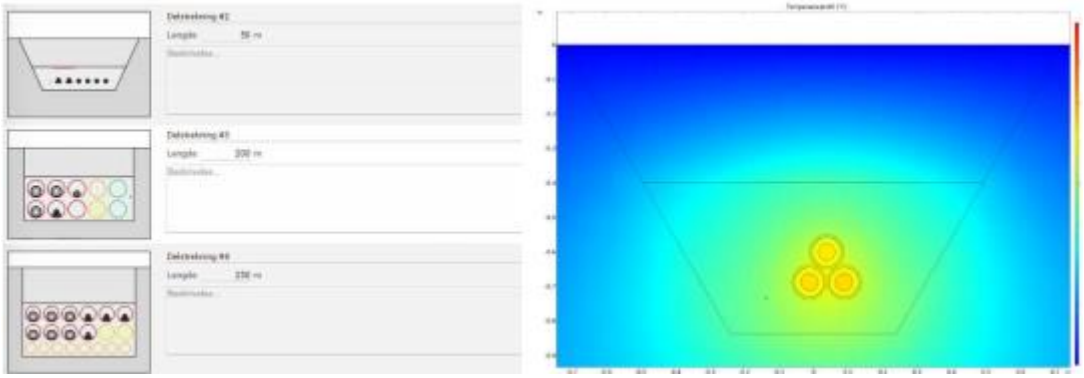

Figure 2.19: Designing cable trench and simulating the temperature profile with REN Trench. [14]

2.4.6 Definition of load factor

Load factor is defined is the ratio of average load or energy consumed in given period of the time to the peak load or maximum demand occurring in that period. The load factor can be calculated as [31]

$$\text{Load factor} = \frac{Average\ load}{Maximum\ load\ in\ given\ period} \tag{2.25}$$

The load factor is significant for describing the consumption characteristic of electricity over a given period. High load factor implies that load is utilizing the electric system more efficiently, while low load factor indicates that occasionally a high demand is set.

The period of the load factor calculation can be the number of hours in days, weeks, months, or years and a power supply normally have a cyclic 24-hour period. Then the daily load factor is calculated from the 24-hour load cycle as [31]

$$\text{Daily load factor} = \frac{\int_0^{24h} i(t)\,dt}{I_{max} \cdot 24\ h} \tag{2.26}$$

where numerator is the total energy during 24-hour period while the denominator is the peak current in that period. The conductor temperature of a power cable is usually delayed hours after the load changes due to the thermal capacity of the cable system including the power cable and surrounding environment. The delay time depends on its thermal time constant. [12], [8]

Figure 2.20 shows an example of a daily load factor where the solid line indicates the instantaneous load, while the dotted line is the load factor of this load profile [26].

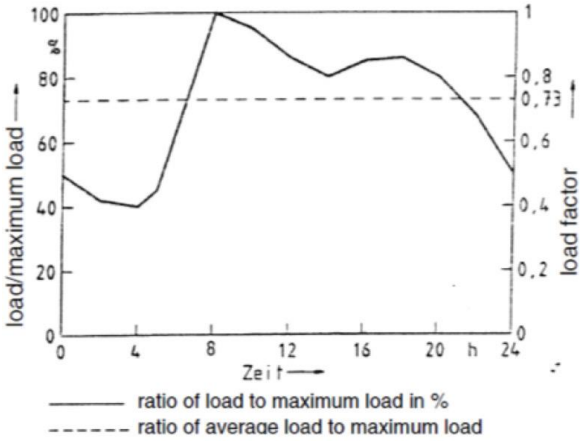

Figure 2.20: Calculation of load factor of a 24-hour load cycle. The load profile has a load factor of 0.73. [27]

Three different shapes of load curves are shown in Figure 2.21 where all has a load factor of 0.5. Curve a and b have the same shape but different peak values, and curve c and b have different shapes but same peak values. Consequently, the ratio between peak load current and the average loading capability is approximately constant. [8]

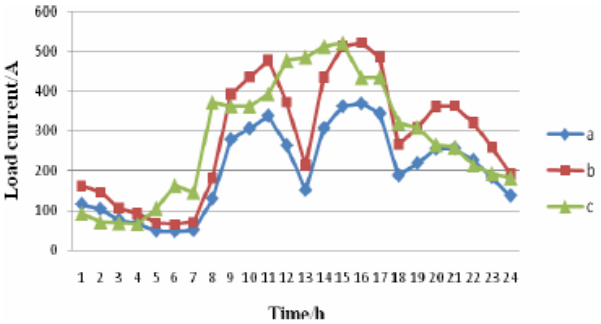

Figure 2.21: Three different shapes of load curves with a load factor of 0.5. [8]

The ratio between the tolerable peak current and the average current depends on the load factor and is not much influenced by the shape of the daily load curve. This is explained by the long thermal time constant which reduce the resulting temperature the conductor and cable insulation reaches. [30]

2.4.7 Thermal-electrical analogy

In engineering, thermal-electrical analogy is often used since there is a similarity between diffusion of heat and electrical charge (dynamic thermal dimensioning). The temperature difference between conductor and environment is related to the total heat losses and the law of heat flow. Table 2.17 and Figure 2.22 shows the units and the circuit diagram of the thermal-electrical analogy. The voltage is analogous to temperature, the current through electrical circuit is corresponds to heat flow rate and the electrical resistance corresponds to thermal resistance. [45]

Table 2.17: The units for thermal-electrical analogy. [45]

Charge q [C]	Current i [A]	Voltage V [V]	Resistance R [Ω]	Capacitance C [F]	Inductance L [H]
Heat Q [J]	Heat flow rate $\dot{Q}$ [J/s]	Temperature T [℃]	Thermal resistance R_t [K/W]	Thermal capacitance C_t [J/K]	-

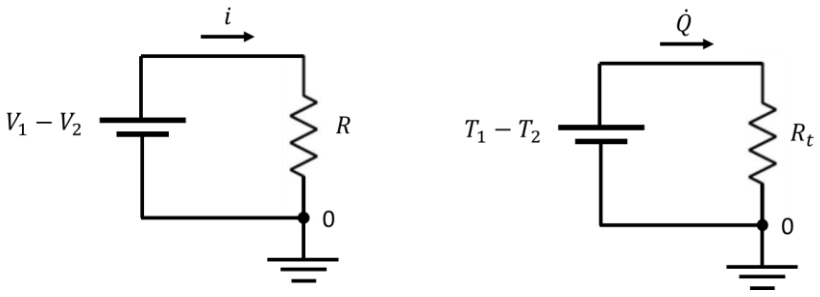

Figure 2.22: Thermal-electrical analogy with different components and properties.

The thermal-electrical analogy can further be extended into the type of circuit diagram as shown in Figure 2.23. It shows how the heat input is related to the different layers, represented by thermal resistances. The thermal resistivity must be measured for all the materials involved. [17]

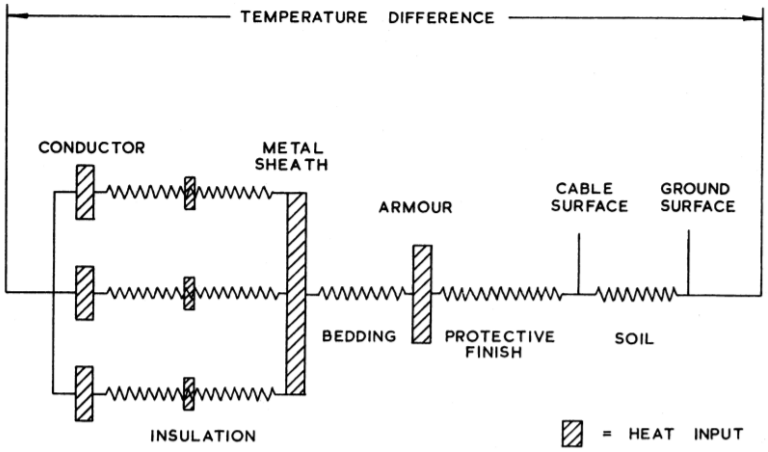

Figure 2.23: Equivalent circuit diagram for the heat flow in a three-phase cable. [17]

Papers in [7] and [9] presents an established thermal circuit model to calculate the conductor temperature. Figure 2.24 shows a simplified thermal circuit under cable transient state where Q is heat, T is temperature, R is thermal resistances and C is thermal capacitances [9].

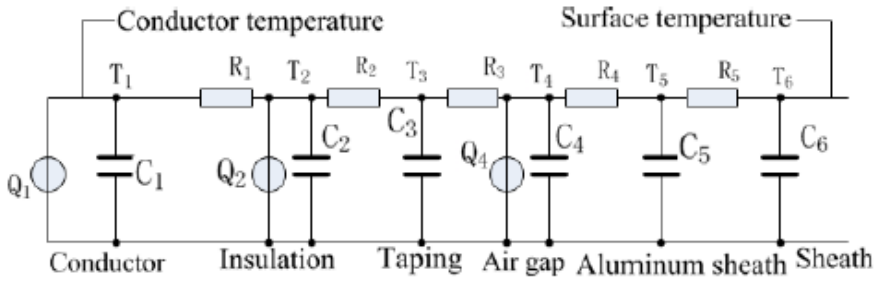

Figure 2.24: Simplified model on the cable transient thermal circuit model. [9]

Electrical circuits have a form of "time-delay" between its input and output signal. This delay is circuit's time delay called RC time constant which represents the time response of the RC circuit when a signal is applied. In other words, the time required to charge a circuit capacitor C through a circuit resistor R from an initial charge voltage to 63.2 % of its maximum possible fully charged voltage. The thermal time constant τ, explained in chapter 2.3.1, can be expressed as the RC time constant as [21]

$$\tau = R_t C_t \tag{2.27}$$

where R is thermal resistance in Ω, and C is thermal capacitance in Farads.

2.5 XLPE cable

Most common modern medium and high voltage power cables are made with XLPE insulation and are sheathed with PVC material. For the long life of the cable installation, XLPE must be resistant to thermal degradation throughout the cable manufacture process and operation at the maximum cable temperature. The most important part is the design and manufacturing of the polymer, and technique of the appropriate crosslinking and stabilizing packages. [23]

The manufacturing techniques used for XLPE needs to ensure the top level of cleanliness over all process of the production line. The process consists of three parts: base polymer manufacture, addition of stabilizing package and crosslinking package. The main two types of crosslinking process are peroxide cure and moisture cure. [23]

2.5.1 Characteristic

XLPE is produced from polyethylene under high pressure with organic peroxides as additives. Application of heat and pressure affects the cross-linking in XLPE such that the individual molecular chains to link with one another. This causes the materials to transform from a thermoplastic to an elastic material. Figure 2.25 shows linear molecular structure of polyethylene and XLPE. As shown in figure, polyethylene molecules are not chemically bounded and it can easily deform at high temperature, while XLPE molecules are bonded chemically such that it needs strong resistance to deformation even at high temperature. [46]

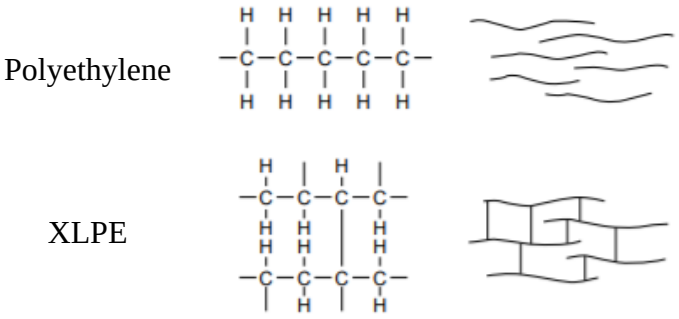

Figure 2.25: Polyethylene and XLPE structure. [46]

The most important advantage of XLPE as insulation for power cables is low dielectric loss and low mutual capacitance. Consequently, reducing the currents and earth-leakage currents can be obtained without the rigid star-point earthing. [46]

XLPE cable constitutes the best power cable for transmission and distribution lines due to the excellent electrical and physical properties. The excellent property of XLPE cable permit the resistance to thermal deformation to carry large current under different conditions. Furthermore, XLPE cables allow for easy and reliable installation since it withstands smaller radius bending and is lighter in weight. It can be also installed anywhere without special consideration of the height limitations since oil is not contained which means it is free from failures due to oil migration. XLPE cable does not require a metallic sheath so the failure peculiar to metallic-sheathed cable is negligible, such as corrosion and fatigue. [46]

2.5.2 Designations

The capital letter combinations are used to describe the construction of the various power cables and their application areas. Each country has its own designations, and there are also systems that are common to Europe such as CENELC cable identification.

Norwegian type designations for power cables normally consist of three or four main clauses. The first main clause usually consists of four capital letters that describes the structure of the cable and the materials used in the various elements of the cable. The capital letters describe insulation, sheath, armoring and outer sheath, see Table 2.18. The capital letters in the table do not apply to micro-cables and is only chosen for different XLPE power cable types. The second main clause indicate the maximum permissible operating voltage of the cable. The third main clause indicates the number of conductors and conductor cross-sections. A possible fourth main clause indicates whether the cable has a special structure of or what standard the cable is produced and tested after. [44]

Table 2.18: The structure and the materials of the cables are described in Norwegian type designations with four capital letters. [44]

code / cable	First letter	Second letter	Third letter	Forth letter
	Insulation	**Sheath and similar**	**Armoring**	**Outer sheath, corrugated protection**
TSLE	Cross-linked Polyethylene PEX	Filling jacket/band ring + concentric conductor	Aluminum laminate	PE or PP
TSLF	Cross-linked Polyethylene PEX	Filling jacket/band ring + concentric conductor	Aluminum laminate	Semiconductors PE
TSLI	Cross-linked Polyethylene PEX	Filling jacket/band ring + concentric conductor	Aluminum laminate	Other plastics e.g. TPE
TSLP	Cross-linked Polyethylene PEX	Filling jacket/band ring + concentric conductor	Aluminum laminate	PVC
TXSI	Cross-linked Polyethylene PEX	No jacket	Concentric conductor	Other plastics e.g. TPE
TXSE	Cross-linked Polyethylene PEX	No jacket	Concentric conductor	PE or PP
TXSP	Cross-linked Polyethylene PEX	No jacket	Concentric conductor	PVC

2.5.3 Structural design and components

The design of XLPE cables fulfill to international standards such as IEC 60502 and IEC 60840. The structure design of XLPE insulated power cable will always involve the following components. The stranded aluminum or copper conductor carries the current and ensure a smooth profile, free from sharp juts that could damage the insulation due to high local electric stress. Inner semi-conductor screen is to prevent electric field and flux concentration since there is an interface of ultra-smooth XLPE between the conductor and the insulation. [46]

2.5.4 Current ratings

The cross-section of a conductor is determined by the transmission capacity or the current transmitted by each phase as [47]

$$I = \frac{S}{\sqrt{3}\,V} \tag{2.28}$$

where

- I is current rating
- S is apparent power of the line in kVA
- V is rated phase-to-phase voltage

The cross-section of a conductor must be in such a way that the heating of the cable insulation generated in the cable is compatible to its resistance to heat. Heat generation in HV cables is covered in chapter 2.2. The rated temperatures of XLPE cable under different conditions are shown in Table 2.19 for XLPE insulation. [47]

Table 2.19: Temperature limits of XLPE cable. [47]

Temperature under rated operating conditions	90 ℃
Temperature under emergency operating conditions	105 ℃
Temperature in the event of a short-circuit (< 5 sec)	250 ℃

The current ratings in amps given in the following tables need to be corrected according to different parameters as the laying conditions in Table 2.20, the thermal resistivity of the ground in Table 2.21, ground temperature shown in Table 2.22, and temperature of air shown in Table 2.23. [47]

Table 2.20: Correction factors for the power cable laying conditions. [47]

Laying depth [m]	1.0	1.2	1.3	1.5	2.0	2.5	3.0	3.5	4.0	4.5	5.0
Correction factor	1.03	1.01	1.00	0.98	0.95	0.93	0.91	0.89	0.88	0.87	0.86

Table 2.21: Correction factor for thermal resistivity of the ground. [47]

Thermal resistivity of the ground	0.8	1	1.2	1.5	2.0	2.5
Correction factor	1.09	1.00	0.93	0.85	0.74	0.67

Table 2.22: Correction factor for temperature of the ground. [47]

Ground temperature [℃]	10	15	20	25	30	35	40
Correction factor	1.07	1.04	1.00	0.96	0.92	0.88	0.84

Table 2.23: Correction factor for temperature of the air. [47]

Air temperature [℃]	10	20	30	40	50	60
Correction factor	1.07	1.04	1.00	0.96	0.92	0.88

3 Color Line cable

The Color Hybrid ferry has both conventional diesel engines and battery operation. The lithium-ion battery pack has a capacity of 4.7 MWh from Siemens and can provide up to 1 hour of maneuvering and sailing. The battery is used for peak shaving at peak loads which results in a lower fuel consumption, and it reduces the noise and emissions. The battery pack is quick charged around three times a day through an onshore-based power supply, normally between 30 minutes to 1 hour at Sandefjord. The onshore power is supplied via 12 kV and 24 kV power cables, referred to as the Color Line cable, in Lede's grid. Color Line wants to optimize charging profiles in terms of the thermal development in the Color Line cable. There are in total seven wireless temperature sensors placed on the 12 kV Color Line cable to measure surface temperatures of the cable and environment temperatures. SINTEF have assessed the thermal conditions around the cable to verify that the nominal load currents will not exceed maximum allowed temperature rise.

In this chapter, the Color Line cable and sensor placements will be presented together with the SINTEF assessment for thermal development. A standard example of a loading profile will also be presented.

3.1 The 12 and 24 kV cable

The charging system in Sandefjord has a power of 6,5 MW [48]. The Color Line cable begins at the substation left in Figure 3.1 and goes through a culvert together with several other cables. After the culvert, the cables pass through a concrete wall in pipes before being placed directly in the ground. After a few meters, the cables splits into two groups (see the split in Figure 3.1) where one of the groups goes toward the charging station. Note that at this point, the 12 kV Color Line cables is in trefoil formation. Some distance after the split, the cables is spliced into a 24 kV cable, before traveling approximately 1.23 km to the charging station. In the last parts of the installation, the cable comes out of the ground and goes into the charging station. [49]

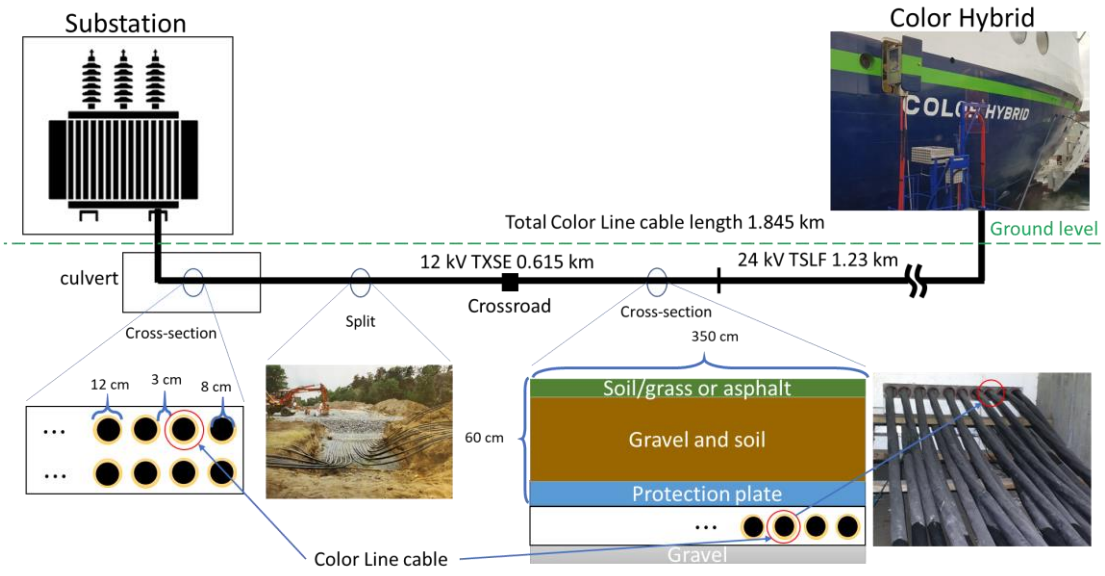

Figure 3.1: Illustration of Color Line cable configuration.

The Color Line cable consists of two different types of XLPE cables. The first part is an older TXSE 12 kV 1x3x240 Al, and the second, newer part is a TSLF 24 kV 3x1x240 Al. The TXSE cable is a three-phase cable with a common shielding while the TSLF cable is three single-conductor cables. Figure 3.2 shows the geometric cross-section of the TXSE cable where the temperature sensor is placed on the common shielding marked with red color. Dimensions and parameters of the TXSE cable is shown in Table 3.1 and Table 3.2, respectively. The material properties such as thermal conductivity and heat capacity are based on data in IEC 60278, and given in the SINTEF report [15].

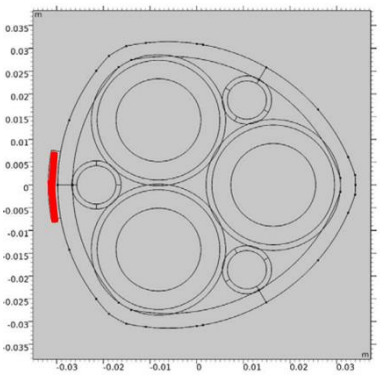

Figure 3.2: Geometric cross-section of TXSE 1x3x240 Al cable. [15]

Table 3.1: Dimension of the TXSE cable. [15]

Component		Dimension [mm]
diameter	Conductor	18.2
	Outer insulation	26.3
	Outer sheath	68
thickness	Insulation	3.4
	Outer sheath	3.2

Table 3.2: Parameter of the cable component. [15]

Component	Material	Thermal resistivity [mK/W]	Density [kg/m^3]	Specific heat capacity [J/kgK]
Conductor	Al	0.0042	2700	900
Insulation	PEX	2.6	930	1900
Semiconductor	PE	1.38	930	1900
Filling pipe	PVC	10	1760	1700
Outer pipe	PE	2.6	930	1900

As given in Table 3.2, the thermal resistivity of insulation (PEX) has the same value as the thermal resistivity of outer pipe (PE). Notice that the resistivity of the semiconductor (PE + carbon black) has much lower value than the two mentioned.

3.2 Loading profile

The Color Hybrid ferry has several short charging periods during the day, and a longer charging period during the night, as illustrated in Figure 3.3. The blue plot is loading profile on winter day (February 24th, 2020) while the red plot is on summer day (June 15th, 2020). The overnight charging is not enough to give the batteries sufficient energy for a day. Therefore, two- or three quick charges is done throughout the day. The currents are given in Appendix B (confidential) which is not published for USN but only shared with Lede and the supervisor. The maximum current value of the winter and the summer day is noted as $I_{max,winter}$ and $I_{max,summer}$, respectively. [49]

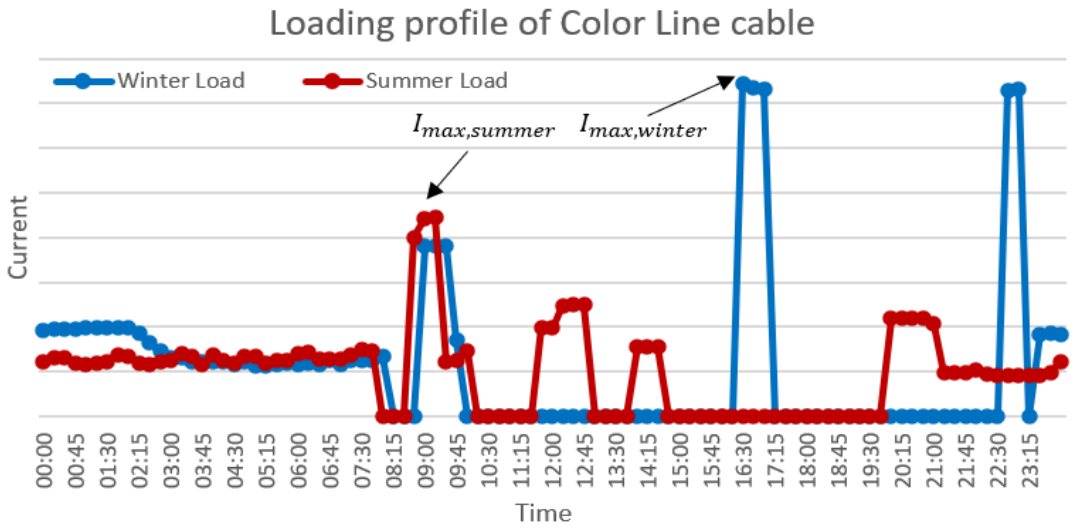

Figure 3.3: Loading profile of Color Line cable for winter and summer day. Data from [49]

The efficiency of the electrical energy usage during a 24-hour period is calculated through the load factor, as defined in chapter 2.4.6. One can use either load factor or daily load factor calculation to obtain the load factor of the winter and the summer day. The load factor of the winter and summer day is 0.12 and 0.21, respectively. The calculation of the load factors is shown in Appendix B (confidential).

3.3 Sensor

The thermal conditions in the culvert are difficult to determine quantitively. Further it is difficult to formulate a good thermal model since the Color Line cable is laid close together with other power cables. To determine the thermal conditions in the culvert, temperature sensors are installed on the surface of the Color Line cable and in the culvert.

The Wireless Temperature Sensors from Disruptive Technologies, see Figure 3.4, makes it easy to measure temperatures and transmit the data wirelessly to the Cloud Connector with 15 minutes intervals. The sensors are placed on the 12 kV TXSE cable and measures the surface temperature of the cable. Sensors on the wall is also measuring the surrounding temperature. The size of this sensor is 19x19x2.5 mm, weighing 2.0 g. The temperature range is -40 to 85 ºC and tolerates 0 to 100 % relative humidity at 25 ℃. [50]

Figure 3.4: The Wireless Temperature Sensor from Disruptive Technologies where the right picture shows an example of sensor placement. [50]

A total of seven wireless sensors are installed in three different places and description of the sensor placement is shown in Table 3.3. The sensors are divided into three groups: I, II and III. The location of these sensor groups on the Color Line cable is illustrated in Figure 3.5. The sensor numbers 1 – 4 (I) and the sensor numbers 5 – 6 (II) is placed close to each other while the sensor number 7 (III) is placed outside of the cable culvert where the coldest environment is.

Table 3.3: Grouping the temperature sensors into three groups.

Sensor number	Name of sensors	Sensor group
1	Ranvik field 20	I
2	Isolated with glass wool	I
3	Isolated with cushion and extra antenna	I
4	Cable straight out from the field	I
5	Cable culvert 20 cm from the wall	II
6	Pipe penetrations from the inside	II
7	Out of the cable culvert	III

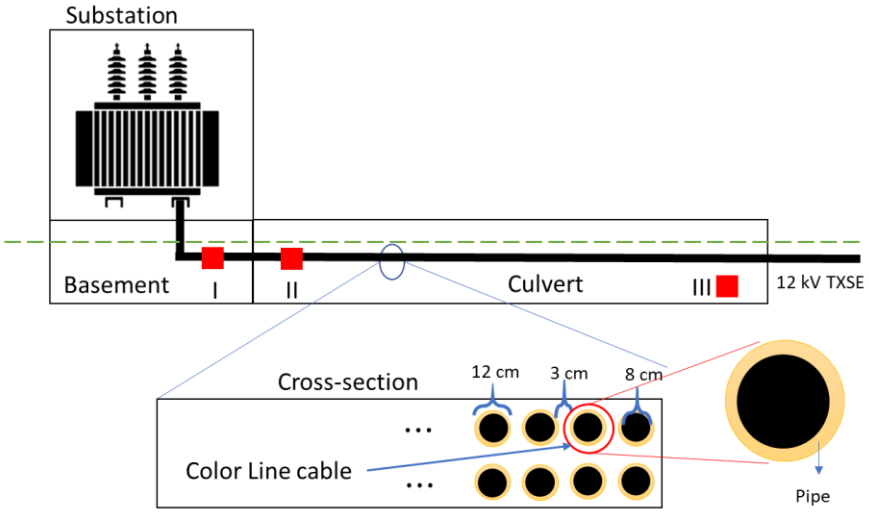

Figure 3.5: Illustration of sensors location on Color Line cable.

3.4 Temperature data

Figure 3.6 shows the temperature data of sensor number 1, Ranvik field 20, in the same days as the loading profiles shown in Figure 3.3 and one can observe that the temperature changes when the load changes. One can also observe that the average temperature of the summer day is slightly higher than the winter day. [49]

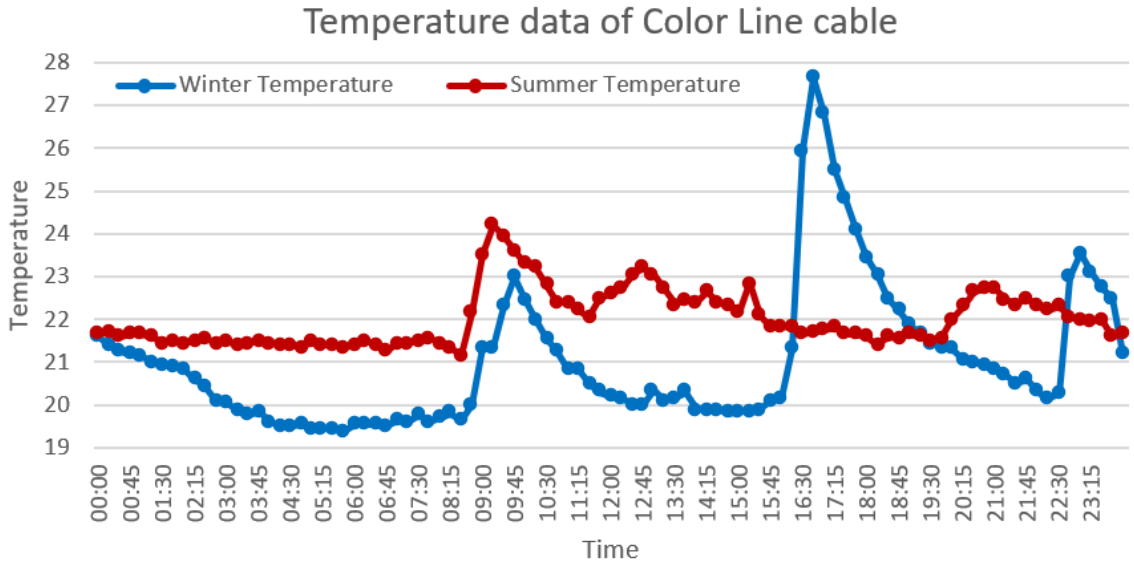

Figure 3.6: Temperature data of Color Line cable for a winter and summer day. Data from [49]

The rough time constant of the Color Line cable is calculated from the period 16:00 to 22:15 of the winter day. The total temperature rise at steady state can be calculated by subtracting the highest temperature 27.65 ºC with the initial temperature 20.15 ºC. The total temperature rise is 7.5 ºC and the temperature rise at the time constant is approximately 4.7 ºC. The temperature at time constant is then 24.9 ºC and the time constant can be read visually from the temperature

data, see Figure 3.7. The time constant is roughly estimated to be 45 minutes. Note that the temperature data is only given every 15 minutes, so there is high uncertainty, $\pm$ 15 minutes, in the estimated time constant of the Color Line cable.

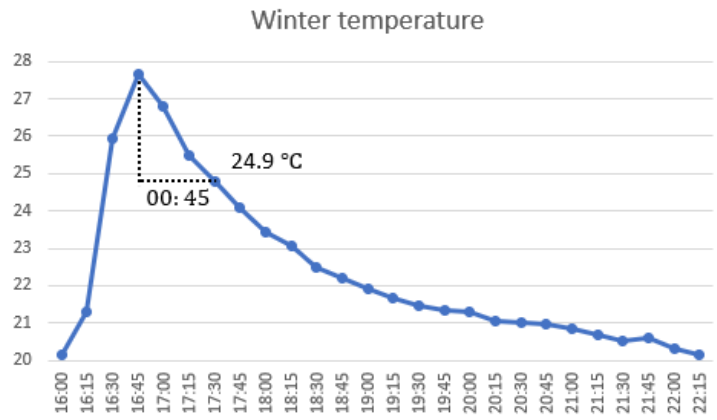

Figure 3.7: Temperature and load data of Color Line cable for the winter day. Data from [49]

Figure 3.8 shows the seven temperatures measurements of the Color Line cable on the winter day. The dynamics of the temperature measurements is similar for all the measurements. The four uppermost sensors (brown, red, orange, and yellow) are in close proximately in the temperature range. The two sensors in the middle (blue and cyan) have the same similarity, while the bottom sensor (green) is the coldest one. [49]

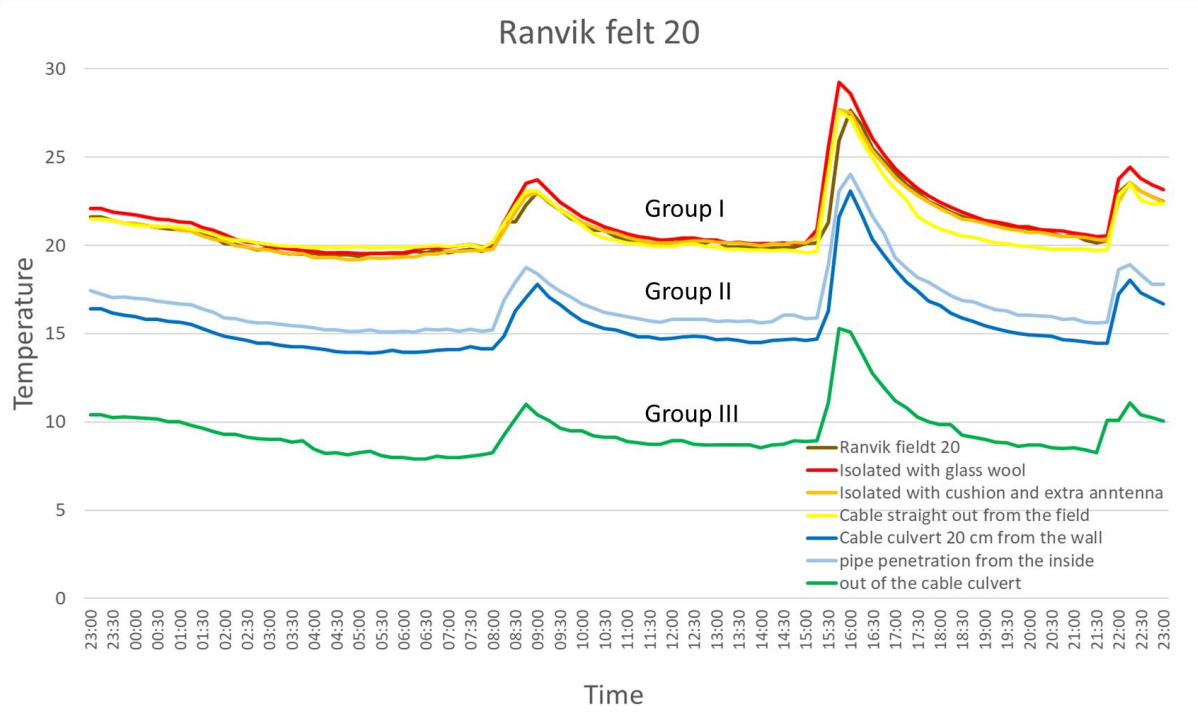

Figure 3.8: Temperature data of Color Line cable on a winter day. Data from [49]

3.5 Thermal conditions

SINTEF has assessed the thermal conditions around the 12 kV TXSE Color Line cable. The maximum stationary temperature development of two different cross-sections has been examined, namely the culvert near the substation and crossroad with 11 power cables. [15]

3.5.1 Culvert

To calculate the thermal behavior of the cable with respect to the culvert, the heat transfer coefficient of the cable must be obtained. This coefficient h is calculated with thermal conductivity of air, Rayleigh number, Prandtl number etc. The calculated average temperature on the cable surface is slightly higher than the measured temperature. The cable in the culvert appears to have sufficient load capacity to be able to supply desired current without the conductor temperature becoming too high. [15]

SINTEF has tested short-term current charging on the Color Line cable where the current is approximately $I_{max,winter}$ with one hour duration. The result shows that the calculated average temperature on the cable surface is slightly higher than the measured cable temperature. However, it seems that the heat dissipation mechanism used in calculation is well suited for estimating the temperature since there is a good agreement between the calculated and the measured cable temperature. [15]

The conductor temperature of the Color Line cable is under 45 ºC for charging profile for Color Hybrid where an ambient temperature in the culvert is 25 ºC. With an ambient temperature of 10 ºC in the culvert, the conductor temperature becomes 30 ºC. The temperature difference between the conductor and the ambient appears to be constant, regardless of the ambient temperature. It concludes that the Color Line cable has sufficient load capacity to be able to supply the desired current without exceeding the temperature limit where the insulation can be degraded. [15]

3.5.2 Crossroad

Thermal modeling of the temperature distribution close to the crossroad shown in Figure 3.1 has been done. The temperature distribution was calculated in "REN Trench" to assess the load capacity of the Color Line cable with 10 other cables. The cables were laid 60 cm under the ground and the distance between the cables was set to 11 cm. [15]

For the intersection, it is assumed conservative values for the thermal resistance in the ground and both surrounding masses under the road and the road body itself. The thermal resistance to the ground, both in the cable trench and for surrounding masses was set to 2.5 mKW^{-1} which have the same thermal resistance as dry masses. Surrounding masses usually have lower thermal resistance due to the moisture content, however the conservative values are assumed. The ground temperature was set to 15 ºC. [15]

The stationary load capacity of the Color Line cable was found to achieve the maximum conductor temperature limit of 90 ºC. The temperature distribution of the trench section is shown in Figure 3.9 where the Color Line cable is the farthest right one and marked with the red circle. [15]

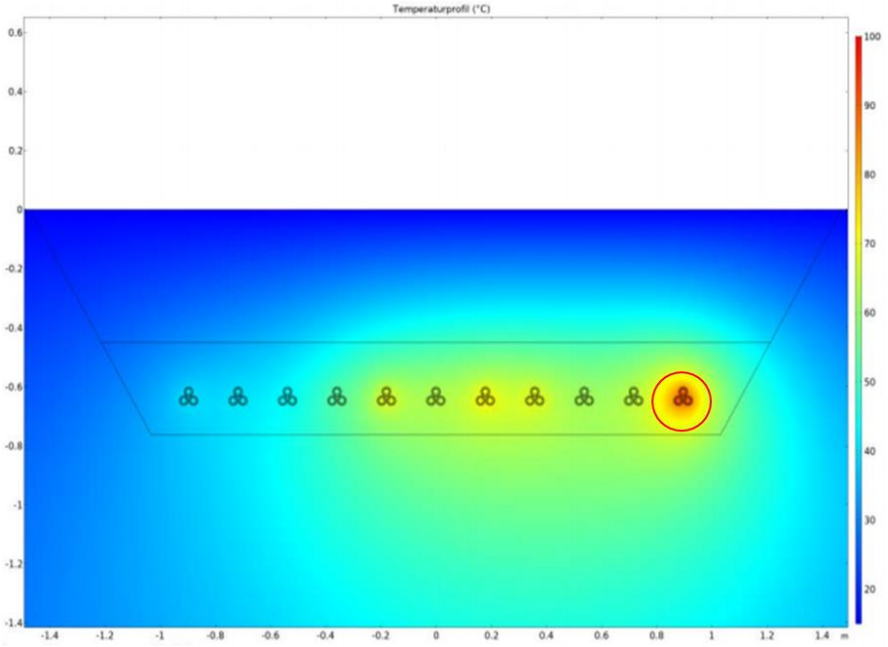

Figure 3.9: Temperature in Color Line cable with a maximum stationary load. [15]

SINTEF has approved that the Color Line cable charging current does not lead to a dangerous temperature rise. However, there is still interests to find out the allowed maximum charging current and minimum resting time between the short charges.

4 Laboratory work

The High Current Laboratory at University of South-Eastern Norway arranges for several different high-current, low voltage experiments. In the late 2020 a new section in the laboratory was constructed for thermal testing with power cables. USN has provided a cable system containing XLPE 24 kV cable from Nexans installed on a cable tray, with K-type thermocouples to investigate thermal property of the power cable. The 8.5 m long cable tray contains six parallel power cables and sixteen thermocouples. Thermocouples have been installed both on the aluminium conductor surface and on the cable outer sheath.

The installed laboratory cable is designed such that it can imitate the new section of the Color Line cable, with focus on the parts in the air. This chapter will look at the installed experiment cables and experiment setup, and long-term and short-term charging will be tested. In addition, a simple thermal model of the power cables will be made, where the thermal model must work for different charging profiles.

4.1 The installed 24 kV XLPE power cable

The structure of a single core TSLF 24 kV 240 mm^2 Al power cable from Nexans is shown in Figure 4.1. TSLF is one type of XLPE insulated cable where T indicates cross-linked polyethylene PEX, S indicates filling jacket/band ring and concentric conductor, L indicate aluminum laminate armoring, and E indicate semiconductors PE outer sheath.

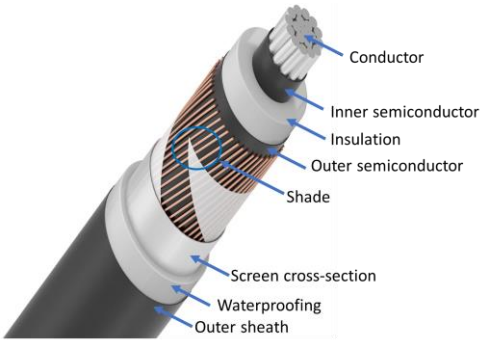

Figure 4.1: Nexans TSLF 24 kV single core power cable. [47, edited]

The aluminum conductor of the TSLF cable is multi-wire compressed aluminum conductor filled with swelling powder. Inner semiconductor and outer semiconductor are extruded cross-linked semiconductor PEX while the insulation is extruded dry-vulcanized polyethylene (PEX). Shade consists of a layer of annealed copper wires and aluminum foil. Standard screen cross-section is the sum of copper threads and aluminum foil. Screen cross-section is the physical cross-section of the copper wires in the screen. The longitudinal water proofing is a layer of swelling tape to prevent longitudinal penetration of water where the swelling tape is applied with a joint to ensure electrical contact between the screen and the aluminum laminate (diffusion barrier). The radial waterproofing is a layer of aluminum laminate glued to the outer sheath. Outer sheath consists of inner layer and exterior layer. Inner layer is the insulating part of the outer mantle and is UV resistant and white to create an optical separation between the inner and outer layers. The exterior layer is conductive black PE. [52]

Table 4.1 shows parameters of the installed 24 kV single-core XLPE cable where the exterior diameter was given in Nexans TSLF cable book [34], and the thermal resistivity are the values given in Table 2.7. The diameter of the aluminum conductor was calculated mathematically by knowing the conductor cross-section, while the rest of the diameters were measured by hand. The weight of this cable is approximately 1.64 kg/m [40].

Table 4.1: Parameters and properties of the installed 24 kV single-core XLPE cable.

Component	**Diameter [mm]**	**Thermal resistivity [Km/W]**
Aluminum conductor	17.4	0.0042
Inner semiconductor (PEX)	19	2.5
XLPE Insulation	28	3.5
Outer semiconductor (PEX)	29.5	2.5
Shade	30	-
Waterproofing	35	-
Outer sheath (PE)	38.1[51]	2.5

The installed cable has the identification codes as A 2X 2Y with respect to the DIN VDE given in Table 2.3. These identification codes means that the cable is aluminum conductor, XLPE insulated and PE outer sheath.

4.2 Laboratory experiment setup

Figure 4.2 shows the experiment setup where the blue panel on the bottom is the high current injection transformer. This setup allows for two different cable formations, namely flat and trefoil formation on the same cable tray.

Figure 4.2: An overview of the experiment setup.

The two sets of three parallel power cables are illustrated in Figure 4.3. At the left side of the setup there is the possibility for connecting a three-phase power source to one of the cable sets (flat formation). At the other end, the first set is connected in series with the second cable set (trefoil formation). At the end of the second set, all three phases are short-circuited, effectively making the three parallel cables connected as a star load.

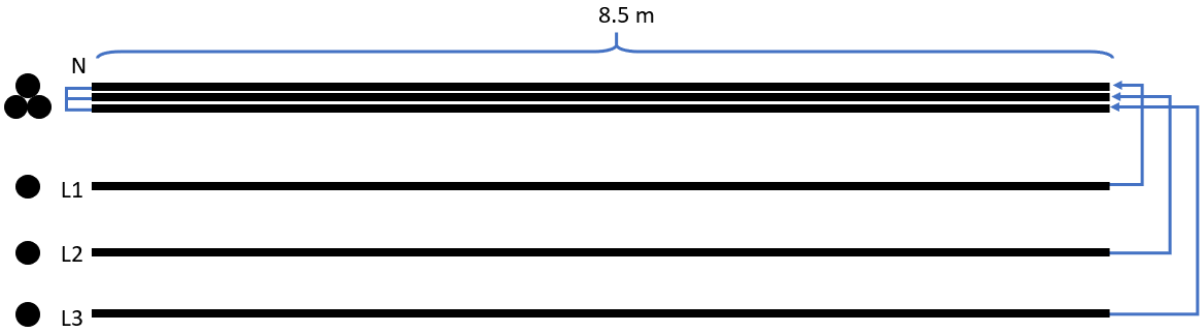

Figure 4.3: Illustration of the experimental power cable setup.

The backside of the high current injection transformer is shown in Figure 4.4 where I_1, I_2, and I_3 is connected to cable terminals L_1, L_2, and L_3 indicated on the left in Figure 4.2.

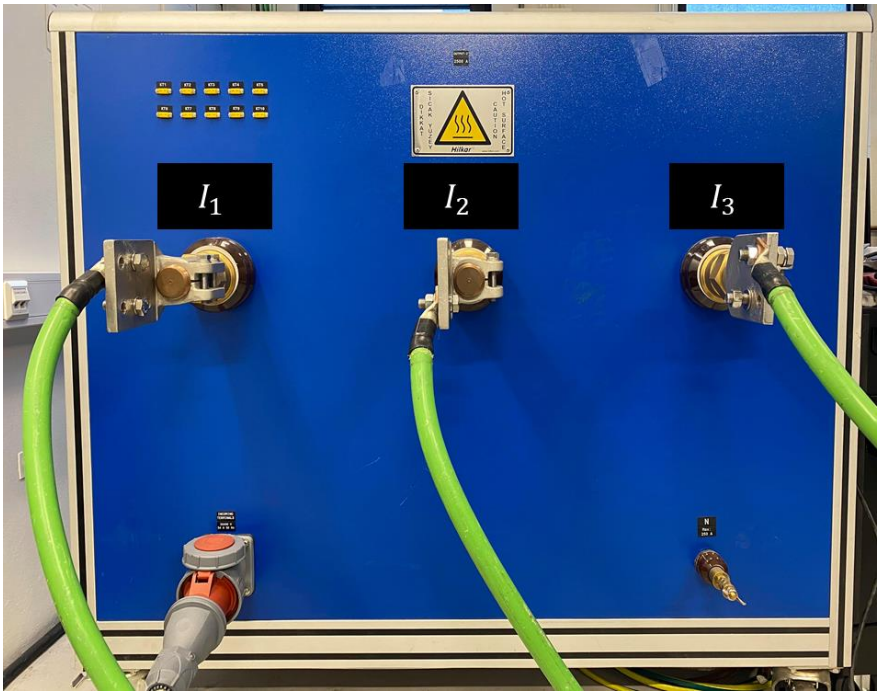

Figure 4.4: Backside of the high current injection transformer where the green cables are the three-phase output.

4.2.1 Cable setup

The most common cable formations for power cables in a three-phase circuit are flat and trefoil (triangular). The choice of cable formation depends on factors such as load, conductor area, cooling retention, available space for installation, screen bonding method etc. Both formations were installed in the laboratory setup. The flat formation was laid with 80 mm distance between each phase, and the distance between the flat and trefoil formation is 225 mm as shown in Figure 4.5. From Table 2.16 and [44], the distances between the phases must be at least 1 cable diameter. Because of available space, two cable diameters are chosen in the laboratory. The circumference of a single cable is calculated to be 120 mm and for the cable bundle of trefoil formation is measured to be 300 mm by hand.

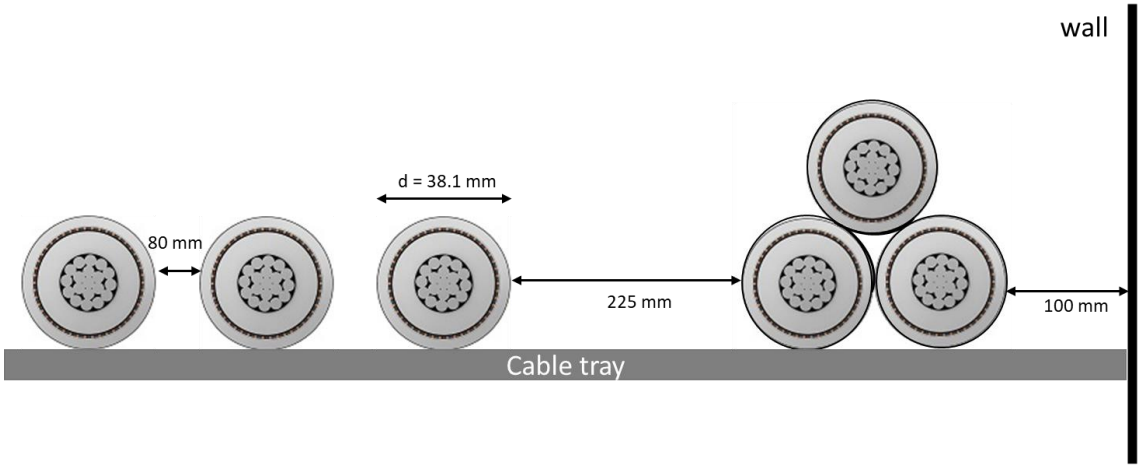

Figure 4.5: Circumferences of the cable and the trefoil bundle.

Figure 4.6 shows close-up pictures of the experimental setup at the High Current Laboratory where (a) shows overall view of the cable setup with both cable formation, (b) and (c) shows flat and trefoil formation, separately, (d) shows the cable arranged on the wall down to the current injection and the short-circuit. Finally, (e) and (f) shows the connection between flat and trefoil and three phases are physically separated with planks.

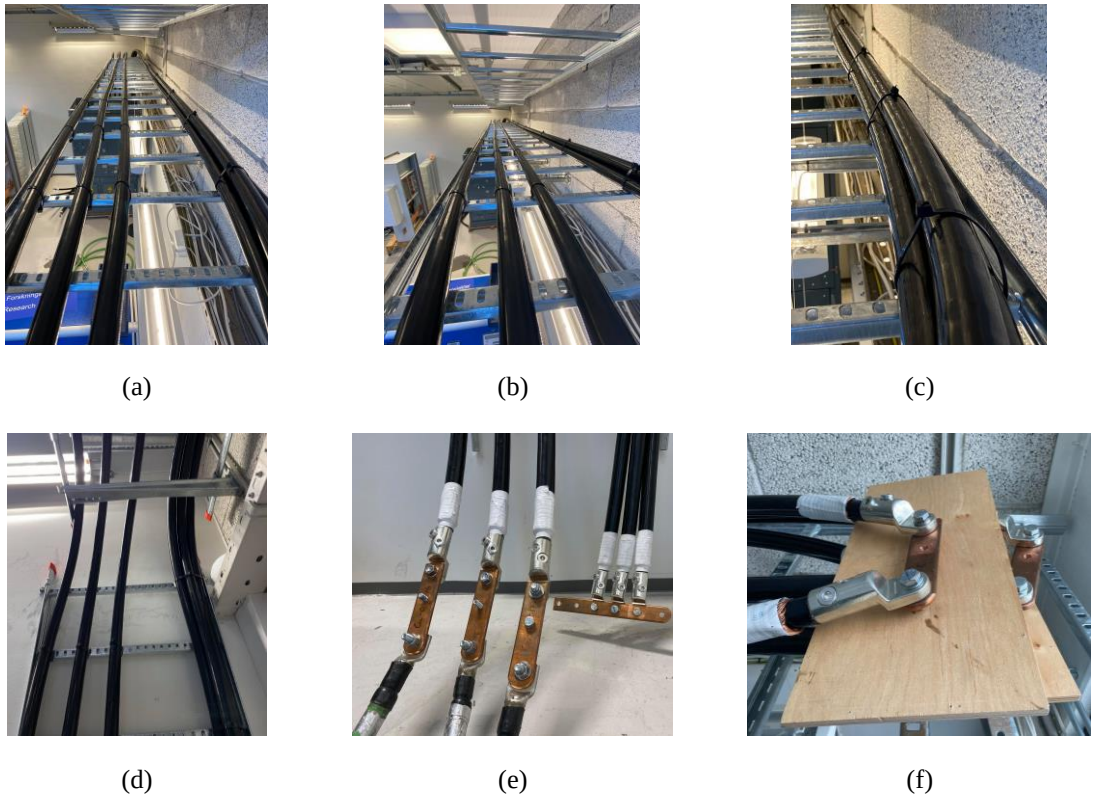

(a) (b) (c)

(d) (e) (f)

Figure 4.6: The experimental cable setup where (a) overall (b) flat formation (c) trefoil formation (d) cables arranged on the wall (e) current injection and neutral point (f) connection between flat and trefoil.

The cold resistance is found by injecting a 100 A DC current between L2 and L3, and measuring the voltage drop in L2-N, L3-N and L2-L3. From there the resistance values is calculated using Ohms law. This resistance is later used to estimate the hot resistance during testing. The calculated values for both L2-N and L3-N are 2.275 m**Ω** when the room temperature is 22.4 ºC. For L2-L3, the cold resistance is measured to 4.55 m**Ω** which is the sum of the phase resistances. Note that the measured cold resistance for L2-N and L3-N contains both the cable resistances of flat and trefoil formation. However, the cold resistance for each formation is assumed to be equally distributed in each phase. In other words, one cable length of 8.5 m has a cold resistance of 1.1375 m**Ω** and cold resistance per unit length of the experimental cable is the assumed to be 0.134 m**Ω**/m. The warm resistance at 90 ºC, which is the temperature limit for the XLPE cable, can be calculated by using Equation (2.3). The cold resistance is only including the ohmic and contact resistance, and do not include skin effect, proximity effect, induced losses, or dielectric losses.

$$R_{90} = 1.1375\ m\Omega\ [1 + 3.9 \cdot 10^{-3}(90℃ - 22.4℃)] = 1.4375\ m\Omega$$

4.2.2 Sensor setup

There are 8 thermocouple sensors in each formation allowing for temperature measurement both on the aluminum conductor surface and on the cable outer sheath. The thermocouples used for temperature measurements are RS PRO type K, with a temperature range between -10 to 105 ℃. The conductor material of the positive side is nickel chromium (green), and the negative side is nickel aluminum (white), see Figure 4.7. [52]

Figure 4.7: RS PRO thermocouple type K. [52]

Of the sixteen temperature measurements, eight is installed close to the aluminum conductor, inside the cable insulation, while the other eight thermocouples are placed on the cable surface. Figure 4.8 shows the method of thermocouple installations on the cable. The upper pictures show the thermocouple installation close to the aluminum conductor while the pictures below show the thermocouple installation on the surface of the cable. The thermocouples on the conductor are installed by drilling a hole through the cable insulation all the way to the conductor surfaces, approximately 15 mm depth.

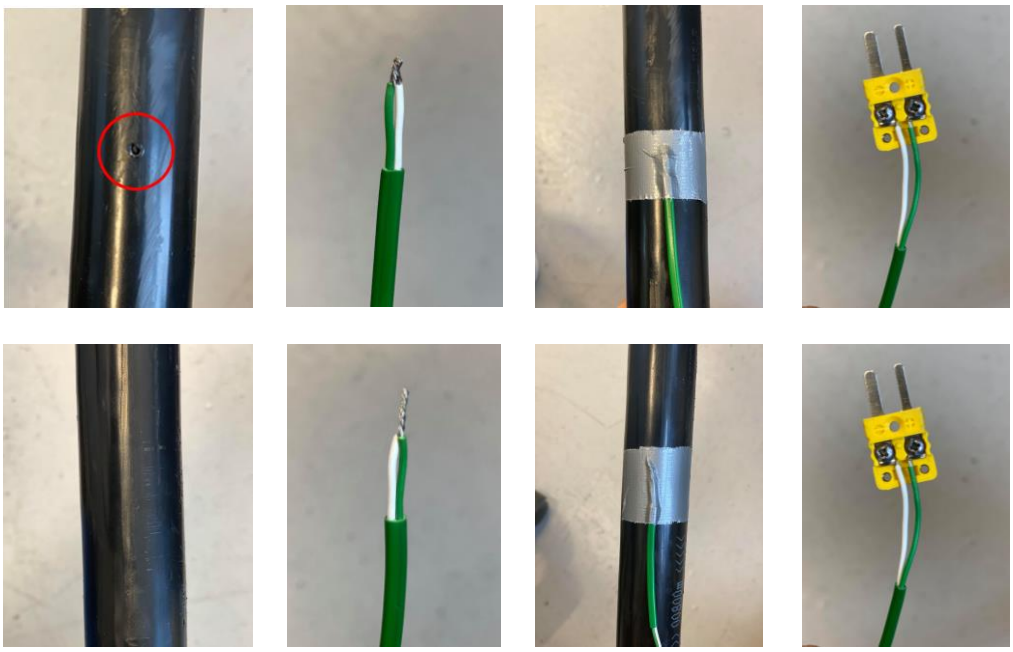

(a) (b) (c) (d)

Figure 4.8: Method of thermocouples installation where (a) cable surface (b) twisted sensor conductor (c) sensors held on with tape (d) thermocouple plug.

The thermocouples are divided into three thermocouple groups A, B, and C and installed as shown in Figure 4.9 where upper pictures show more details of thermocouples placement. All thermocouples are collected and comes down from the cable tray on the right side of the setup.

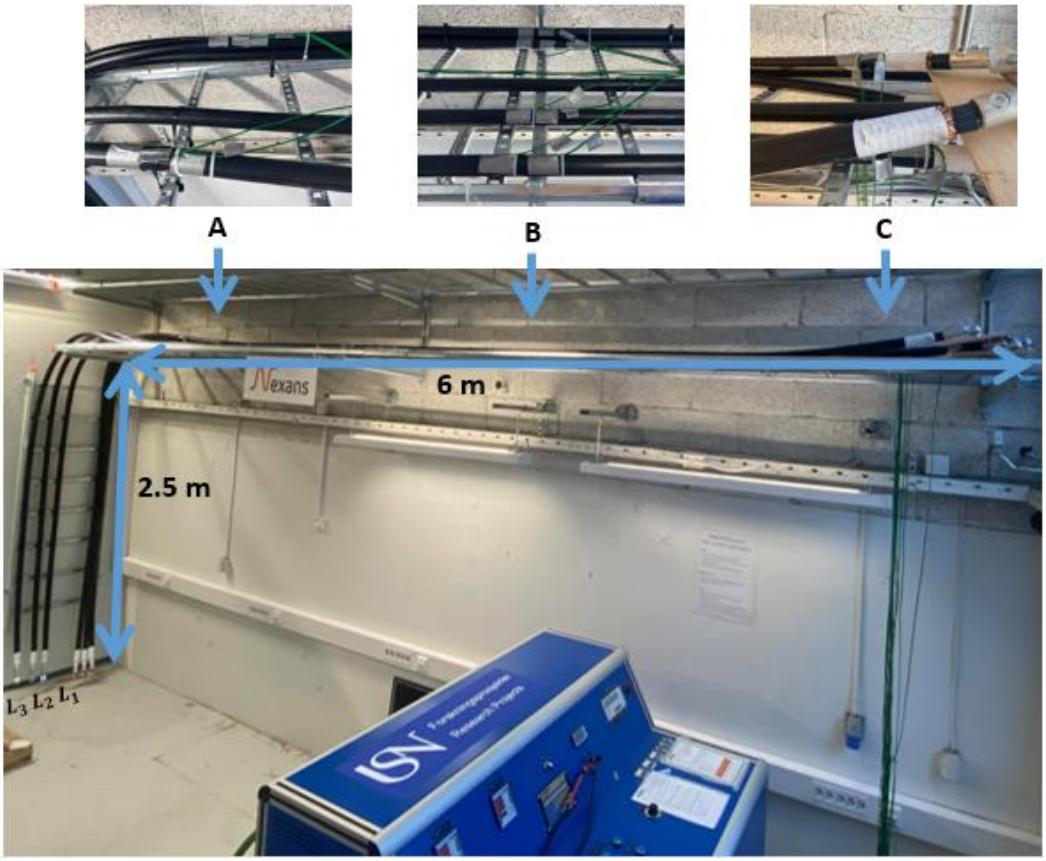

Figure 4.9: The overview of three sensor group placement.

The sixteen thermocouples are indicated as red squares in Figure 4.10 where odd thermocouple numbers are installed on the conductor surface while the even thermocouple numbers are installed on the surface of the cable.

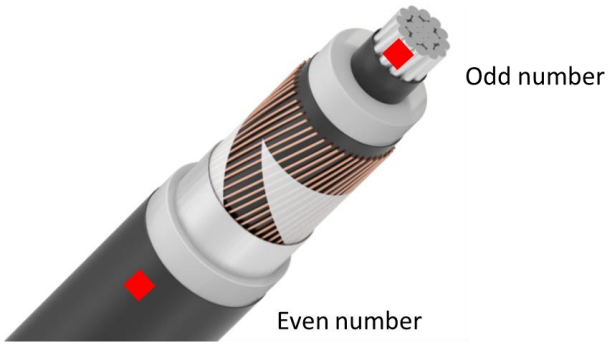

Figure 4.10: Thermocouple placement and numbering. [47, edited]

Figure 4.11 shows an overview of the installed thermocouples on both trefoil and flat formation, where a red solid square includes both conductor and surface measurement. The three thermocouple groups include the following sensor numbers: group A (1, 2, 15, 16), group B (3, 4, 5, 6, 11, 12, 13, 15), and group C (7, 8, 9, 10). Note that thermocouple nr. 9 and nr. 10 are installed in a part where the trefoil formation is separated in order to make the necessary connections. Because of this, the measurements from these sensors are neglected in the analysis for trefoil formation.

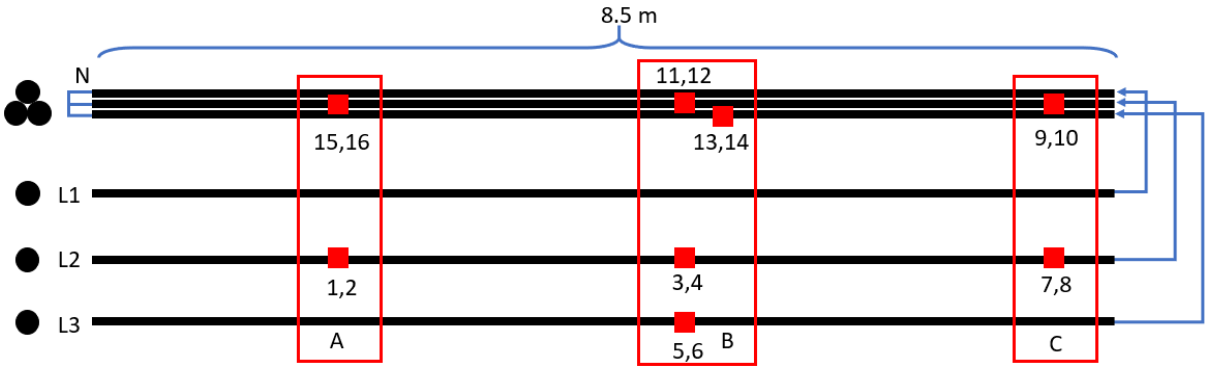

Figure 4.11: Overview of the thermocouple groups, and their respective placements.

The thermocouples are connected to a data logger through two connection boxes shown in Figure 4.12. The room temperature sensor is placed around 2 meters from the installed cables and is screwed between a bolt and a nut to increase the thermal time constant of the measurement. This will act as a first order filter for the room temperature measurement that gives greater thermal inertia and is therefore not affected by fast local air/temperature variations. The data logger is connected to the software Agilent BenchLink Data Logger 3 to collect the temperature data from the power cables during testing.

(a) (b) (c)

Figure 4.12: The set of temperature measurements where (a) connection boxes (b) ambient temperature sensor (c) data logger

4.3 Laboratory long-term testing and thermal response

Before running the first tests on the experiment setup, appropriate testing currents must be decided. Table 4.2 includes a comparison of the maximum current from different references, in addition to indicating the maximum currents that have been tested by Lede, shown in Figure 3.3, and given in Appendix B (confidential) [45]. Permitted load of the power cable at 15 ºC room temperature is 465 A for flat formation and 445 A for triangle formation [51]. General permitted load for 24 kV cable for open cover/screen and air/ground arrangement type is shown in the center of Table 4.2 [44].

Table 4.2: Comparison of the maximum current from Nexans and maximum current operated by Lede given in Appendix B (confidential).

TSLF cable (Nexans) 240 mm2 24kV [51]		**open cover/screen (Nexans) air/ground 12 and 24kV[44]**		**Data from Lede (Confidential) Color Line cable [49]**	
Flat	Trefoil	Flat	Trefoil	Winter day	Summer day
465	445	570/510	505/465	$I_{max,winter}$	$I_{max,summer}$

The correction factor f_1 is 1.08 for the power cable in air with a room temperature of 20 ºC following Table 2.15, while the correction factor f_2 is 1 according to the number of grouping cables following Table 2.16. Since the correction factors are quite small, they are neglected when assessing the maximum current rate for the tests.

Load data from Lede has a lower current value than the others in Table 4.2, and therefore the highest current value of the winter day ($I_{max,winter}$) was chosen to determine the thermal property of the cable. In addition, 465 A and 520 A was also selected for thermal testing. The collection of this data will then make the foundations for calculating the thermal model parameters.

4.3.1 Testing with $I_{max,winter}$ to steady state

The current indicated as $I_{max,winter}$ was tested on the laboratory setup. The current from the injection transformer was adjusted manually to be constant from the beginning of the experiment until the temperature reached approximately steady state. Steady state was defined when the temperature difference at any point was less than 1 ºC in one hour.

The temperature stabilized after 3 hour and 45 minutes. Figure 4.13 shows all measured temperatures of the cables with a current of $I_{max,winter}$, including the room temperature. The solid lines indicate conductor surface temperatures or inner temperatures (odd thermocouple numbers), and dashed lines indicate outer sheath or outer temperature measurements (even thermocouple numbers). The maximum measured temperature is 51.4 ºC with a room temperature of 22 ºC.

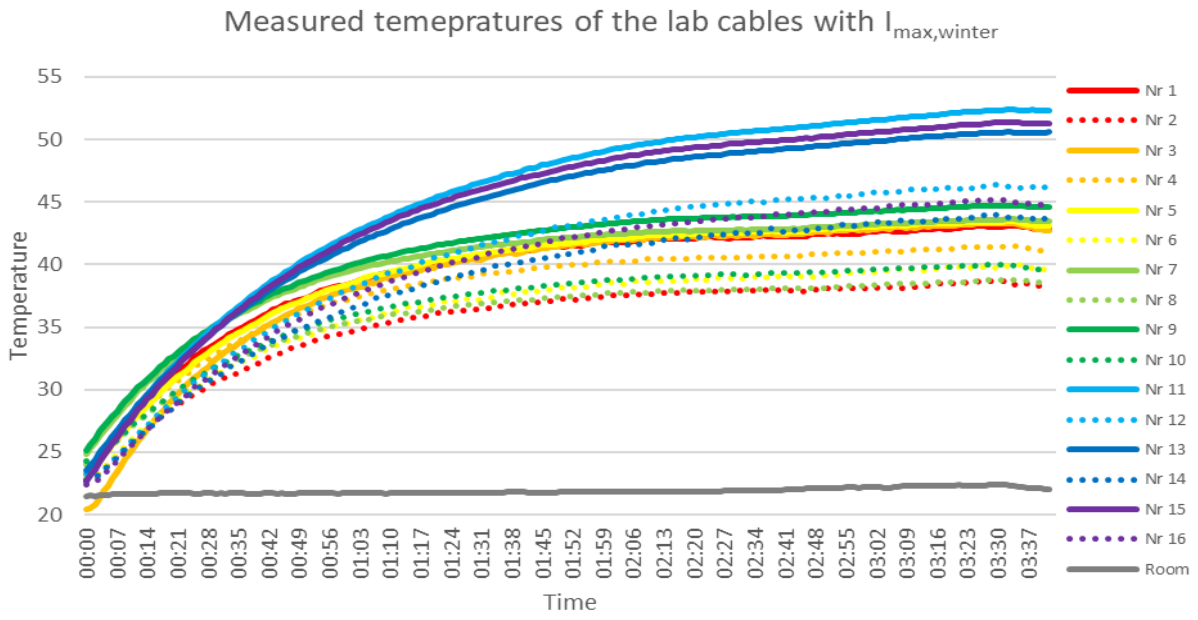

Figure 4.13: Measured temperatures of the cables with $I_{max,winter}$ where solid lines are conductor surface temperatures and dashed lines are outer sheath temperatures.

It is clear to see that the highest final temperature is thermocouple nr. 11 which is the inner conductor on the upper most cable in the trefoil formation, located in the middle of the setup. One can also see that the temperature of the trefoil formation (thermocouple nr. 9-16) has higher values than the temperatures of the flat formation (thermocouple nr. 1-8). This is due to a smaller total surface area of the outer sheath for trefoil compared to flat formation. In addition, a stronger proximity effect of the trefoil formation leads to a higher apparent resistance, which results in larger ohmic losses.

Table 4.3 shows the temperature differences between steady state temperature of each sensor and the room temperature of 22 ºC. One can observe that the temperature difference is higher for the trefoil formation than flat for formation. Sensor group A and B, indicated in bold, are used further to obtain parameters for a simplified thermal model.

Table 4.3: The temperature differences between steady state temperature of each sensor and room temperature.

Cable formation		**Conductor temperature**				**Surface temperature**			
Flat	Sensor nr.	1	**3**	**5**	7	2	**4**	**6**	8
	ΔT	22.8	**22.7**	**23.1**	23.4	18.1	**21.1**	**19.6**	18.5
Trefoil	Sensor nr.	9	**11**	**13**	15	10	**12**	**14**	16
	ΔT	24.6	**32.4**	**30.6**	31.3	19.6	**26.3**	**23.9**	24.8

To better illustrate the temperature responses, the measured temperatures of flat and trefoil formation is plotted separately and shown in Figure 4.14 and Figure 4.15.

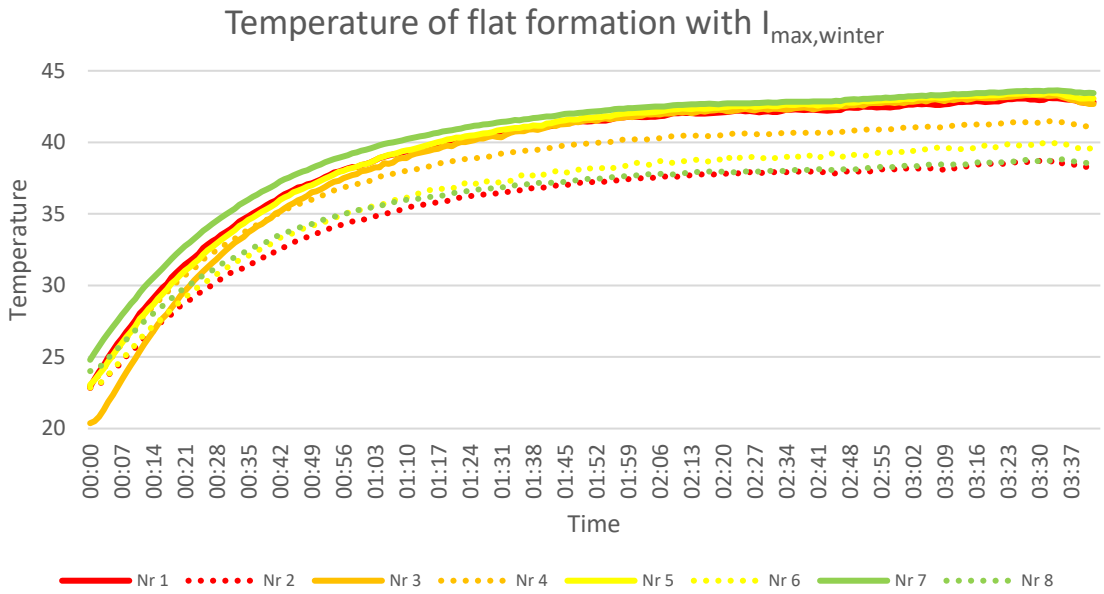

Figure 4.14: Measured temperature of the flat formation with $I_{max,winter}$.

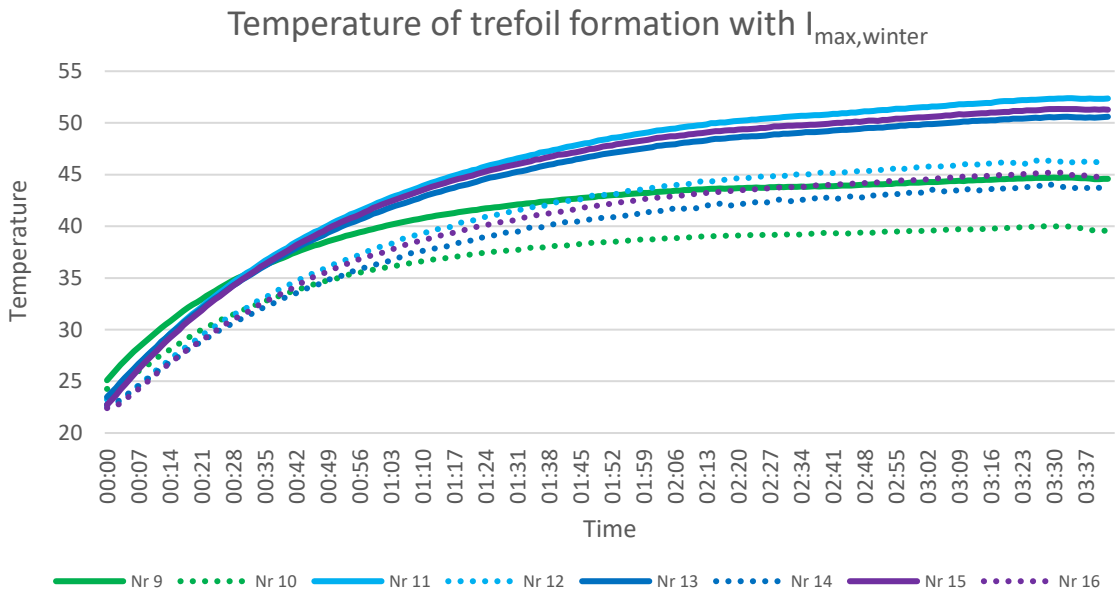

Figure 4.15: Measured temperature of the trefoil formation with $I_{max,winter}$.

For flat formation, there is a clear divide between the surface measurements and the conductor measurements. This divide can also be found in the trefoil formation measurements, with one outlier. Measurement nr. 9 reads of a much lower value than the other conductor temperatures. The main reason for this is that this sensor is placed in Group C, shown in Figure 4.9, where the trefoil formation is not contained. The space that is made between the cables leads to better cooling conditions, and this can explain the low value that is measured.

4.3.2 Testing with 465 A to steady state

The thermal response in the cables for a 465 A constant current is shown in Figure 4.16. The maximal temperature measured in this case was 71.2 ºC, which were reached after 5 hours. One can observe that the room temperature is increasing over the test duration, with an end value of 24 ºC.

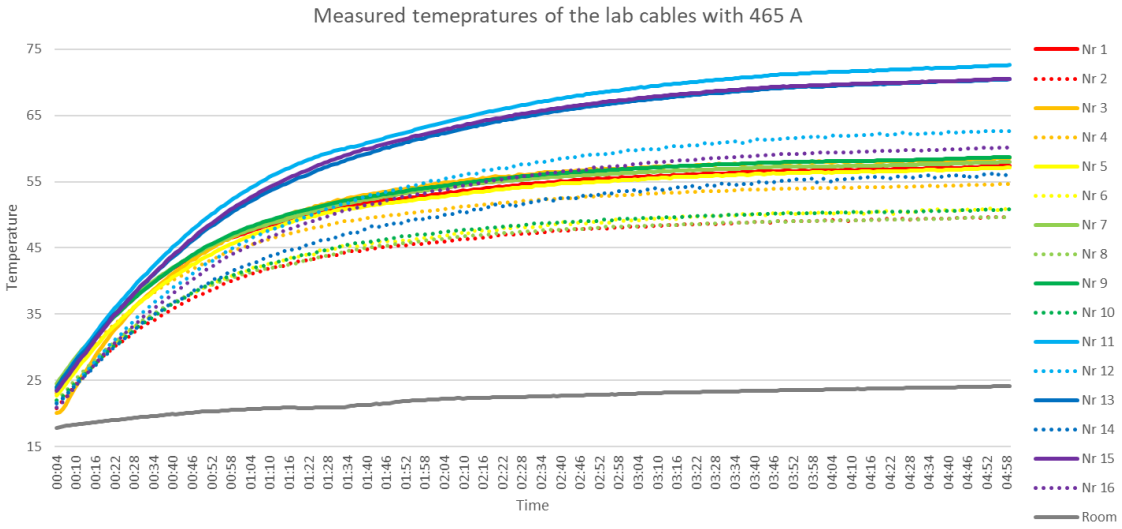

Figure 4.16: Measured temperatures of the cables with 465 A.

4.3.3 Testing with 520 A to steady state

The thermal response in the cables for a 520 A constant current is shown in Figure 4.17. The maximal temperature measured in this case was 83.4 ºC, which were reached after 4.5 hours. The room temperature is increasing over the test duration, with an end value of 25.1 ºC.

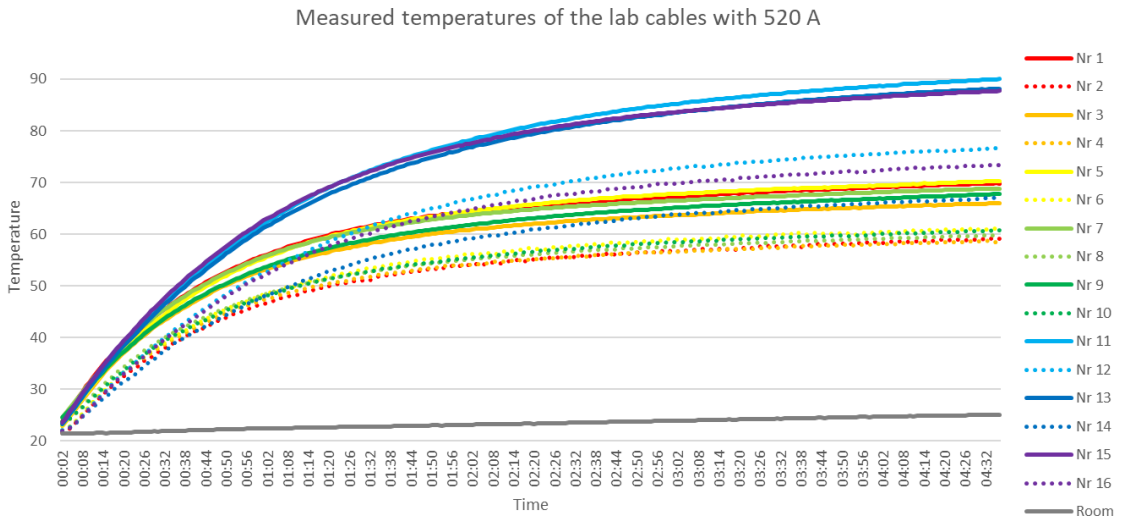

Figure 4.17: Measured temperatures of the cables with 520 A.

4.4 Thermal responses for short-term charging

Data from short-term charging in the Color line cable is taken from time period 16:15 to 20:00 on February 24th, 2020 from Figure 3.6. The same load current is applied to the laboratory setup for the same duration, where the data from trefoil formation is used. Figure 4.18 shows the short-term charging temperature responses the measured values. Since the temperature sensor of the Color Line cable is placed on the outer sheath of the cable, it is expected that this measurement is somewhat lower than what is found in the laboratory. One can see from the figure below that he Color Line cable temperature is just 2 and 3 ºC lower than laboratory cable surface measurements.

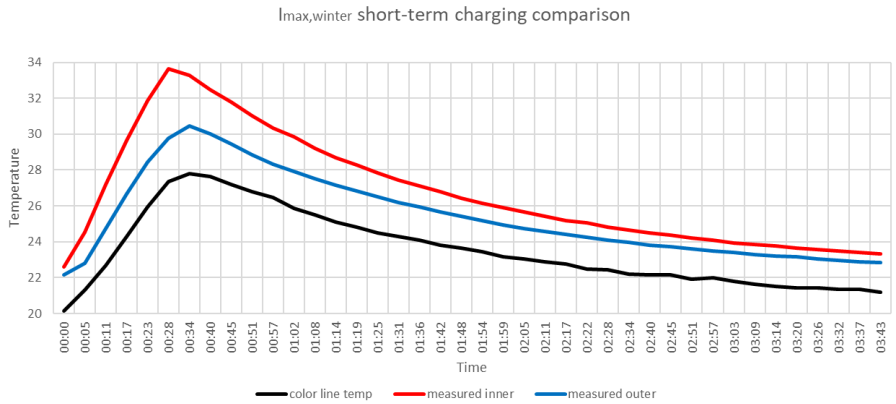

Figure 4.18: Temperature of Color Line cable, measured and simulated for inner and outer.

To compensate for the different air temperatures surrounding the cables, the figure above is plotted with temperature difference between the cable and the environment on the y-axis, and this is shown in Figure 4.19. The environment temperature of the Color Line cable in culvert is assumed to be 15 ºC, based on the cable temperature measurements in the culvert (Group II), given in Figure 3.8. The temperature difference of the Color Line cable has the largest value. However, there are uncertainties in the Color Line temperature measurements because of the sensor placement on the outside of the ground cable and because of an unknown environment temperature.

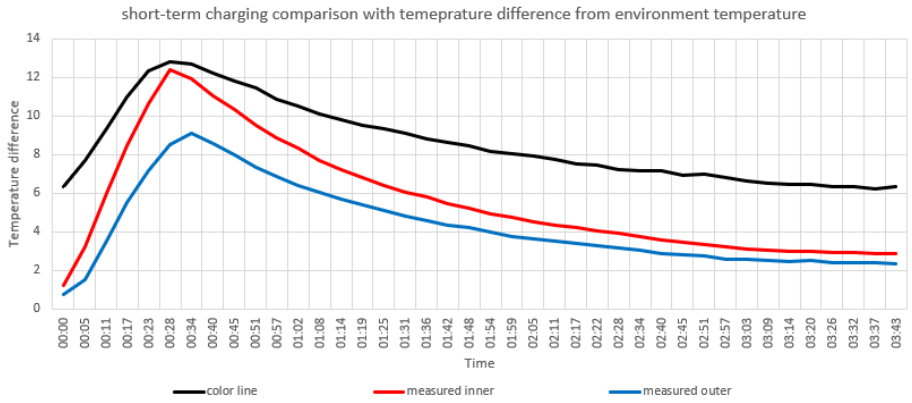

Figure 4.19: Temperature difference from the environment temperature of Color Line cable, and measured temperature for inner and outer in laboratory.

4.4.1 Testing with 700 A for 30 minutes

The thermal response in the cables for a 700 A current in 30 minutes is shown in Figure 4.20. The maximal temperature measured in this case was 64.3 ºC in sensor nr. 15. The room temperature is measured to be 20.9 ºC.

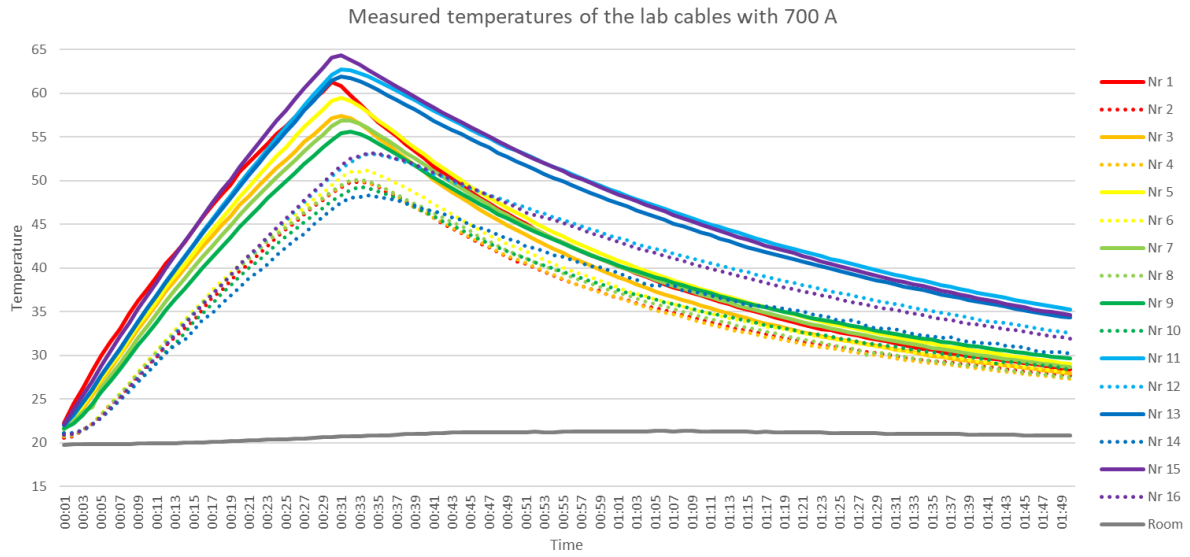

Figure 4.20: Measured temperatures of the cables with 700 A.

4.4.2 Testing with 850 A for 30 minutes

The thermal response in the cables for an 850 A current in 30 minutes is shown in Figure 4.21. The maximal temperature measured in this case was 86.7 ºC in sensor nr. 15. The room temperature is measured to be quite constant at 23.4 ºC.

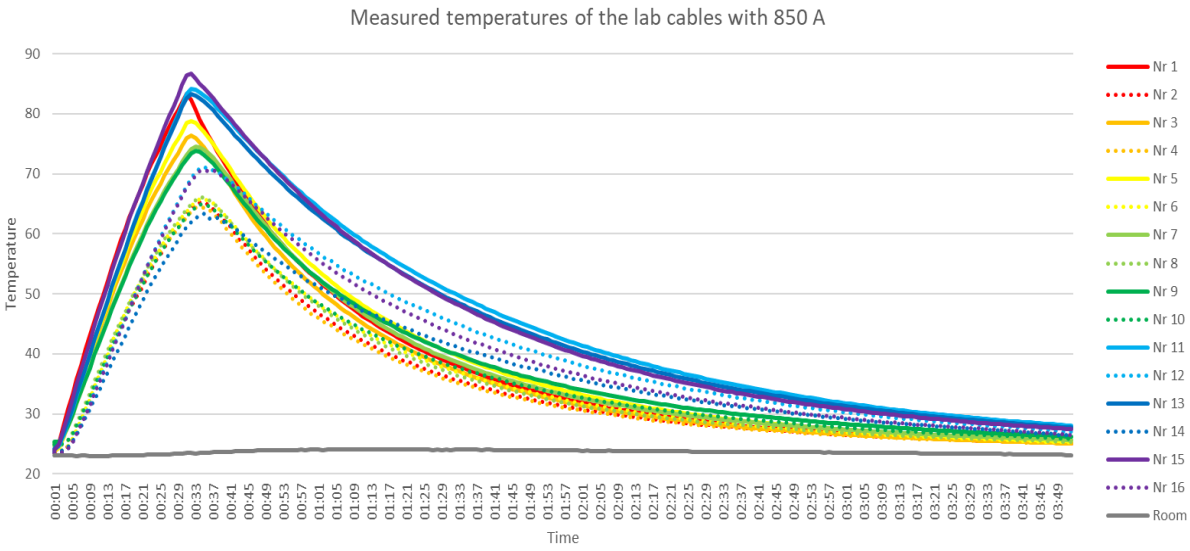

Figure 4.21: Measured temperatures of the cables with 850 A.

4.5 Thermal property of the experimental cable

Thermal properties such as thermal time constant, heat capacity and heat transfer coefficients can be calculated using the data obtained from the steady state experiment done in chapter 4.3.

4.5.1 Thermal Time constant from $I_{max,winter}$

Thermocouples nr. 3 (flat) and nr. 11 (trefoil) in the middle of the setup is chosen to calculate the thermal time constant of the cable formations. First the total temperature rise at steady state is calculated by subtracting the steady state temperature with the initial temperature. Then 63.2 % of the temperature rise is calculated and added to the initial temperature to get the temperature at the time constant. Lastly, the time constant can be visually found using the temperature measurements of those thermocouples, and this is illustrated in Figure 4.22 and Figure 4.23. Table 4.4 shows the time constant calculation procedures.

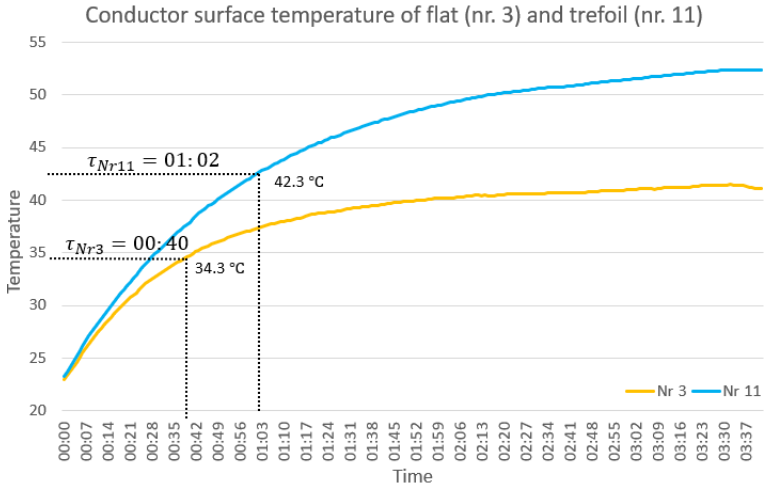

Figure 4.22: Time constant of the conductor surface measurements for flat (nr. 3) and trefoil (nr. 11).

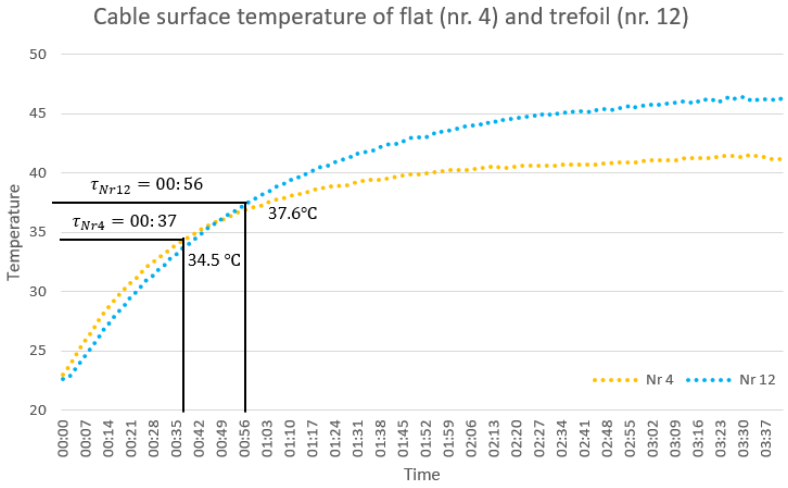

Figure 4.23: Time constant cable surface measurements for flat (nr.4) and trefoil (nr. 12).

Table 4.4: Time constant calculation of flat (nr.3) and trefoil (nr.11).

Conductor surface temperature	**Flat (nr. 3)**	**Trefoil (nr. 11)**
Temperature rise at steady state	$41.1 - 22.7 = 18.4\,℃$	$52 - 23 = 29\,℃$
Temperature rise at time constant	$18.4\,℃ \cdot 63.2\,\% = 11.6\,℃$	$29\,℃ \cdot 63.2\,\% = 19.3℃$
Temperature at time constant	$11.6\,℃ + 22.7\,℃ = 34.3℃$	$19.3\,℃ + 23\,℃ = 42.3\,℃$
Time constant	40 minutes	1 hour 2 minutes

In order to compare the Color Line cable with the laboratory cable, the time constant of thermocouple nr. 12 is compared since the Color Line cable has trefoil formation. With the same time constant calculation method as shown above, time constant of thermocouple nr. 4 and nr. 12 are calculated to be 37 minutes and 56 minutes, respectively. As shown in chapter 3.4, the Color Line cable had a time constant of 45 minutes, which is comparable with the laboratory results. The time constant calculation from the Color Line cable has some uncertainty because of the low data resolution of 15 minutes per measurement. In addition, the environment temperature is different between the laboratory and the Color Line measurements, and the difference in conditions may affect the calculations.

One can see that the flat formation has a lower time constant than the trefoil formation. This is because the larger surface area of flat formation gives a better heat transfer to the air and a larger surface emissivity. This is why the flat formation permit higher currents than trefoil, which is also indicated in Table 4.2. In other words, one can say that the thermal resistance from the cable to the surrounding air for flat formation is lower than for trefoil formation. Equation (2.27) describes that with equal thermal capacities, the lower thermal resistance must have a lower thermal time constant.

4.5.2 Heat transfer coefficient and thermal conductivity

To estimate the heat transfer coefficient of the two different cable formation, the thermal systems is assumed as a lumped parameter system for simplicity. This effectively means that the temperatures of the defined subsystems have uniformly distributed temperature. As shown in Figure 4.24, there are two subsystems considered, namely the inner (conductor) and outer (insulation) part of the cable. These subsystems are chosen because they can be referred to as the two different measurements taken at the cable. The outer subsystem will include all the different layers from the inner semiconductor to the outer sheath as a simplification, see Figure 4.1 for the different layers.

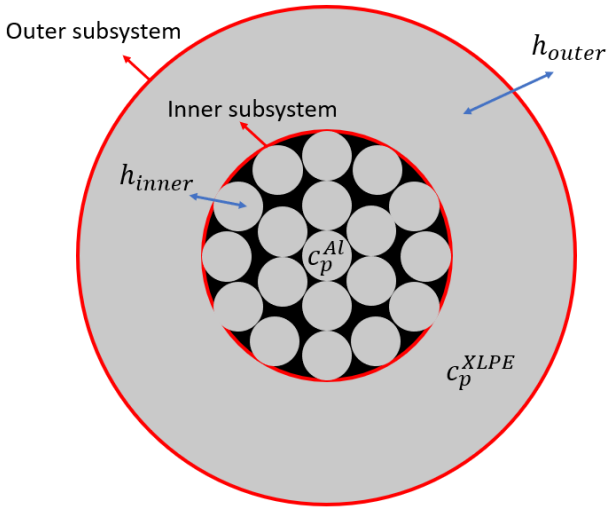

Figure 4.24: Illustration of the lumped parameter system of the cable.

For the inner part of the cable, the heat transfer mechanism (h_{inner}) is dominated by conduction between the conductor and the insulation. Heat transfer from the cable surface to the surrounding air (h_{outer}) is mainly affected by convection and radiation.

There are four different temperature measurements that are important in calculating the thermal heat transfer coefficients, namely the inner and outer temperatures of the flat and trefoil formation. To obtain representative values for these temperatures, averages from the appropriate thermocouples was used, which were introduced in chapter 4.2.2.

It is assumed that the heat transfer coefficient h is the same for both cable formation because they are the same cables. This is assumed because h depends on the physical material, internal layout in the cable, and the interface between the cable and the environment. The main reason for the difference in thermal properties between flat and trefoil formation is the surface area between the cable and the environment, which is the only place for the generated heat to flow.

The area of the outer sheath of each formation is calculated by using the diameters given in Table 4.1. The area between the inner and outer subsystems can be calculated from the circumference of the conductor. Area from the conductor surface is calculated in a similar way, by using the outer circumference of the cable.

$$A_{inner} = d_{inner} \cdot \pi \cdot 1m = 0.0174\ m \cdot \pi \cdot 1m = 0.0547\ m^2/m$$

$$A_{outer} = d_{outer} \cdot \pi \cdot 1m = 0.0381\ m \cdot \pi \cdot\ 1m = 0.119\ m^2/m$$

However, in trefoil formation the generated heat from the conductor will not spread out evenly as the adjacent cables creates less temperature gradients toward the center of the trefoil formation. This is illustrated in Figure 4.25 where the size of the red arrows indicates the amount of heat flow, and the blue line indicating the outer circumference. To address this, some adjustment factors for the trefoil areas κ_{inner} and κ_{outer} are introduced for the thermal heat conductivity calculations.

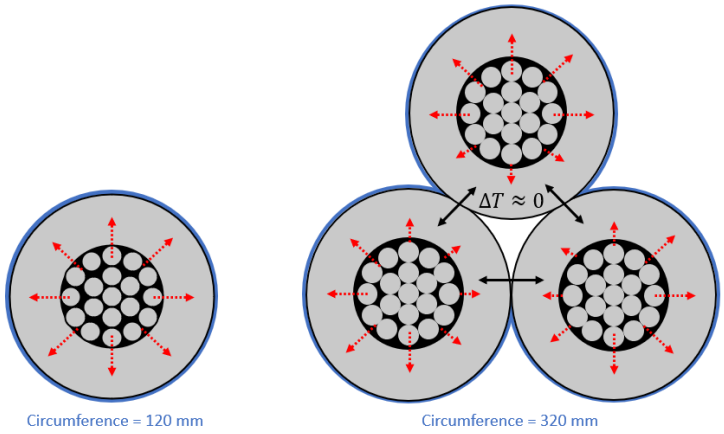

Figure 4.25: Illustration of heat flow and outer circumference of flat (left) and trefoil (right) formation.

The heat transfer coefficient can be calculated by using the Equation (2.14), where ΔT is temperature difference between two points/subsystems. If the adjustment factors are to be considered, the heat transfer coefficients must be calculated using the following equations.

$$h_{inner,-} = \frac{R_- I^2}{A_{inner}\left(T_{inner,-} - T_{outer,-}\right)} \tag{4.1}$$

$$h_{outer,-} = \frac{R_- I^2}{A_{outer}\left(T_{outer,-} - T_{room}\right)} \tag{4.2}$$

$$h_{inner,\Delta} = \frac{R_\Delta I^2}{A_{inner} \cdot \kappa_{inner}\left(T_{inner,\Delta} - T_{outer,\Delta}\right)} \tag{4.3}$$

$$h_{outer,\Delta} = \frac{R_\Delta I^2}{A_{outer} \cdot \kappa_{outer}\left(T_{outer,\Delta} - T_{room}\right)} \tag{4.4}$$

The resistance values in the equations above is calculated separately for each case because the resistance is temperature dependent. R_- is the warm resistance in flat formation while R_Δ is warm resistance for trefoil formation.

All the variables in the equations above are known, except the adjustment factors. These are obtained by using an optimization algorithm from Scipy in Python [53]. To include the data from the laboratory tests presented above, few constraints and assumptions are made:

- It assumes that h_{inner} for both formations is identical for all test scenarios. This is also true for h_{outer}.
- The average values calculated for h_{inner} from the three test cases will be the resulting heat transfer coefficient. This is also true for h_{outer}.

The objective function for the optimization is presented in Equation (4.5). Note that $h_{inner,\Delta}$ and $h_{outer,\Delta}$ is the variables which is affected by the adjustment factors while flat formation is not affected by these.

$$J(\kappa_{inner}, \kappa_{outer}) = \left(h_{inner,-} - h_{inner,\Delta}\right)^2 + \left(h_{outer,-} - h_{outer,\Delta}\right)^2 \tag{4.5}$$

The Python code for the calculations is shown in Appendix C, where calculation shows that κ_{inner} is 0.68 and κ_{outer} is 0.89. κ_{outer} seems reasonable as the trefoil formation has less contact with the surrounding air. The low value of κ_{inner} may indicate that the heat flow is concentrated mostly in the outwards direction from the center of the trefoil formation as illustrated in Figure 4.25. The resulting heat transfer coefficients and surface areas are presented in Table 4.5, together with the resulting thermal conductivity.

Table 4.5: Calculated heat transfer coefficients and surface areas for the XLPE cable.

	Flat inner	**Flat outer**	**Trefoil inner**	**Trefoil outer**
Heat transfer coefficient h [W/m^2°C]	188.3	18.4	188.3	18.4
Surface area A [m^2/m]	$5.5 \cdot 10^{-2}$	$12.0 \cdot 10^{-2}$	$3.7 \cdot 10^{-2}$	$10.7 \cdot 10^{-2}$
Thermal conductivity hA [W/°C]	10.4	2.2	7.0	2.0

The outer heat transfer coefficient has a reasonable value as the heat transfer mechanisms are mainly convection and radiation. Similar values in MV switchgear have been found by [54]. The inner heat transfer coefficients are 10 times higher than the outer coefficients because the main heat transfer mechanism is conduction between the conductor and the insulation.

4.5.3 Heat capacity

In order to determine the heat capacity of the aluminum and XLPE insulation of the cable, specific heat capacity and density given in Table 2.4 is used. The conductor volume per meter can be calculated by multiplying the cross-section area with one meter cable length. The volume of the XLPE insulation is obtained by taking the conductor outer cross-section and subtracting the cross-section of the aluminum conductor.

$$V_{Al} = 2.4\ cm^2 \cdot 100\ cm/m = 240\ cm^3/m$$

$$V_{XLPE} = \left(\frac{3.81}{2} cm\right)^2 \cdot \pi \cdot 100\ cm/m - 240\ cm^3/m = 900\ cm^3/m$$

Conductor and insulation mass per unit length is calculated by multiplying the respective density with the volume.

$$m_{Al} = \frac{2.7\ g/cm^3 \cdot 240\ cm^3/m}{1000\ g/kg} = 0.648\ kg/m$$

$$m_{XLPE} = \frac{0.965\ g/cm^3 \cdot 900\ cm^3}{1000\ g/kg} = 0.869\ kg/m$$

Finally, heat capacity per unit length can be calculated by multiplying the specific heat capacity with the masses.

$$c_p^{Al} = 900\ J/kg°C \cdot 0.648\ kg/m = 583.2\ J/m°C$$

$$c_p^{XLPE} = 2174\ J/kg°C \cdot 0.869\ kg/m = 1889.2\ J/m°C$$

Calculation values and results are given in Table 4.6. The total heat capacity per unit length can be calculated roughly by adding the two heat capacities c_p = 583 + 1890 = 2473 J/mºC.

Table 4.6: Calculation of different parameters of the aluminum conductor and XLPE insulation.

	Aluminum conductor	**XLPE insulation**
Specific heat capacity	$\hat{c}_p^{Al} = 900\ J/kg℃$	$\hat{c}_p^{XLPE} = 2174\ J/kg℃$
Density	$\rho_{Al} = 2.7\ g/cm^3$	$\rho_{XLPE} = 0.965\ g/cm^3$
Volume per unit length	$V_{Al} = 240\ cm^3/m$	$V_{XLPE} = 900\ cm^3/m$
Mass per unit length	$m_{Al} = 0.65\ kg/m$	$m_{XLPE} = 0.87\ kg/m$
Heat capacity per unit length	$c_p^{Al} = 583\ J/m℃$	$c_p^{XLPE} = 1890\ J/m℃$

4.5.4 Thermal model of the cable

An equivalent thermal circuit of the laboratory cable can be made based on the calculations made above. Figure 4.26 shows the thermal circuit of the cable. The power losses in the cable are modeled as a current source, while the room temperature is modeled as a voltage source.

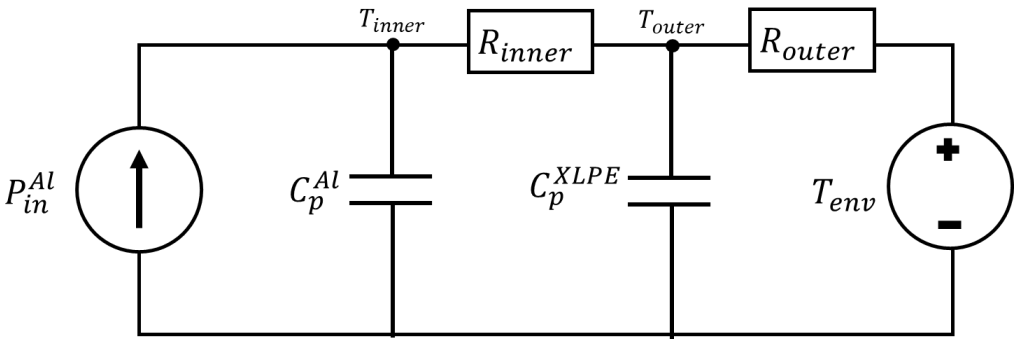

Figure 4.26: Corresponding thermal circuit of the experimental cable.

The mathematical model is based on the thermal energy balance. As mentioned earlier, it is assumed that the cables are modeled as a lumped parameter system with inner and outer temperatures. The inner temperature T_{inner} represents the aluminum conductor surface temperature, and the outer temperature T_{outer} represents the temperature in the insulation and all the way to the cable surface. Therefore, this dynamical system has two states, being the two temperatures, expressed as two differential equations as following.

$$\frac{dT_{inner}}{dt} = \frac{1}{c_p^{Al}}[P_{in}^{Al} - P_{out}^{Al}] \tag{4.6}$$

$$\frac{dT_{outer}}{dt} = \frac{1}{c_p^{XLPE}}[P_{out}^{Al} - P_{out}^{XLPE}] \tag{4.7}$$

Where the power in and out of the subsystems is described by the following equations. The aluminum conductor resistance R_{Al} is the warm resistance that depends on the aluminum conductor temperature. Two constants of the thermal model are temperature coefficient $\alpha = 3.9 \cdot 10^{-3}\ [1/K]$ and reference temperature of the cold resistance $T_{ref} = 22.4$ ℃.

$$P_{in}^{Al} = R_{Al} I^2 \tag{4.8}$$

$$P_{out}^{Al} = h_{inner} A_{inner} (T_{inner} - T_{outer}) \tag{4.9}$$

$$P_{out}^{XLPE} = h_{outer} A_{outer} (T_{outer} - T_{env}) \tag{4.10}$$

$$R_{Al} = R_{cold}\left[1 + \alpha\left(T_{inner} - T_{ref}\right)\right] \tag{4.11}$$

Inputs to the thermal model is current and the room temperature. Total heat capacity of aluminum conductor and XLPE insulator is the same for both flat and trefoil formation. Table 4.7 shows all known parameters per unit length of the thermal model.

Table 4.7: Calculated model parameters in the thermal model of the laboratory cable.

Model parameters	c_p^{Al}	c_p^{XLPE}	h_{inner}	h_{outer}	A_{inner}	A_{outer}	R_{cold}
	[J/ m°C]		**[W/m²°C]**		**[m²/m]**		**[Ω/m]**
Flat	583	1890	188.3	18.4	0.055	0.12	0.134
Trefoil	583	1890	188.3	18.4	0.037	0.107	0.134

5 Data Simulation

The thermal model derived in chapter 4.5.4 can be used for inner and outer temperature estimations for the 24 kV XLPE cable, given some current and room temperature over time. This can be useful for Color Line, as charging currents can exceed the rated current in the cable for short time spans. This is because the thermal inertia of the cable is not instantaneous.

In this chapter, different loading profiles are simulated with the thermal model and tested in the High Current Laboratory to verify the thermal model of the cable. In addition, the thermal model parameters will be adjusted to best fit simulation results with the measurements. The reader should notice that the room temperature in the laboratory at USN is around 22 ºC which is certainly higher than the outside temperature and in culvert where Color Line cable is laid. Because of this fact, the laboratory tests will not lead to identical temperature responses as the Color Line cable. The Python code behind the results in this chapter is shown in Appendix E.

5.1 Simulation of thermal model with calculated parameters

The different loading experiments done in chapter 4.3 and 4.4 is simulated with the presented thermal model. First the long-term cases will be simulated, followed by the short-term experiments. As shown in Figure 5.1, the conductor temperature basically exhibited the same temperature variation tendency as the measured temperature. The temperature difference between the simulated and measured are in range of ± 5 ºC throughout the simulation.

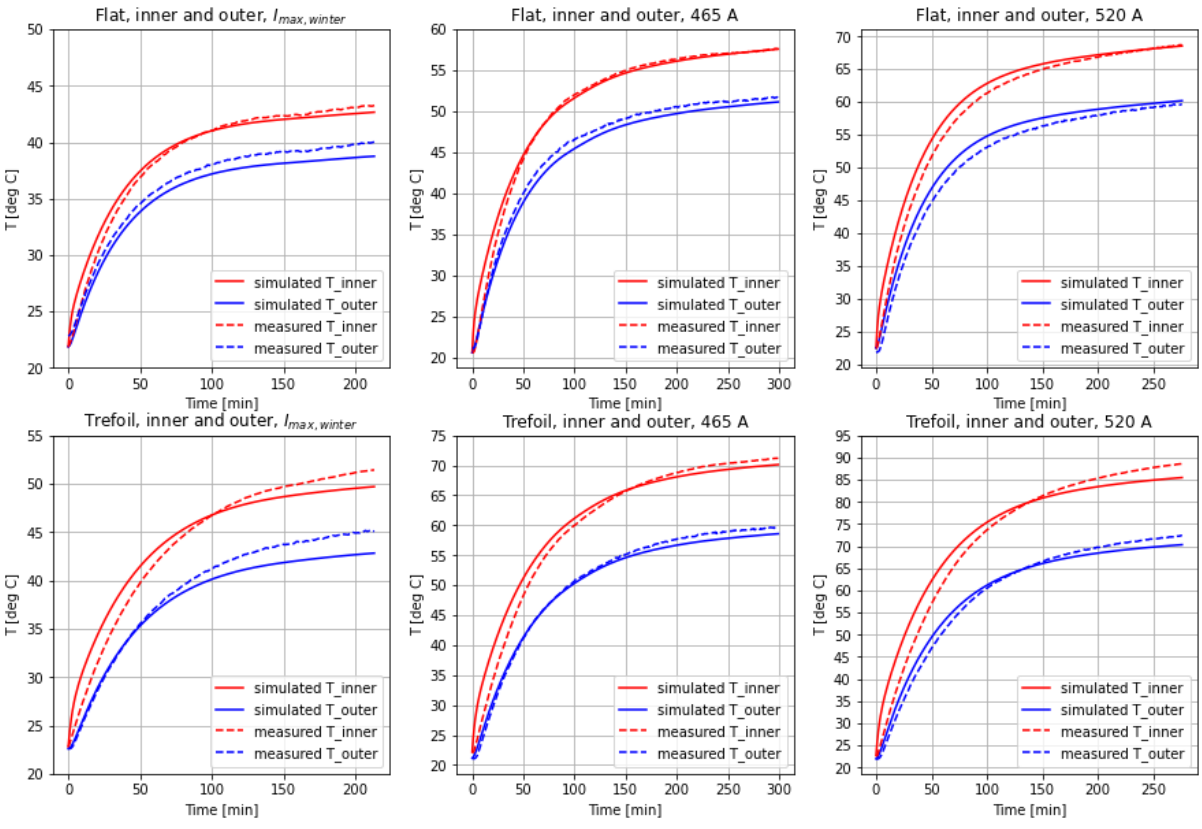

Figure 5.1: Simulated and measured temperature of long-term charging with calculated parameters.

Simulation of the short-term charging cases is shown in Figure 5.2. From the figure, one can see that the simulated inner temperature is much higher than the measured inner temperature for all cases, in both flat and trefoil formation.

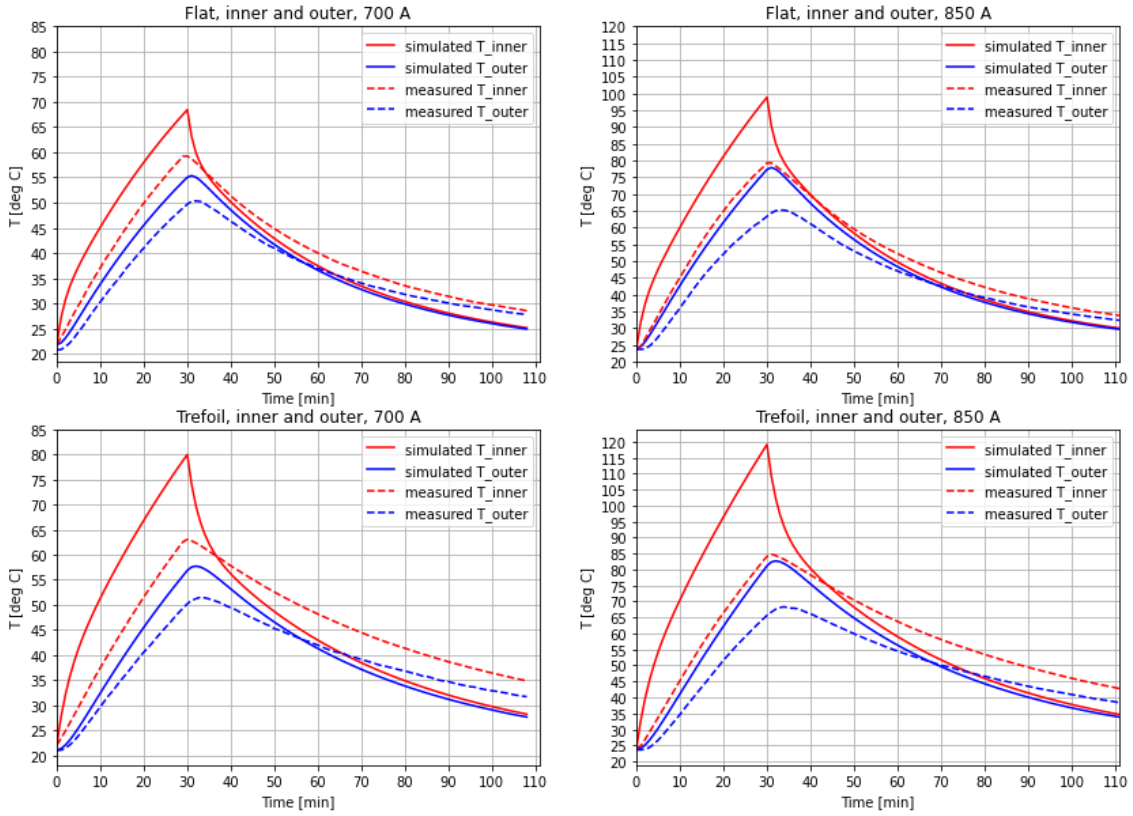

Figure 5.2: Simulated and measured temperature of short-term charging with calculated parameters.

Although the model predicts temperatures for long-term charging well, the short-term simulations are off by up to around 40 ºC. This may be explained because the model parameters were obtained from the long-term responses. Therefore, adjustments for the calculated model parameters are done to better fit simulations to measurements.

5.2 Optimizing model parameters to measurements

A better fit for the thermal model to the laboratory experiments can be obtained by using an optimization algorithm to minimize the mean absolute error (MAE) between simulation and measurements, which can be calculated using Equation (5.1). MAE measures the average magnitude of the errors in a set of predictions, where the errors is defined as simulated values y_i minus measured values $\hat{y}_i$, and n is the total number of data points.

$$MAE = \frac{1}{n}\sum_{j=1}^{n}|y_i - \hat{y}_i| \tag{5.1}$$

An adjustment array is used to scale the calculated model parameters. The model parameters are optimized for both long-term and short-term charging. However, to reduce the number of variables in the optimization, not all parameters are optimized. Instead of optimizing the thermal heat transfer coefficients h and the surface areas A separately, the thermal conductivity hA is instead optimized directly. This results in there being five model parameters that can be adjusted during the optimization, namely c_p^{Al}, c_p^{XLPE}, hA_{inner}, hA_{outer}, and R_{cold}.

The optimization was done in Python, where Scipy dual annealing function was used [53]. In Appendix D, the Python code is shown for the optimization of the model parameters. This was done two separate times, with different boundaries for the adjustment array. First, the optimization was done with a boundary between 0.001 and 10, referred to as the large-bound optimized adjustment. Then another optimization was done with a smaller boundary between 0.5 to 1.5, referred to as the small-bound optimized adjustment. This smaller boundary was set to force the optimization to not make the model parameters deviate too far away from the calculated values. The optimization results for the adjustment arrays are shown in Table 5.1 together with the calculated model parameters. Note that the optimization for flat and trefoil formations is separated, and they therefore get their own adjustment arrays. The non-optimized adjustment is all set to 1 because this adjustment represents a multiplication factor for the calculated parameter values.

Table 5.1: Results from the optimization of model parameters by using mean absolute error.

Model parameter	**Formation**	c_p^{Al}	c_p^{XLPE}	hA_{inner}	hA_{outer}	R_{cold}
Calculated model parameters	Flat	583	1890	10.4	2.2	0.134
	Trefoil	583	1890	7.0	2.0	0.134
Non-optimized adjustments	Flat	1	1	1	1	1
	Trefoil	1	1	1	1	1
Large-bound optimized adjustments	Flat	10.0	1.71	3.1	3.2	3.28
	Trefoil	7.28	0.79	1.97	1.96	2.14
Small-bound optimized adjustments	Flat	1.5	0.5	0.62	0.61	0.63
	Trefoil	1.5	0.71	0.78	0.69	0.75

For the optimization with large bounds, the most significant adjustments are the aluminum heat capacity for both formations. For flat formation, all parameters are scaled up, with the conductor heat capacity scaled most, and the insulation heat capacity scaled the least. The tendency is the same for trefoil formation.

For the optimizations with smaller bounds, the conductor heat capacity is still the most scaled up parameter. However, all other parameters are in this case scaled down.

All the optimizations scaled the conductor heat capacity up more than the other parameters. This may indicate that the boundary for the inner subsystem should be larger than what is defined in the thermal model. In addition, the measurements of the conductor surface may not be a perfect measurement, and may be affected by the insulation temperature, leading to inaccurate parameter calculations in the first place.

5.2.1 Simulations with the large-bound optimization parameters

Figure 5.3 shows the simulated temperatures of long-term loading currents with optimized model parameters from the large-bounded case. The steady-state simulated temperatures for $I_{max,winter}$ and 520 A in trefoil formation fits better with the large-bound optimization parameters compared to the calculated parameters. The temperatures in first hour for all cases is also superior. On the other hand, the error for the simulated temperature for 465 A in trefoil formation has increased.

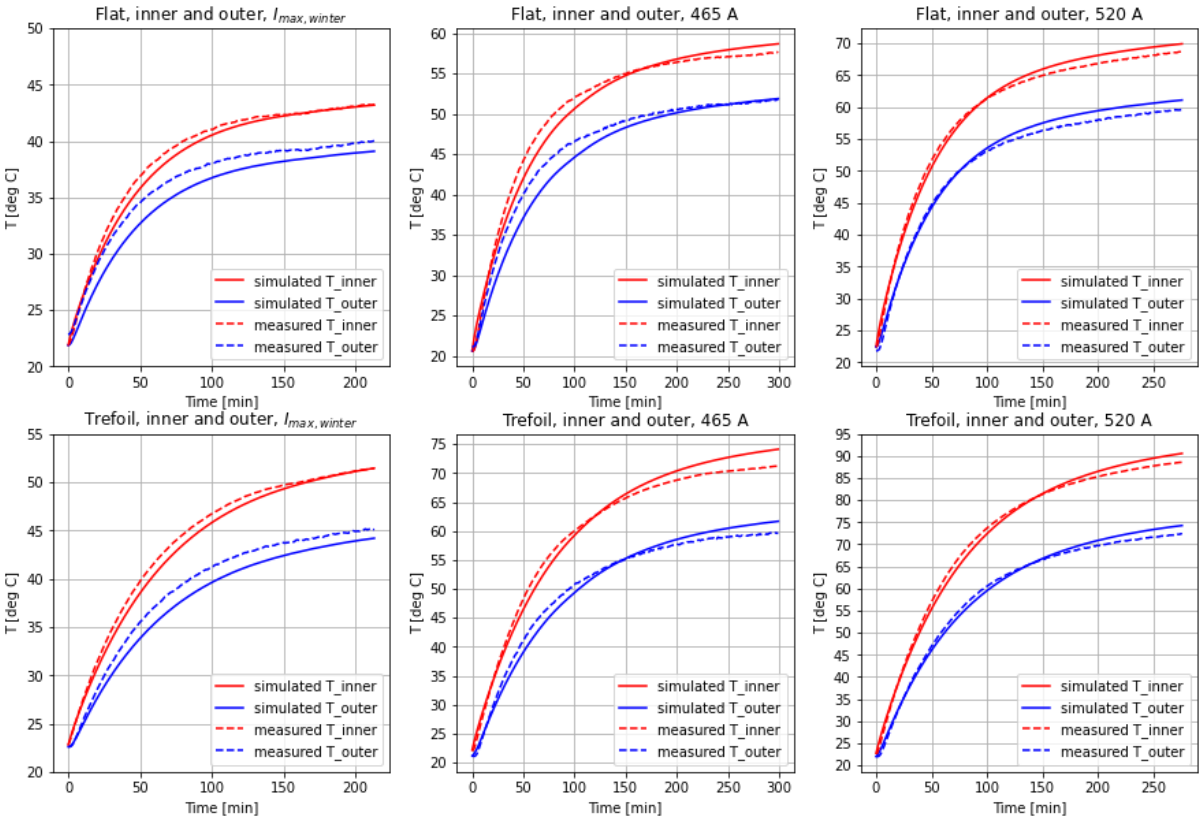

Figure 5.3: Simulated (large-bound) optimization parameters and measured temperature of long-term charging.

Figure 5.4 shows the simulated temperatures of short-term loading currents with optimized model parameters from the large-bound case. The simulated inner temperature is remarkably better than the calculated model parameters, where the maximum temperature difference is approximately 5 ºC.

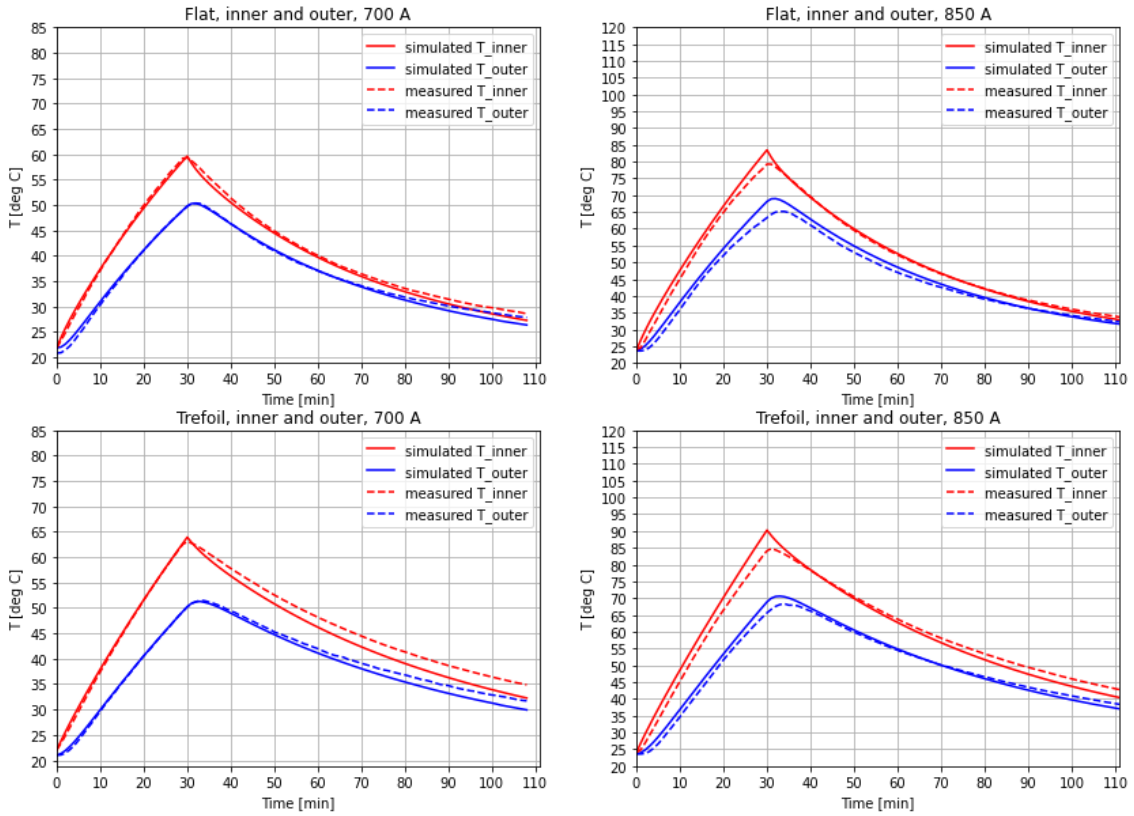

Figure 5.4: Simulated (large-bound) optimization parameters and measured temperature of short-term charging.

The simulated temperature fits the measured temperature well with the large-bound optimization parameters. However, these parameters have values that are not representative for the physical system, as the parameter values has been found as a local minimum in the parameter space with respect to the error between measurement and simulation.

5.2.2 Simulations with the small-bound optimization parameters

Figure 5.5 shows the simulated temperatures of long-term loading currents with optimized model parameters from the small-bounded case. The simulated temperatures for all cases for both flat and trefoil formation is representative since the maximum temperature difference between the simulated and measured values is approximately 3 ºC.

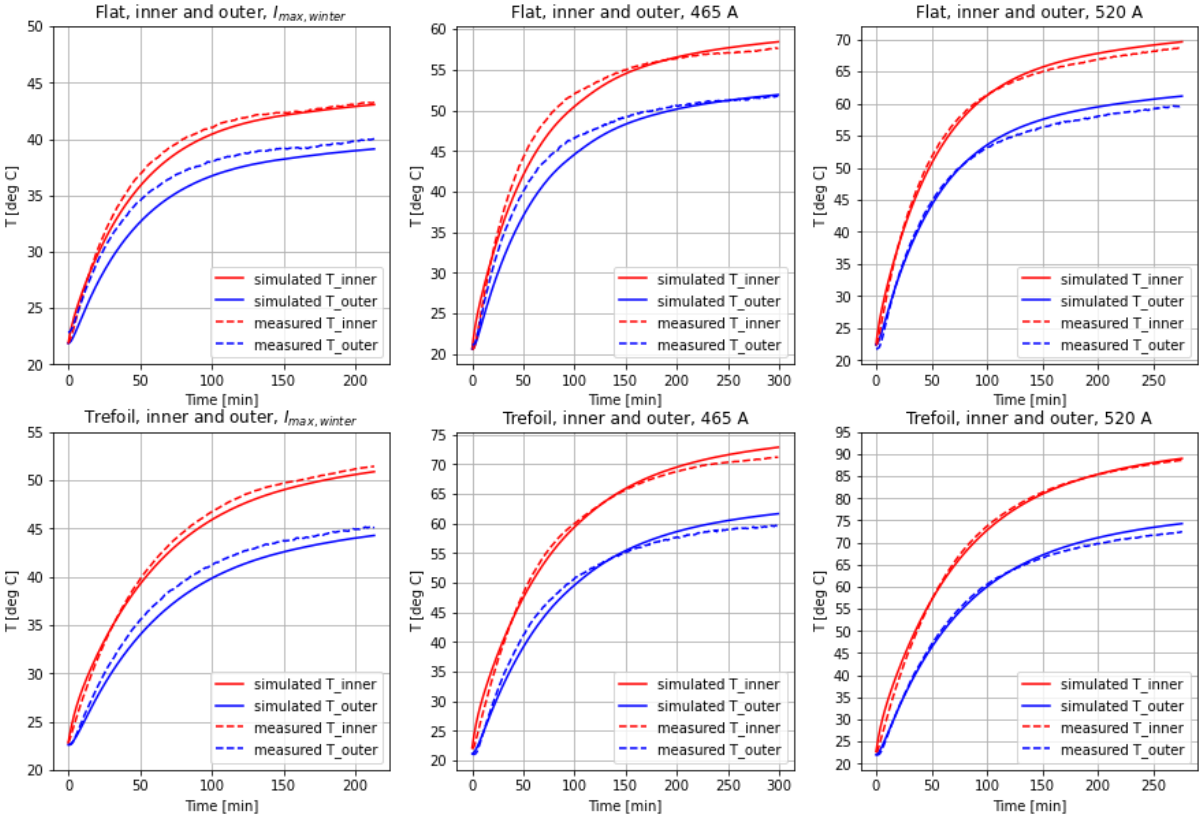

Figure 5.5: Simulated (small-bound) optimization parameters and measured temperature of long-term charging.

Figure 5.6 shows the simulated temperatures of short-term loading currents with optimized model parameters from the small-bound case. The simulated inner temperature has a larger maximum discrepancy (15 ºC) compared to the large-bounded optimization. However, the small-bound optimization parameters perform significantly better than the calculated parameters and are still somewhat representative for the physical system.

Because the resulting model parameters after the small-bounded optimization is similar to the calculated ones, but still yields better simulation results, the rest of the report will use these parameters in further calculations.

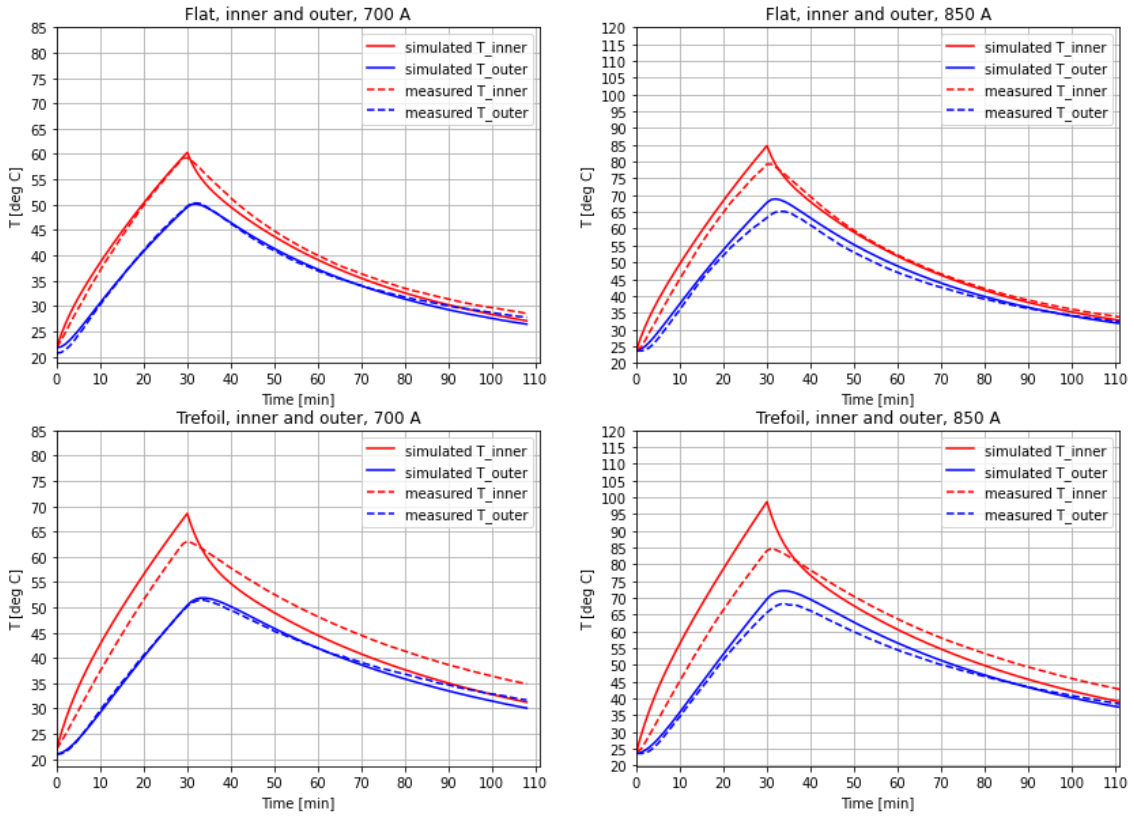

Figure 5.6: Simulated (small-bound) optimization parameters and measured temperature of short-term charging.

5.3 Visualization of maximum allowed current values

The environment temperature has a significant impact on the cooling of the cable. Therefore, it is instructive to visualize how this temperature affects the maximum steady-state currents for both trefoil and flat formation. The Python-code for plots in this chapter is shown in Appendix E.

Figure 5.7 shows contours of the steady-state temperatures in the cable with a given environment temperature on the x-axis and current on the y-axis. The plot is made by simulating with the thermal model, with a duration of 5 hours which is approximately 5 time the thermal time constant of the cable. The blue and orange points represent the 465 and 520 A long-term tests, respectively.

The simulated maximum allowed current for flat and trefoil formation is 600 A and 520 A, respectively, at 25 ºC. The temperatures for any given currents for flat formation is much lower than the trefoil formation for the same environment temperatures because of a higher heat conductivity out of the cable. In addition, the three long-term laboratory tests are shown in context of this figure. The temperature indicators on the given points represents the actual steady-state temperatures from the long-term tests.

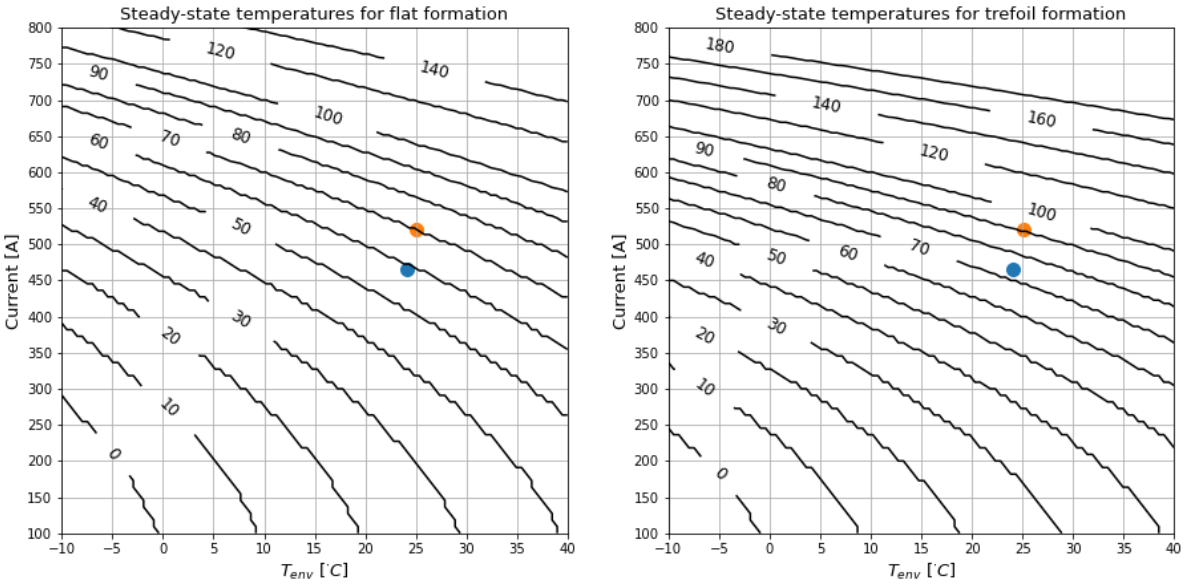

Figure 5.7: Simulated steady-state temperatures [ºC] with respect to long-term current and environment temperature. Points indicates laboratory test results from the long-term loading.

The points indicated in Figure 5.7 fits well with the contour plot. However, the thermal model is already optimized for the scenarios presented in the figure, and one should expect a good fit between them. There is no guarantee that the plot works for different operating conditions, and further testing must be done to validated this.

It is also interesting to know how much the cable can be loaded in short terms before exceeding the maximum temperature limit of 90 ºC. Figure 5.8 shows the simulated temperature difference from the environment temperature with respect to loading currents applied for 30 minutes, where the environment temperature is 20 ºC. The red line is the inner temperature, and the blue line is the outer temperature of the cable. The points in the figure indicates the measurement from the short-term testing currents. One can observe that the measured inner temperature for the trefoil formation has a small discrepancy with the simulated estimate. However, to further validate the graphs one should test with a larger range of current values, and with different environment conditions.

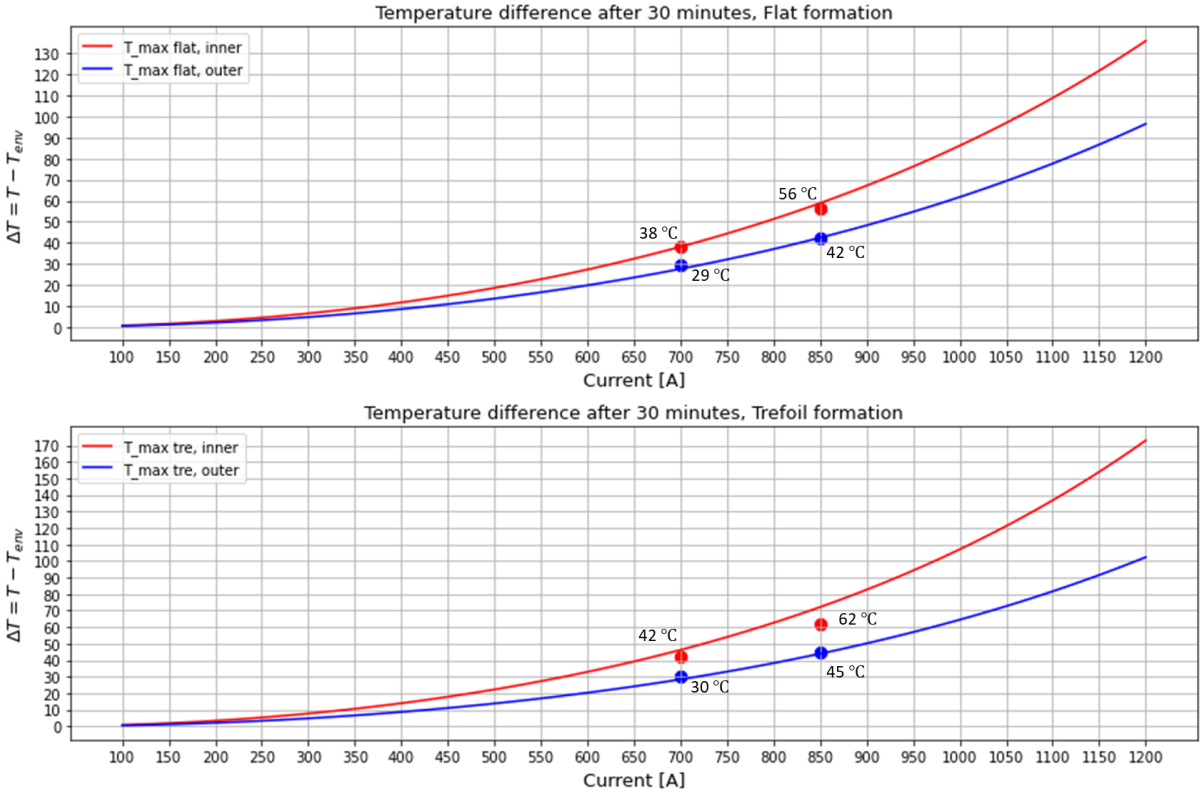

Figure 5.8: Maximum temperature after 30 minutes of loading.

5.4 Periodic short-term loading scenarios

During a day, there might be several ferries that arrives at the charging station to do a short-term charging, and then depart as fast as possible. In the cases where there is more than one ferry that needs charging, it might be necessary to know that the cable is in an appropriate state to handle a new short-time charging. Therefore, two periods of short-term charging will be assessed. Two different periodic loading profiles will be assessed. The first is two charging cycles with the same loading current and charging times. The other scenario is two charging cycles with different currents and equal charging times. The Python-code for generating the results in this chapter is shown in Appendix F and Appendix G.

5.4.1 Short-term loading with the same loading currents

The first periodic loading profile is defined as illustrated in Figure 5.9. Each cycle has a charging time T_{on} where the loading current is constant. This is followed by a resting time T_{off} where the loading current is zero.

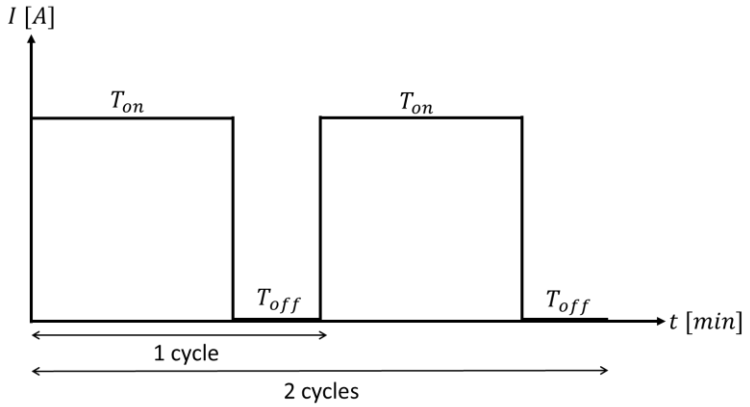

Figure 5.9: Periodic loading profile with the same current for both periods.

Figure 5.10 shows a contour plot of the maximum allowed current I_{max} for the periodic loading where the x-axis is charging time and the y-axis is resting time. With this figure, one can determine the maximum current given a charging time and a resting time that will not reach a maximum cable temperature of 90 ºC in the trefoil formation.

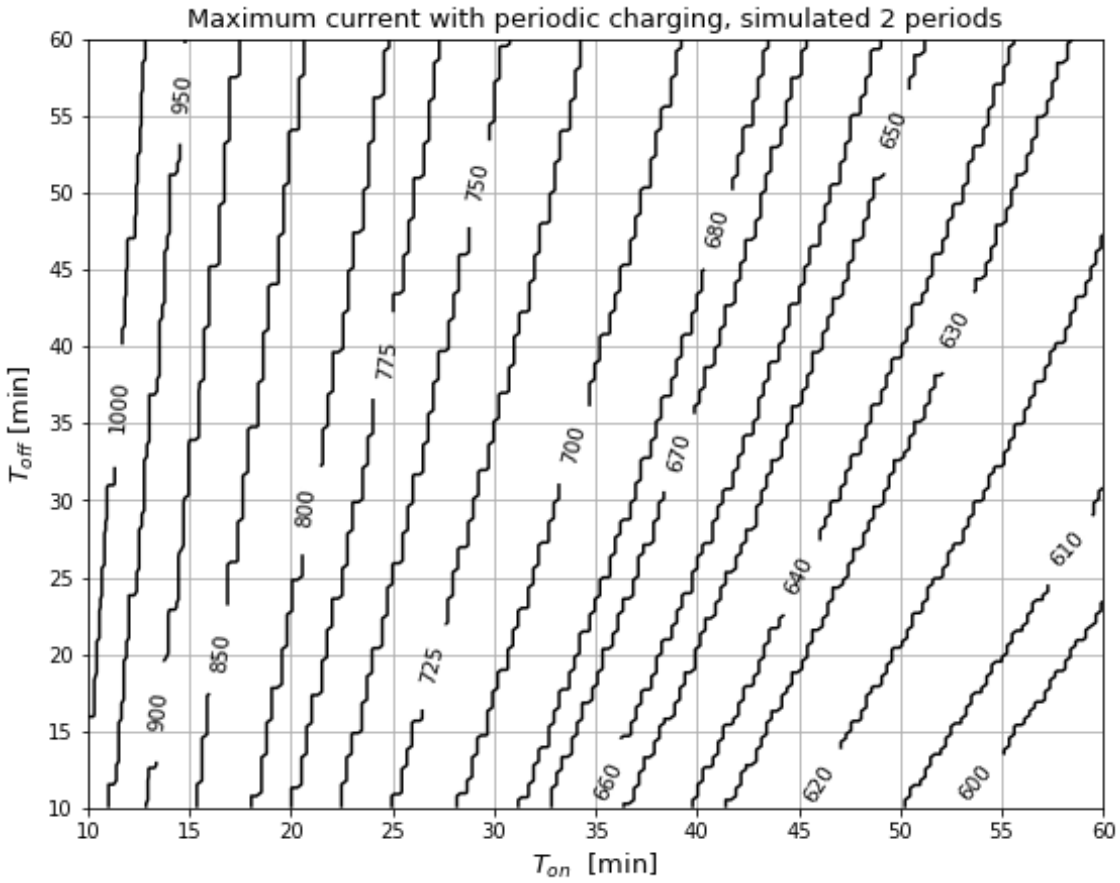

Figure 5.10: Maximum allowed loading currents I_{max} [A] for periodic charging with 2 periods.

The currents given in Table 5.2 is a table representation of Figure 5.10 which allows for exact current value from the charging period.

Table 5.2: Maximum currents with periodic charging of 2 periods.

T_{off} \ T_{on}	10	15	20	25	30	35	40	45	50	55	60
10	996	859	781	722	689	657	637	624	611	598	585
15	1010	872	787	735	696	670	644	631	611	605	591
20	1023	879	801	742	703	676	650	637	618	611	598
25	1036	892	807	755	716	683	657	644	624	611	605
30	1049	905	820	761	722	689	663	644	631	618	605
35	1062	912	827	768	729	696	670	650	637	624	611
40	1068	925	833	774	735	703	676	657	644	624	618
45	1081	931	840	781	742	709	683	663	644	631	618
50	1088	938	853	787	748	716	689	670	650	637	624
55	1101	944	859	794	755	716	689	670	657	637	624
60	1108	957	866	801	755	722	696	676	657	644	631

Based on the results in Figure 5.10 and Table 5.2, three test cases are executed in the laboratory to verify the predictions. The three cases are given in Table 5.3 where I_{tesst} is the testing current.

Table 5.3: Three test cases for the periodic loading with same currents.

Test cases	T_{on} [min]	T_{off} [min]	I_{max} [A]	I_{tesst} [A]
Case 1	45	20	637	630
Case 2	30	30	722	675
Case 3	30	25	716	725

The measured temperature response from the laboratory, together with the simulated values are shown in Figure 5.11. In general, the simulated temperature estimations are somewhat higher than the measured responses. This is similar to the short-term trefoil responses and is therefore expected. The maximum temperature error between measurement and simulation is approximately 10 ℃.

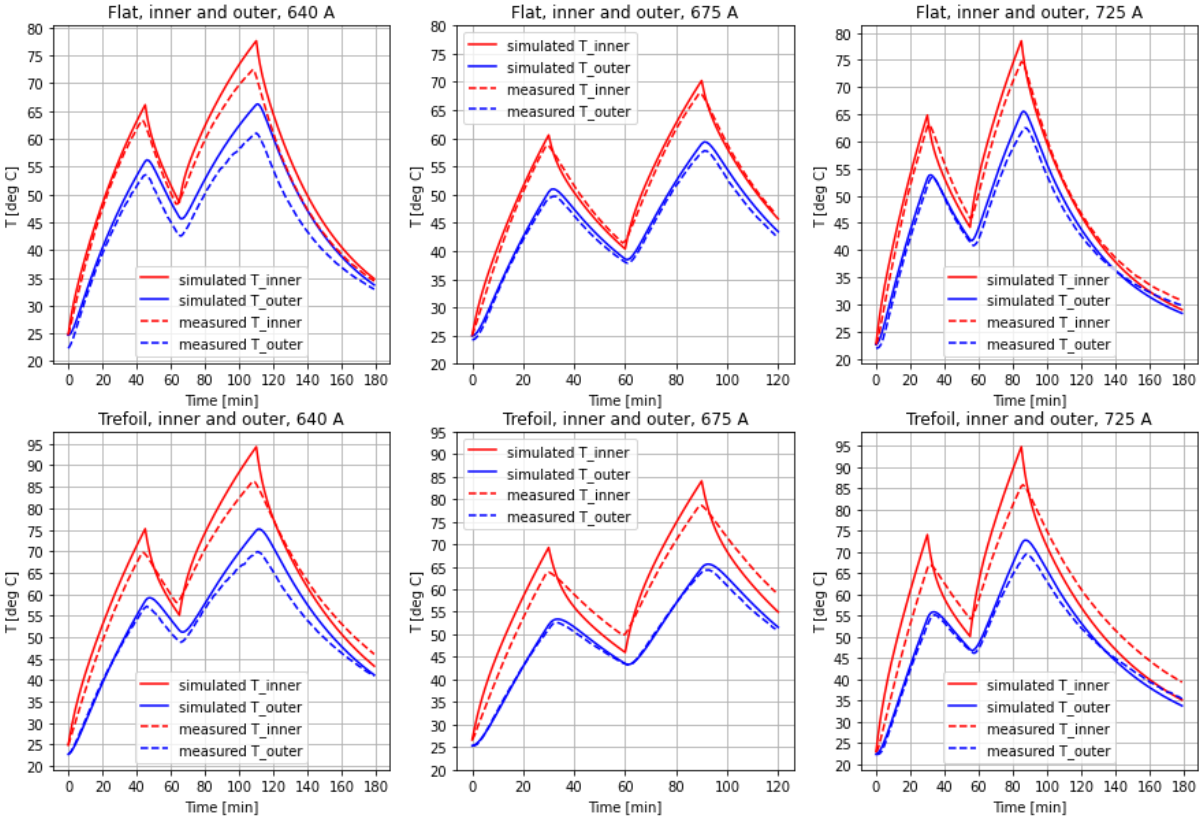

Figure 5.11: Simulated and measured temperature for the periodic loading profile with same currents.

5.4.2 Short-term loading with different loading currents

The second periodic loading profile is defined as illustrated in Figure 5.12. Each charging period has a charging time T_{on}, but the two periods may have different loading currents. Between the two charging periods there is a resting time T_{off} where the loading current is zero. This loading profile allows for different amounts of battery charging for the same charging period T_{on}, which may be useful in the case of several ferries charging sequentially with different charging demands.

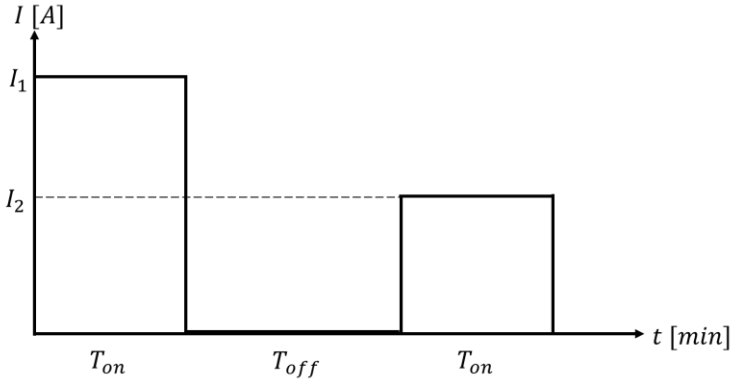

Figure 5.12: Periodic loading profiles with two different currents with the same charging time.

Figure 5.13 show a contour plot of the minimum resting time T_{off} between the two charging periods of 30 minutes. Charging time can be customized in the Python script, and an additional test with 60 minutes are shown in Appendix G. The environment temperature for these simulations is defined as 22 ºC.

The 60 minutes charging period has much lower maximum currents for I_1 and I_2 since the charging period is doubled with respect to the 30 minutes plot. Note that the greyed-out area represents a resting time of 0 minutes, which effectively means that the two charging periods can be done without any resting time and still avoid overheating.

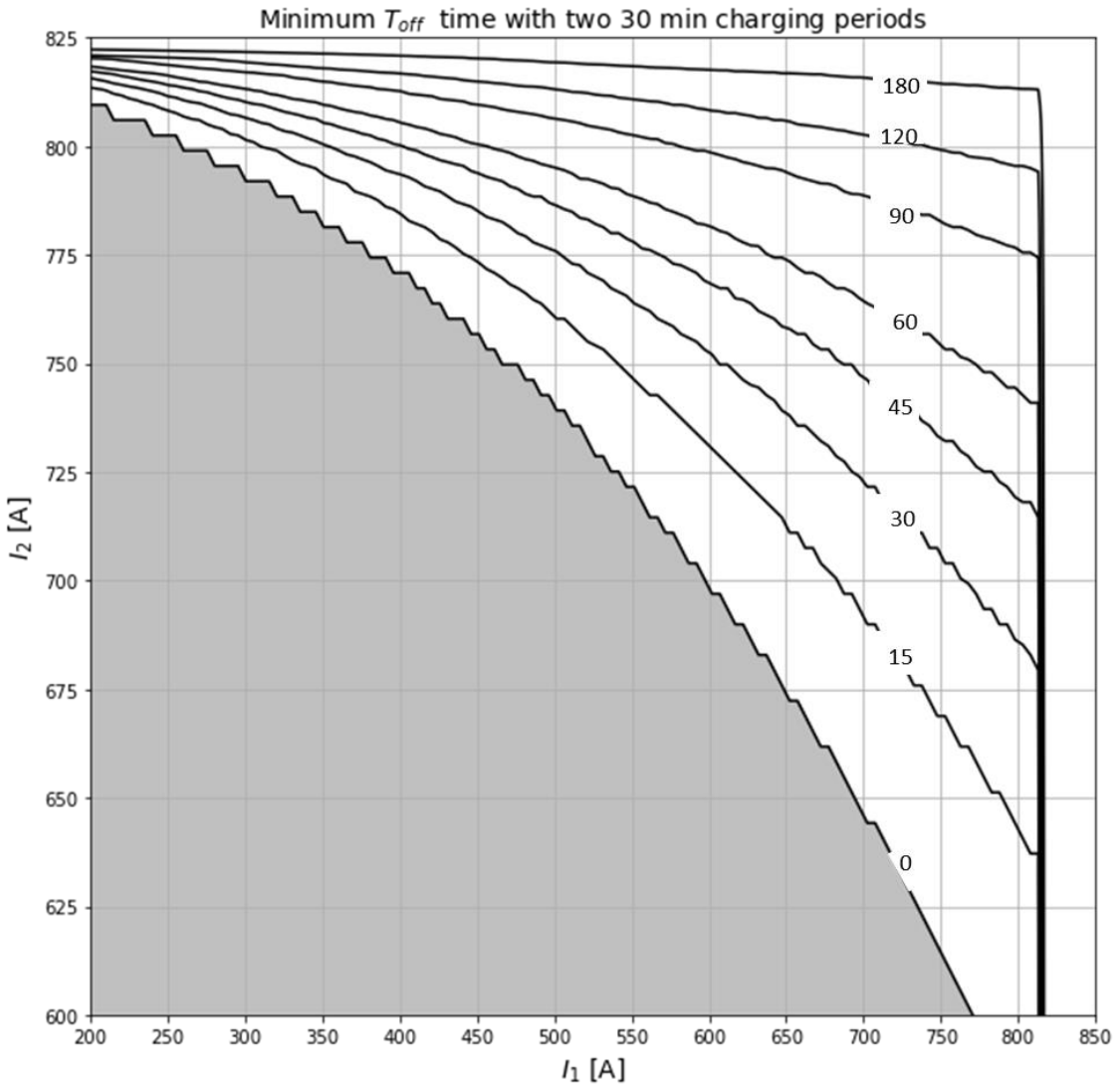

Figure 5.13: Minimum resting time T_{off} [minutes] for 30 minutes charging times.

Two cases with 30 minutes charging time are tested to verify the simplified periodic loading profile with different currents. These test cases are shown in Table 5.4 Table 5.4where T_{off} is minimum resting time and $T_{off,test}$ is tested resting time.

Table 5.4: Two test cases with 30 minutes charging time for the periodic loading with different currents.

Test cases	I_1 [A]	I_2 [A]	T_{off} [min]	$T_{off,test}$ [min]
Case 1	800	660	20	15
Case 2	500	825	180	45

Current values in Case 2 were chosen to test current values close to the upper current limitations shown in Figure 5.13. From the short-term tests, it was shown that the thermal model overestimates the maximum temperature in the cable, and therefore the high I_2 current of 825 A was chosen. Based on the chosen values, the figure predicts a resting time of 180 minutes. However, since the temperature measurements is overestimated from the model, it was chosen to rest for only 45 minutes.

The measurements and simulations for the thermal responses are shown in Figure 5.14. Again, one should note that there is a discrepancy between the maximum temperature, especially for the trefoil formation. The maximum temperature discrepancy is approximately 15 ºC.

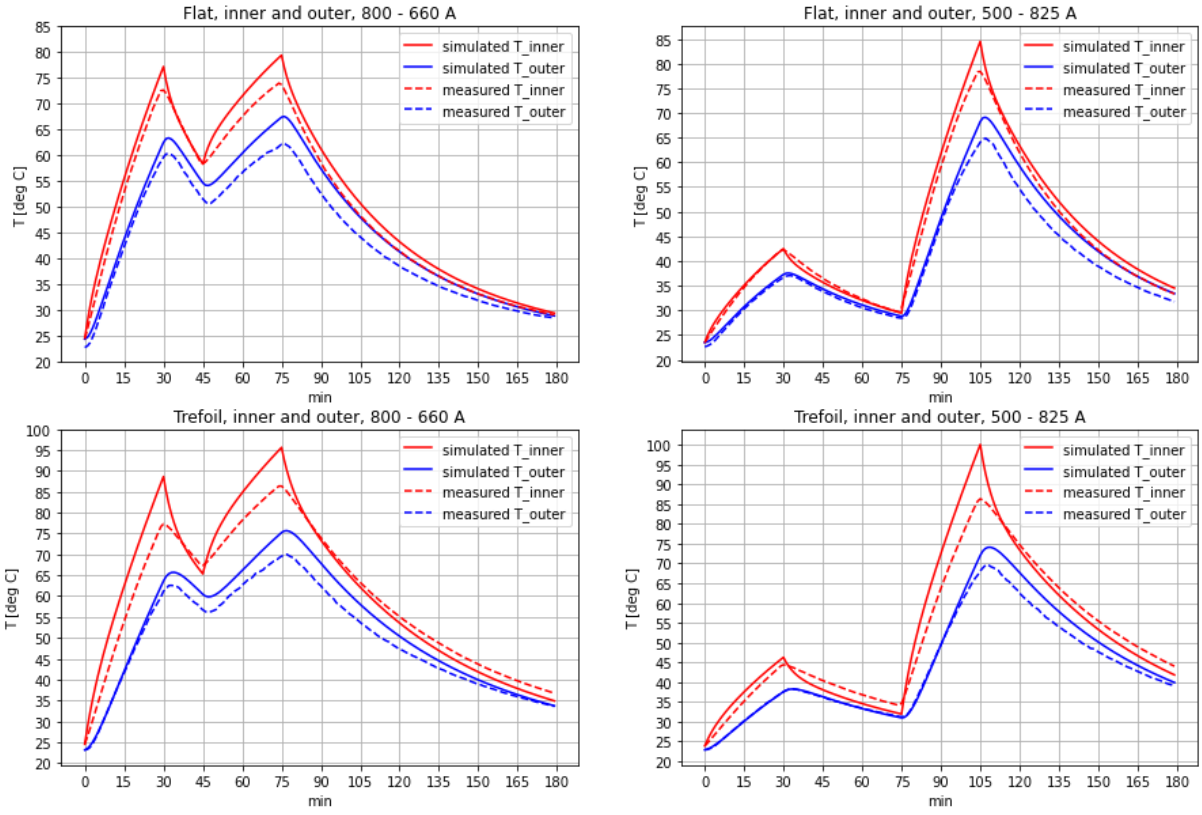

Figure 5.14: Simulated and measured temperatures for the periodic loading profile with different currents.

6 Discussion

Information about the Color Line cable setup has been gathered from conversations and pictures supplied by Lede. The exact sensor placements have some uncertainty, as there has been no visit to the site during the project. The seven sensor measurements from the Color Line cable have been difficult to relate to the laboratory experiment as there are unknowns such as the environment temperature and sensor placement. The data provided by Lede and Color Line was from two days, one winter day and one summer day. With more data, better comparisons may have been done with the laboratory experiments.

Previous studies have been focusing on the long-term thermal responses of the Color Line cable in the culvert. However, research about the short-term responses for the cable in air have not been investigated and is the main topic of this thesis.

6.1 Laboratory setup

6.1.1 Sensors

There are in this thesis two different sensor placements on the cable: one at the conductor surface, and one at the cable surface. The conductor sensor was installed by drilling a 15 mm deep hole in the cable insulation, such that the conductor was not damaged. The sensor was placed directly in the hole, and then the opening was taped in place with the cable. The temperature measurements may be inaccurate because of two factors. Firstly, the heat dissipation may not have been representative where the hole was drilled. This could have been remedied by filling the drilled holes with some sort of epoxy or similar. Secondly, the sensor might not have been exactly placed on the conductor surface, as the tape that held the cable surface sensors in place might have affected the surface temperature by reducing the thermal heat coefficient locally.

Sensors placed in Group C (in Figure 4.6) may have been affected by sun radiation, as this is close to a window. On sunny days, one could measure the effect of the sun on these sensors without any cable loading. In addition, sensor nr. 9 and 10 was affected by a change in the cable formation. These sensors were placed at a location where the flat cables were joined with the trefoil formation. This required the cables to bend out of formations to make the connections. This change is measurable, as sensor nr. 9 and 10 had lower temperature measurements in the trefoil formation than the rest of the sensors.

It might be possible to measure the temperature for several cable layers, such at the outer semiconducting layer or under the sheath. This may be helpful if the thermal model is to be extended with more subsystems.

6.1.2 Current injection and cable formations

The high current injection transformer is in principle a manually adjustable low voltage, high current source. Therefore, the currents had to be adjusted manually in each phase to the desired values. During the experiment, the cable resistances increased because of an increase in conductor temperature, which means that without manual adjustment the current would fall. Because of this, there are some uncertainties and inaccuracies from constant current values in the experiments.

The laboratory setup was configured such that the flat and trefoil formations were connected in series. This may have allowed heat to flow from the hotter trefoil formation, thought the conductors, and into the colder flat formation. In addition, the room temperature around the cables may have been higher with both formations on simultaneously, compared to if only one of the formations was active. The two formations could have been configured to be tested separately, such that they would not affect each other at all.

6.2 Thermal model and properties of the cable

6.2.1 Thermal properties

Some of the thermal properties of the cable was obtained by measurements from the experiments. An essential property is the cold cable resistance, which is the main property in deciding how much heat generation is present in the cable. The cold resistance was measured as the DC-resistance at 22.4 ºC, but the measurement included the contact resistance, and did not include skin- or proximity effects, induced losses in cable sheath or dielectric losses. In addition, because the cable length was measured with some uncertainties, the per unit length quantities may be inaccurate.

The warm resistance was calculated from the cold resistance and used the temperature coefficient α for aluminum. The α factor may have a different value for the conductor, as the exact chemical composition of the aluminum conductor is not known.

The heat capacity calculations were calculated by using specific heat capacity for aluminum and XLPE, and the measured size of the different layers in the cable. There is no guarantee that the specific heat capacity is correct compared to the XLPE cable used in the experiments, and the size of the layers was approximated and simplified to not include other layers than the conductor and insulation layer.

Heat transfer coefficients h in the cable was simplified to be from the conductor to the insulation, and from insulation to the environment. It is assumed that these coefficients are independent of cable formation, meaning that both inner and outer coefficients are constants. It is thought that the difference between cable formations should come from changing the contact areas instead of the heat transfer coefficients.

From calculations of the heat transfer coefficients from the individual long-term cases, one can observe that higher currents (and therefore higher temperatures) resulted in higher heat transfer coefficient values. This may be explained because the heat transfer coefficient may be temperature dependent, and heat transfer from radiation and convection were not included. In the end, the average calculated coefficients for both inner and outer parts were used in the thermal model.

During the long-term tests, one can see that higher currents led to higher room temperatures at the end of the test. In addition, there were no air temperature measurements close to the cables, which was probably significantly higher than the general room temperature. This may have been a source of error when calculating the thermal properties of the cable.

6.2.2 Thermal model

The main objective for this thesis was not to create the most realistic thermal model of the XLPE cable, but to create a model which is able to emulate measurements based on correct inputs. The resulting model had five model parameters which could be fine-tuned to achieve best predictions to measurements. However, the resulting parameters from the optimization algorithm was not close to what was expected in the physical system when the optimization boundaries were large. This may indicate that the model was not complete. Indeed, additions could have been implemented to the thermal model to make it a better representation of the cable, such as heat loss from radiation and convection from the surface of the cable.

The XLPE cable has several layers of different materials. Each layer could have been modeled as a separate subsystem, resulting in more differential equations, and more model parameters. One could also have used Finite Element Methods (FEM) to simulate temperature distribution over the whole cable cross-section. However, the point of the model in this thesis was to make a simple thermal representation of the cable, and a lumped parameter system with two subsystems was appropriate, as the two subsystems represented the measurements taken at the lab. This simple model may also be implemented in other cable types without many modifications. A flaw of the thermal model, which may make it incompatible for the Color Line cable, is that there is no way of incorporating weather like sun, rain, or wind.

6.3 Results from experiments and simulations

6.3.1 Laboratory tests

There were in total three different long-term, and two short-term tests done in the laboratory, which made the basis for parameter optimization. However, experiments with low current values could have made the thermal model more robust, as there is no validation of, for instance, 100 A long-term thermal response.

6.3.2 Simulation results

From Figure 5.7, the maximum cable temperatures were presented as a function of the environment temperature and the current in steady state. It was assumed that approximately 5 times the thermal time constant of the cable as simulation time was enough to reach steady state temperature. In Figure 5.8 the environment temperature was set to 20 ºC. The results would have been different with different environment temperatures.

For the periodic loading scenarios, two different types of loading profiles were presented, namely two cycles of equal currents, or two cycles of different currents. These loading profiles may not be relevant for Color Line but serves as an illustration to how one can plan optimal charging profiles without overheating the cable. These types of simulations are flexible and can be extended to as many cycles as is preferred. The illustration shown in Figure 5.13 works only for two charging cycles, as additional cycles will add additional dimension to the plot, which quickly becomes unfeasible to illustrate.

The simulations from the testing of periodic loading scenarios were not a part of the parameter optimization. However, from the results shown in Figure 5.11 and Figure 5.14, the simulated response matches reasonably well with the measurements in the laboratory.

7 Conclusion and future work

7.1 Conclusion

The first laboratory tests were long-term loading tests to reach steady-state temperatures. The three scenarios tested the maximum Color Line cable current given (confidential), 465 A and 520 A. Further, short-term loading test with 30 minutes duration was done with 700 A and 850 A currents. During all the tests, both inner and outer temperatures was logged for both the flat and trefoil formations.

Based on the thermal energy balance and basic thermodynamics, a lumped parameter thermal model of the laboratory cable was made. Model parameters was calculated from the long-term laboratory tests. It was found that the thermal time constants depended on cable formation and whether the measurement was at the conductor or the cable surface. The lowest thermal time constant was 37 minutes for the cable surface measurement in the flat formation, while the highest thermal time constant was 62 minutes for the conductor surface measurement in the trefoil formation. The heat transfer coefficients in the cable are calculated as 18.4 $Wm^{-2}K^{-1}$ between the insulation and the surrounding air. The heat capacity was also divided into two parts, namely the aluminum part and the insulation plus cable sheath part. The heat capacity was calculated as a per meter quantity, with the aluminum heat capacity being 583 $Jm^{-1}K^{-1}$ and the XLPE insulation being 1890 $Jm^{-1}K^{-1}$.

All the laboratory tests were used to do a bounded optimization of the model parameters by minimizing the simulation error with respect to the temperature measurements. After the optimization, the thermal model overestimated the short-term temperature responses with a maximum error of approximately 15 ºC.

The thermal model predicts that in the laboratory setup, with a room temperature of 25 ºC, the maximum steady-state current for flat formation is 600 A while it is 520 A for the trefoil formation. From simulations of short-term loading profiles with a charging time of 30 minutes, the results show that the most critical temperature is the conductor temperature for both cable formations. It is also shown that the flat formation has a larger short-term current capacity.

A loading profile with two cycles of the same loading current with a resting time in between was assessed. Simulations of this loading profile was done, and three cases of this was replicated in the laboratory. It was shown that the resting time only increases the maximum allowed charging current slightly in this loading profile. The main limitation for the charging current is the charging time. Two cycles with different loading currents were also assessed with resting time as a variable. This profile was assessed with a constant charging time of 30 minutes and two different cases has been tested in the laboratory. The simulations from the thermal model and laboratory tests shows that if the resting time is increased, either of the loading currents may be increased. This is, however, limited by the short-term current capacity of the cable. The maximum error between measurement and simulation for the two different loading profiles was found in trefoil inner temperature as 15 ºC.

By developing the thermal model of the cable, the loading profiles can be predetermined and optimized based on the thermal response of the cable. Based on the illustrations and approaches taken in this thesis, charging time and resting time can be scheduled to maximize the charging capabilities while limiting the maximum cable temperature to a safe level.

7.2 Future work

The thermal model of the cable can be upgraded by implementing thermal energy dissipation equations of conduction, convection, and radiation, separately. Here the correct thermal properties should be measured and obtained. In addition, more subsystems in the lumped parameter model can be added to better represent the different layers in the XLPE cable.

The experiments in the laboratory can be tested with colder room temperatures to better imitate the Color Line cable conditions.

More measurements can be taken from the Color Line cable, especially from the cable-in-air section at the 24 kV cable at the intake of the charging station. In addition, a measure of the environment temperature can be beneficial. If these measurements are obtained, test cases done in this thesis can be tested for the Color Line cable to verify or disapprove and update the thermal model.

A study of the importance of short-term loading capacity can be assessed to verify if the ferry/ferries have enough charging possibilities for future expansion.

References

[1] ‘Klimagassutslipp fra transport - Miljøstatus for Norge’. https://miljostatus.miljodirektoratet.no/tema/klima/norske-utslipp-av-klimagasser/klimagassutslipp-fra-transport/ (accessed Feb. 01, 2021).

[2] ‘Visitor Information’, *Telemarkskanalen*. https://www.telemarkcanal.com/visitor-information (accessed Apr. 29, 2021).

[3] ‘Autonomous ship project, key facts about YARA Birkeland’. https://www.kongsberg.com/no/maritime/support/themes/autonomous-ship-project-key-facts-about-yara-birkeland/ (accessed Apr. 29, 2021).

[4] ‘Longship’, *Langskip*, Sep. 11, 2020. https://langskip.regjeringen.no/longship/ (accessed Apr. 29, 2021).

[5] ‘Kort vei til Danmark fra Langesund Ferry Terminal’, *Grenland havn*. https://grenland-havn.no/en/our-terminals/langesund-ferry-terminal/ (accessed Apr. 29, 2021).

[6] ‘Color Line - Color Hybrid| Sandefjord–Strömstad | Our crossings’. https://www.colorline.com/sandefjord-stroemstad (accessed Apr. 09, 2021).

[7] L. Yang *et al.*, ‘Comparison of Conductor-Temperature Calculations Based on Different Radial-Position-Temperature Detections for High-Voltage Power Cable’, *Energies*, vol. 11, no. 1, p. 117, Jan. 2018, doi: 10.3390/en11010117.

[8] X. Zhuang, H. Niu, J. Wang, Y. You, and G. Sun, ‘Experimental Study on the Cyclic Ampacity and Its Factor of 10 kV XLPE Cable’, *EPE*, vol. 05, no. 04, pp. 1221–1225, 2013, doi: 10.4236/epe.2013.54B231.

[9] Lei Cheng-hua, Liu Gang, and Liu Yi-gang, ‘An accuracy assessment method of calculating cable conductor temperature through surface temperature and actual loading current’, in *2010 IEEE International Symposium on Electrical Insulation*, San Diego, CA, Jun. 2010, pp. 1–3. doi: 10.1109/ELINSL.2010.5549814.

[10] X. W. Wang, J. P. Zhao, Q. G. Zhang, S. Y. Wang, Y. P. Gao, and Q. Ying, ‘Fast Calculation for Temperature Rise of Trench Laying Cables Based on Thermal Circuit Model and Assessments of the Cable Life’, in *2019 IEEE Conference on Electrical Insulation and Dielectric Phenomena (CEIDP)*, Richland, WA, USA, Oct. 2019, pp. 190–193. doi: 10.1109/CEIDP47102.2019.9009937.

[11] M. A. Hanna, A. Y. Chikhani, M. Baxter, and M. M. A. Salama, ‘Thermal modelling of cables in conduits: (air gap consideration)’, in *Proceedings 1995 Canadian Conference on Electrical and Computer Engineering*, Montreal, Que., Canada, 1995, vol. 1, pp. 578–581. doi: 10.1109/CCECE.1995.528203.

[12] S. Czapp, S. Szultka, and A. Tomaszewski, ‘CFD-based evaluation of current-carrying capacity of power cables installed in free air’, in *2017 18th International Scientific Conference on Electric Power Engineering (EPE)*, Kouty nad Desnou, Czech Republic, May 2017, pp. 1–6. doi: 10.1109/EPE.2017.7967271.

[13] A. Sedaghat and F. de Leon, ‘Thermal Analysis of Power Cables in Free Air: Evaluation and Improvement of the IEC Standard Ampacity Calculations’, *IEEE Trans. Power*

Delivery, vol. 29, no. 5, pp. 2306–2314, Oct. 2014, doi: 10.1109/TPWRD.2013.2296912.

[14] 'Grøft', *REN*. https://www.ren.no/verktoy/groft (accessed Apr. 01, 2021).

[15] S. M. Hellesø, 'Color Hybrid Kabel - belastningevne', SINTEF Energi AS, Feb. 2020.

[16] 'Overhead Conductors - About Circuit'. https://www.aboutcircuit.com/overhead-conductors/ (accessed Jan. 31, 2021).

[17] M. A. Laughton and D. F. Warne, Eds., *Electrical engineer's reference book*, 16. ed. Oxford: Newnes, 2003.

[18] 'What is Electrical Power Cable? Definition & Construction of Cable - Circuit Globe'. https://circuitglobe.com/electrical-power-cable.html (accessed Jan. 31, 2021).

[19] 'What is the history of electrical cables?', *Eland Cables*. https://www.elandcables.com/the-cable-lab/faqs/faq-what-is-the-history-of-electrical-cables

[20] Fjeld E., Hagen, S. T., *High Votlage Technology*, 2017th ed. May 31.

[21] R. L. Boylestad, *Introductory circuit analysis*. Harlow: Pearson Education, 2016. Accessed: May 18, 2021. [Online]. Available: http://search.ebscohost.com/login.aspx?direct=true&scope=site&db=nlebk&db=nlabk&AN=1419376

[22] 'Lv/mv /hv Electrical Cable/ Power Cabel From Factory Only - Buy Xlpe Cable 3x150 Al 50 Cu,185mm2 Copper Conductor,3 Core Shielded Power Cable Product on Alibaba.com'. https://www.alibaba.com/product-detail/LV-MV-HV-electrical-cable-power_62131889220.html (accessed May 05, 2021).

[23] A. Haddad, D. F. Warne, and Institution of Electrical Engineers, Eds., *Advances in high voltage engineering*. London: Institution of Electrical Engineers, 2004.

[24] 'Construction of Power Cable'. https://electricalconstruction2019.wordpress.com/2019/10/20/construction-of-power-cable/ (accessed Feb. 05, 2021).

[25] 'EHV/HV Cable Sheath Earthing', *Electrical Notes & Articles*, Dec. 21, 2011. https://electricalnotes.wordpress.com/2011/12/21/ehvhv-cable-sheath-earthing/ (accessed May 05, 2021).

[26] 'Medium Voltage Cable Shield Grounding – Voltage Disturbance'. https://voltage-disturbance.com/power-engineering/medium-voltage-cable-shield-grounding/ (accessed May 05, 2021).

[27] H. Gremmel, ABB-Calor-Emag-Schaltanlagen AG, and ABB-Calor-Emag-Mittelspannung GmbH, Eds., *Switchgear manual*, 10., rev. Ed. Berlin: Cornelsen, 2001.

[28] R. A. Serway, *Principles of physics*, 2nd ed. Fort Worth: Saunders College Pub, 1998.

[29] 'IEC 60287-1-1 ed2.0; Electric cables - Calculation of the current rrating - Part 1-1: Current rating equations (100 % load factor) and calculation of losses'. International Electrotechnical Commision (IEC), 2006. [Online]. Available: www.iec.ch

[30] 'Skin effect'. https://en.wikipedia.org/wiki/Skin_effect (accessed Feb. 08, 2021).

[31] E. Fjeld and W. Rondeel, *Physics of Electrical Power Engineering*.

[32] ‘Luvata | Hollow Conductors’. https://www.luvata.com/products/hollow-conductors (accessed Feb. 08, 2021).

[33] J. T. Smith, ‘Cable cleaning solvents: their use and evaluation’, *IEEE Electrical Insulation Magazine*, vol. 9, no. 1, pp. 18–21, Jan. 1993, doi: 10.1109/57.249921.

[34] R. Holm, ‘Electric Contacts: Theory and Application’.

[35] A. J. Wileman and S. Perinpanayagam, ‘Integrated vehicle health management: An approach to dealing with lifetime prediction considerations on relays’, *Microelectronics Reliability*, vol. 55, no. 9, pp. 2165–2171, Aug. 2015, doi: 10.1016/j.microrel.2015.06.013.

[36] M. Ohring, *Engineering materials science*. San Diego: Academic Press, 1995.

[37] L. Chen, Ed., *Microwave electronics: measurement and materials characterisation*. Chichester: John Wiley, 2004.

[38] S. Mo, J. Zhang, D. Liang, and H. Chen, ‘Study on Pyrolysis Characteristics of Cross-linked Polyethylene Material Cable’, *Procedia Engineering*, vol. 52, pp. 588–592, 2013, doi: 10.1016/j.proeng.2013.02.190.

[39] F. P. Incropera, *Fundamentals of Heat and Mass Transfer*. Erscheinungsort nicht ermittelbar: John Wiley & Sons Ltd, 2007.

[40] ‘Numerical modeling of the thermal behavior of XLPE Power Cable’, *EMWorks*. /application/numerical-modeling-of-the-thermal-behavior-of-xlpe-power-cable (accessed Mar. 10, 2021).

[41] G. Wypych, *Handbook of polymers*, 2nd edition. Toronto: CP, ChemTec Publishing, 2016.

[42] The Engineering ToolBox, ‘Specific Heat of some common Substances’, Nov. 04, 2021. https://www.engineeringtoolbox.com/specific-heat-capacity-d_391.html (accessed Apr. 11, 2021).

[43] ‘Polymers - Specific Heats’, *The Engineering ToolBox*, Nov. 04, 2021. https://www.engineeringtoolbox.com/specific-heat-polymers-d_1862.html (accessed Apr. 11, 2021).

[44] V. D. Antoniello, ‘Underground Power Cable Considerations: Alternatives to Overhead’. https://docplayer.net/16373365-Ii-cable-components-and-system-types.html (accessed May 19, 2021).

[45] ‘Underground Power Cable Installations: Soil Thermal Resistivity’, *ICT International*. https://ictinternational.com/casestudies/underground-power-cable-installations-soil-thermal-resistivity/ (accessed Mar. 31, 2021).

[46] Nexans Norway AS, ‘Kabelboka’. Nexans. [Online]. Available: https://www.nexans.no/Norway/2009/Kabelboka_final_2009.pdf

[47] ‘Massachusetts Institute of Technology (MIT) web education - 16.4 Thermal Resistance Circuits’. https://web.mit.edu/16.unified/www/FALL/thermodynamics/notes/node118.html (accessed May 18, 2021).

[48] Universal Cable, ‘UC XLPE Catalogue (Co. No.: 7042-D)’. Universal Cable (M) BERHAD. [Online]. Available: http://www.ucable.com.my/images/products/UC%20XLPE%20Catalogue.pdf

[49] Nexans, ‘60-500 kV High Voltage Underground Power Cables (XLPE insulated cables)’, p. 64.

[50] O.-F. E. Kvalnes, C. Stålesen, I. M. Svansson, and M. A. Svenneby, ‘Bachelor Thesis - Establishment of automated optimal hybrid ferry charging’, 2020.

[51] Lede (Skagerak Nett), ‘Color Line cable information, temperature and load data (confidential) given by Lede’. Jan. 14, 2021.

[52] ‘Wireless Temperature Sensor’, *Disruptive Technologies*. https://support.disruptive-technologies.com/hc/en-us/articles/360010342900-Wireless-Temperature-Sensor (accessed Feb. 27, 2021).

[53] Nexans Norway AS, ‘24 - 36 Distribusjonskabel TSLF’. Jan. 13, 2021.

[54] ‘RS PRO Extension Cable Type K, 100m | RS Components’. https://uk.rs-online.com/web/p/thermocouple-extension-wire/6117889/ (accessed Feb. 28, 2021).

[55] ‘Optimization and root finding (scipy.optimize) — SciPy v1.6.3 Reference Guide’. https://docs.scipy.org/doc/scipy/reference/optimize.html (accessed May 14, 2021).

[56] Fjeld E., Rondel W., Saxegaard M., and Hagen S.T., ‘Estimating the temeprature rise of load break switch contacts in enclosed MV switchgear.’, CIRED, 24 th International Conference on Electricity Distribution Paper 0349. [Online]. Available: http://cired.net/publications/cired2017/pdfs/CIRED2017_0349_final.pdf

Appendices

Appendix A Task Description of the Master Thesis

Appendix B Confidential Document for Supervisor and Lede (confidential)

Appendix C Thermal Heat Transfer Coefficient and Resistance Calculations in Python

Appendix D Parameter Optimization in Python

Appendix E Lab Measurement and Simulations in Python

Appendix F Periodic Loading with Same Currents in Python

Appendix G Periodic Loading with Different Currents in Python

Appendix A

FMH606 Master's Thesis

Title: Thermal dimensioning of HV cables in air

USN supervisor: Elin Fjeld

External partner: Skagerak Nett

Task background:
XLPE insulated cables are the most common power cables in the MV grid. The insulation condition is related to the conductor temperature, which means it limits the loadability of the cable. This will depend on the laying of the cable and the surroundings.

Underground cables have lower stationary loadability than cables in air, but may have relatively long thermal time constants, depending on the cross-section and the soil. This characteristic permits cables to have high short term ratings, which can be utilized e.g. when charging electric vehicles and ferries. In such a case, any part of the cable laid in air (e.g. the cable terminations) may be the limiting factor due to shorter time constant.

The conductor temperature of a cable in service is difficult to measure directly, but may be obtained by calculations, especially if the temperature of the outside (on the surface of the insulation) is measured. In order to make an estimate for the conductor temperature, a thermal model of the cable is required. Based on such a thermal model, the optimal charging pattern may be obtained.

Task objectives:

- Do a survey on thermal dimensioning of cables.
- Search the literature for similar studies and gather relevant data.
- Build a test set-up in the high current laboratory for loadability of cables in air both flat and triangle arrangement.
- Measuring the conductor temperature and the outside of the insulation.
- Run steady state temperature rise tests with cables in different configurations to determine the time constants, total heat transfer coefficient etc.
- Simulate different dynamic load profiles of the cables.
- Compare temperatures measured in the laboratory with temperature data gathered from the field during charging of the hybrid ferry in Sandefjord.
- Make an initial, simplified thermal model for the cables in air.

Student category: EPE

Is the task suitable for online students (not present at the campus)? No

Practical arrangements:
The high power laboratory at USN can provide load currents up to 2500 A. Temperature sensors are available in the laboratory. 60 meters XLPE 24 kV cable (240 mm2) will be provided by Nexans. Load and temperature data from cables in operation in the grid, will be provided by Skagerak Nett.

Supervision:
As a general rule, the student is entitled to 15-20 hours of supervision. This includes necessary time for the supervisor to prepare for supervision meetings (reading material to be discussed, etc).

Signatures:
Supervisor (date and signature):
25/1-21
Eun

Student (write clearly in all capitalized letters):

HYEONYOUNG KWAK

Student (date and signature):
25/01-2021
Hyeonyoung Kwak

Appendix B (confidential)

This appendix contains confidential information.

Appendix C

Thermal heat transfer coefficient and resistance calculations

In [1]:

```
import numpy as np
from scipy.optimize import minimize
```

In [2]:

```
d_inner = 17.4e-3 #m
d_outer = 38.1e-3 #m
R_cold = 1.34e-4 #ohm
alpha = 0.039
T_ref = 22.4 #deg C
R_warm = lambda T: R_cold*(1 + alpha*(T - T_ref))

#Values for the CL case
I_CL = [redacted] #A
T_env_CL = 22.0 #deg C
T_inner_flat_CL = 43 #deg C
T_outer_flat_CL = 39.34 #deg C
T_inner_tre_CL = 51.4 #deg C
T_outer_tre_CL = 45 #deg C

#Values for the 465 A case
I_465 = 465
T_env_465 = 24.0
T_inner_flat_465 = 57.8
T_outer_flat_465 = 51.2
T_inner_tre_465 = 71.2
T_outer_tre_465 = 57.4

#Values for the 520 A case
I_520 = 520
T_env_520 = 25.1
T_inner_flat_520 = 68.7
T_outer_flat_520 = 59.7
T_inner_tre_520 = 83.4
T_outer_tre_520 = 69.4

#Collecting the values into arrays
I = np.array([I_CL, I_465, I_520])
T_env = np.array([T_env_CL, T_env_465, T_env_520])
T_inner_flat = np.array([T_inner_flat_CL, T_inner_flat_465, T_inner_flat_520])
T_outer_flat = np.array([T_outer_flat_CL, T_outer_flat_465, T_outer_flat_520])
T_inner_tre  = np.array([T_inner_tre_CL, T_inner_tre_465, T_inner_tre_520])
T_outer_tre  = np.array([T_outer_tre_CL, T_outer_tre_465, T_outer_tre_520])
```

In [3]:

```
#Calculating the surface areas of the inner and outer parts
A_inner = d_inner*np.pi
A_outer = d_outer*np.pi

#Calculating or defining the calculation of the heat transfer coefficients
h_inner_flat = R_warm(T_inner_flat)*I**2 / (A_inner*(T_inner_flat - T_outer_flat))
h_outer_flat = R_warm(T_outer_flat)*I**2 / (A_outer*(T_outer_flat - T_env))
h_inner_tre = lambda k_inner: R_warm(T_inner_tre) *I**2 / (A_inner*k_inner*(T_inner_tre - T_o
h_outer_tre = lambda k_outer: R_warm(T_outer_tre) *I**2 / (A_outer*k_outer*(T_outer_tre - T_e
```

In [4]:

```
#Make the objective function:
def objective(k):
    k_inner = k[0]
    k_outer = k[1]
    h_in_tre = h_inner_tre(k_inner)
    h_out_tre = h_outer_tre(k_outer)
    error_inner = (np.average(h_inner_flat) - np.average(h_in_tre))**2
    error_outer = (np.average(h_outer_flat) - np.average(h_out_tre))**2
    return error_inner + error_outer

#Minimize the error in the h calculations.
k0 = np.ones(2)
sol = minimize(objective, k0)
```

In [5]:

```
print("The values from the optimization is as follows:")
print("k_inner = " + str(round(sol.x[0], 4)))
print("k_outer = " + str(round(sol.x[1], 4)))
```

```
The values from the optimization is as follows:
k_inner = 0.6805
k_outer = 0.8907
```

Appendix D

Parameter Optimization code

In this notebook the following model parameters will be optimized, based on the calculated parameters from steady-state measurements.

- C_p^{Al} $[\frac{J}{K.m}]$- Inner heat capacity of the XLPE cable
- C_p^{XLPE} $[\frac{J}{K.m}]$ - Outer heat capacity of the XLPE cable
- hA_{Al2ins} $[\frac{W}{K}]$ - Heat conductivity from inner to outer layer
- $hA_{ins2env}$ $[\frac{W}{K}]$ - Heat conductivity from outer layer to environment
- R_{cold} $[\frac{\Omega}{m}]$ - Ohmic resistance of the aluminum conductor at 22.4 degrees celsius

In [1]:

```
#Importing the relevant modules
import numpy as np
from scipy.optimize import minimize, dual_annealing
import pandas as pd
import matplotlib.pyplot as plt
from Thermal_models import ThermalModel

#Used to import measurement data from Excel to a pandas dataframe, and doing some prepr
def import_data_excel(filename, sheet_name):
    data = pd.read_excel(filename, sheet_name=sheet_name, index_col="time")
    data["mean_inner_flat"] = data[sensor_id_flat_inner].mean(axis=1)
    data["mean_outer_flat"] = data[sensor_id_flat_outer].mean(axis=1)
    data["mean_inner_tre"] = data[sensor_id_tre_inner].mean(axis=1)
    data["mean_outer_tre"] = data[sensor_id_tre_outer].mean(axis=1)
    data.drop(columns=["Nr1", "Nr2", "Nr3", "Nr4", "Nr5", "Nr6", "Nr7", "Nr8", "Nr9", '
    data.drop(columns=["Nr11", "Nr12", "Nr13", "Nr14", "Nr15", "Nr16"], inplace=True)
    return data

#Preparing initial conditions and the model inputs for simulation.
def prepare_data(data):
    I = np.array(data["current"])
    T_env = np.array(data['env'])
    u = np.array([I, T_env], dtype=np.float32).T
    x0_flat = np.array([data["mean_inner_flat"].iloc[0], data["mean_inner_flat"].iloc[(
    x0_tre = np.array([data["mean_inner_tre"].iloc[0], data["mean_outer_tre"].iloc[0]],
    return u, x0_flat, x0_tre

#Defining which sensor numbers that are included in the average temperature measuremen
sensor_id_flat_inner = ['Nr1', 'Nr3', 'Nr5']
sensor_id_flat_outer = ['Nr2', 'Nr4', 'Nr6']
sensor_id_tre_inner = ['Nr11', 'Nr13', 'Nr15']
sensor_id_tre_outer = ['Nr12', 'Nr14', 'Nr16']
```

In [2]:

```python
#Calculates the absolute error between simulated and measured temperatures, inner and c
def calc_error_flat(cable_flat, x0_flat, u, data):
    error = 0
    T_sim_flat = cable_flat.sim(x0_flat, u)
    error += np.mean(np.abs(T_sim_flat[:, 0] - data["mean_inner_flat"]))
    error += np.mean(np.abs(T_sim_flat[:, 1] - data["mean_outer_flat"]))
    return error

#Calculates the absolute error between simulated and measured temperatures, inner and c
def calc_error_tre(cable_tre, x0_tre, u, data):
    error = 0
    T_sim_tre = cable_tre.sim(x0_tre, u)
    error += np.mean(np.abs(T_sim_tre[:, 0] - data["mean_inner_tre"]))
    error += np.mean(np.abs(T_sim_tre[:, 1] - data["mean_outer_tre"]))
    return error

#Objective function for optimizing model parameters for flat formation.
def opt_func_flat(adj):
    error = 0
    adj = np.array(adj, dtype=np.float32)
    theta_flat_opt = theta_flat*adj
    dt = 60
    cable_flat = ThermalModel(theta_flat_opt, dt=dt)
    error += calc_error_flat(cable_flat, x0_CL_flat, u_CL, data_CL)
    error += calc_error_flat(cable_flat, x0_465_flat, u_465, data_465)
    error += calc_error_flat(cable_flat, x0_520_flat, u_520, data_520)
    error += calc_error_flat(cable_flat, x0_700_flat, u_700, data_700)
    error += calc_error_flat(cable_flat, x0_850_flat, u_850, data_850)
    return error

#Objective function for optimizing model parameters for trefoil formation.
def opt_func_tre(adj):
    error = 0
    adj = np.array(adj, dtype=np.float32)
    theta_tre_opt = theta_tre*adj
    dt = 60
    cable_tre = ThermalModel(theta_tre_opt, dt=dt)
    error += calc_error_tre(cable_tre, x0_CL_tre, u_CL, data_CL)
    error += calc_error_tre(cable_tre, x0_465_tre, u_465, data_465)
    error += calc_error_tre(cable_tre, x0_520_tre, u_520, data_520)
    error += calc_error_tre(cable_tre, x0_700_tre, u_700, data_700)
    error += calc_error_tre(cable_tre, x0_850_tre, u_850, data_850)
    return error
```

```python
#Defining the model parameters from the steady-state calculations.
C_al = 583 #J/K.m
C_ins = 1890 #J/K.m
h_inner = 92.707
h_outer = 10.010
A_al2ins_flat = 0.055 #flat
A_ins2a_flat = 0.120 #flat
A_al2ins_tre = 0.032
A_ins2a_tre = 0.098
R_cold = 0.134e-3 #Ohm/m

#Collecting model parameters into numpy arrays, and formating to float32 datatype.
theta_flat = np.array([C_al, C_ins, h_inner*A_al2ins_flat, h_outer*A_ins2a_flat, R_cold
theta_tre = np.array([C_al, C_ins, h_inner*A_al2ins_tre, h_outer*A_ins2a_tre, R_cold],
```

In [4]:

```
#Importing lab test data from excel
filename = "Data_full.xlsx"

#LT - Long Term measurements
data_CL = import_data_excel(filename, 'LT_CL')
data_465 = import_data_excel(filename, 'LT465')
data_520 = import_data_excel(filename, 'LT520')

#ST - Short Term measurements
data_700 = import_data_excel(filename, 'ST700')
data_850 = import_data_excel(filename, 'ST850')

u_CL, x0_CL_flat, x0_CL_tre = prepare_data(data_CL)
u_465, x0_465_flat, x0_465_tre = prepare_data(data_465)
u_520, x0_520_flat, x0_520_tre = prepare_data(data_520)

u_700, x0_700_flat, x0_700_tre = prepare_data(data_700)
u_850, x0_850_flat, x0_850_tre = prepare_data(data_850)
```

Optimization with large boundaries

Boundaries for allowed parameter adjustments is between 0.001 and 10

In [7]:

```
# Running the dual_annealing optimization algorithm on both flat and trefoil formations
# parameter adjustments.
res_flat = dual_annealing(opt_func_flat, bounds=[[1e-3,10]]*5, x0=np.ones(5), maxiter=
res_tre = dual_annealing(opt_func_tre, bounds=[[1e-3, 10]]*5, x0=np.ones(5), maxiter=3

print(f"Adjustment flat: {res_flat.x}")
print(f"Adjustment trefold: {res_tre.x}")
```

```
Adjustment flat: [9.999932  1.712864  3.096757  3.19802   3.2842934]
Adjustment trefold: [7.2784424  0.79451984 1.970478   1.9604963  2.1360586 ]
```

Optimization with small boundaries

Boundaries for allowed parameter adjustments is between 0.5 and 1.5

In [8]:

```
#Running the dual_annealing optimization algorithm on both flat and trefoil formations,
#parameter adjustments.
res_flat = dual_annealing(opt_func_flat, bounds=[[0.5, 1.5]]*5, x0=np.ones(5), maxiter=
res_tre = dual_annealing(opt_func_tre, bounds=[[0.5, 1.5]]*5, x0=np.ones(5), maxiter=3

print(f"Adjustment flat: {res_flat.x}")
print(f"Adjustment trefold: {res_tre.x}")
```

```
Adjustment flat: [1.4989872  0.5        0.61660844 0.60746086 0.6258046 ]
Adjustment trefold: [1.4999229  0.7145247  0.77748907 0.6902083  0.7545206 ]
```

Appendix E

Lab measurement and simulation code

In this notebook, lab measurements is plotted together with simulated temperatures. The notebook contains two sections, where the first section is simulations with non-optimized model parameters, and the second section is simulation with the optimized model parameters from the Parameter Optimization notebook.

In [1]:

```
#Importing the relevant modules
import pandas as pd
import numpy as np
import matplotlib.pyplot as plt
from Thermal_models import ThermalModel

#Used to import measurement data from Excel to a pandas dataframe, and doing some preprocessing
def import_data_excel(filename, sheet_name):
    #Created an excel-file with only the data points
    data = pd.read_excel(filename, sheet_name=sheet_name, index_col="time")
    data["mean_inner_flat"] = data[sensor_id_flat_inner].mean(axis=1)
    data["mean_outer_flat"] = data[sensor_id_flat_outer].mean(axis=1)
    data["mean_inner_tre"] = data[sensor_id_tre_inner].mean(axis=1)
    data["mean_outer_tre"] = data[sensor_id_tre_outer].mean(axis=1)
    data.drop(columns=["Nr1", "Nr2", "Nr3", "Nr4", "Nr5", "Nr6", "Nr7", "Nr8", "Nr9", "Nr10"],
    data.drop(columns=["Nr11", "Nr12", "Nr13", "Nr14", "Nr15", "Nr16"], inplace=True)
    return data

#Preparing initial conditions and the model inputs for simulation.
def prepare_data(data):
    I = np.array(data["current"])
    T_env = np.array(data['env'])
    u = np.array([I, T_env], dtype=np.float32).T
    x0_flat = np.array([data["mean_inner_flat"].iloc[0], data["mean_inner_flat"].iloc[0]], dtyp
    x0_tre = np.array([data["mean_inner_tre"].iloc[0], data["mean_outer_tre"].iloc[0]], dtype=r
    return u, x0_flat, x0_tre

#Defining which sensor numbers that are included in the average temperature measurements.
sensor_id_flat_inner = ['Nr1', 'Nr3', 'Nr5']
sensor_id_flat_outer = ['Nr2', 'Nr4', 'Nr6']
sensor_id_tre_inner = ['Nr11', 'Nr13', 'Nr15']
sensor_id_tre_outer = ['Nr12', 'Nr14', 'Nr16']
```

In [2]:

```
def plot_long_term(T_CL_flat, T_CL_tre, T_465_flat, T_465_tre, T_520_flat, T_520_tre):
    #Plotting both simulated and measured temperature data for inner and outer layers, for both
    #The following plots are for long-term charging.
    fig, ax = plt.subplots(2,3)
    ax[0,0].set_title("Flat, inner and outer, $I_{max,winter}$ ")
    ax[0,0].plot(data_CL.index/60, T_CL_flat[:, 0], 'r', label="simulated T_inner")
    ax[0,0].plot(data_CL.index/60, T_CL_flat[:, 1], 'b', label="simulated T_outer")
    ax[0,0].plot(data_CL.index/60, np.array(data_CL['mean_inner_flat']), 'r--', label="measured
    ax[0,0].plot(data_CL.index/60, np.array(data_CL['mean_outer_flat']), 'b--', label="measured
    ax[0,0].legend()
    ax[0,0].grid()
    ax[0,0].set_xlabel("Time [min]")
    ax[0,0].set_ylabel("T [deg C]")
    ax[0,0].set_yticks(np.arange(20,51,5))
```

```
    ax[0,1].set_title("Flat, inner and outer, 465 A")
    ax[0,1].plot(data_465.index/60, T_465_flat[:, 0], 'r', label="simulated T_inner")
    ax[0,1].plot(data_465.index/60, T_465_flat[:, 1], 'b', label="simulated T_outer")
    ax[0,1].plot(data_465.index/60, np.array(data_465['mean_inner_flat']), 'r--', label="measur
    ax[0,1].plot(data_465.index/60, np.array(data_465['mean_outer_flat']), 'b--', label="measur
    ax[0,1].legend()
    ax[0,1].grid()
    ax[0,1].set_xlabel("Time [min]")
    ax[0,1].set_ylabel("T [deg C]")
    ax[0,1].set_yticks(np.arange(20,61,5))

    ax[0,2].set_title("Flat, inner and outer, 520 A")
    ax[0,2].plot(data_520.index/60, T_520_flat[:, 0], 'r', label="simulated T_inner")
    ax[0,2].plot(data_520.index/60, T_520_flat[:, 1], 'b', label="simulated T_outer")
    ax[0,2].plot(data_520.index/60, np.array(data_520['mean_inner_flat']), 'r--', label="measur
    ax[0,2].plot(data_520.index/60, np.array(data_520['mean_outer_flat']), 'b--', label="measur
    ax[0,2].legend()
    ax[0,2].grid()
    ax[0,2].set_xlabel("Time [min]")
    ax[0,2].set_ylabel("T [deg C]")
    ax[0,2].set_yticks(np.arange(20,71,5))

    ax[1,0].set_title("Trefoil, inner and outer, $I_{max,winter}$ ")
    ax[1,0].plot(data_CL.index/60, T_CL_tre[:, 0], 'r', label="simulated T_inner")
    ax[1,0].plot(data_CL.index/60, T_CL_tre[:, 1], 'b', label="simulated T_outer")
    ax[1,0].plot(data_CL.index/60, np.array(data_CL['mean_inner_tre']), 'r--', label="measured
    ax[1,0].plot(data_CL.index/60, np.array(data_CL['mean_outer_tre']), 'b--', label="measured
    ax[1,0].legend()
    ax[1,0].grid()
    ax[1,0].set_xlabel("Time [min]")
    ax[1,0].set_ylabel("T [deg C]")
    ax[1,0].set_yticks(np.arange(20,56,5))

    ax[1,1].set_title("Trefoil, inner and outer, 465 A")
    ax[1,1].plot(data_465.index/60, T_465_tre[:, 0], 'r', label="simulated T_inner")
    ax[1,1].plot(data_465.index/60, T_465_tre[:, 1], 'b', label="simulated T_outer")
    ax[1,1].plot(data_465.index/60, np.array(data_465['mean_inner_tre']), 'r--', label="measure
    ax[1,1].plot(data_465.index/60, np.array(data_465['mean_outer_tre']), 'b--', label="measure
    ax[1,1].legend()
    ax[1,1].grid()
    ax[1,1].set_xlabel("Time [min]")
    ax[1,1].set_ylabel("T [deg C]")
    ax[1,1].set_yticks(np.arange(20,76,5))

    ax[1,2].set_title("Trefoil, inner and outer, 520 A")
    ax[1,2].plot(data_520.index/60, T_520_tre[:, 0], 'r', label="simulated T_inner")
    ax[1,2].plot(data_520.index/60, T_520_tre[:, 1], 'b', label="simulated T_outer")
    ax[1,2].plot(data_520.index/60, np.array(data_520['mean_inner_tre']), 'r--', label="measure
    ax[1,2].plot(data_520.index/60, np.array(data_520['mean_outer_tre']), 'b--', label="measure
    ax[1,2].legend()
    ax[1,2].grid()
    ax[1,2].set_xlabel("Time [min]")
    ax[1,2].set_ylabel("T [deg C]")
    ax[1,2].set_yticks(np.arange(20,96,5))

    fig.set_figheight(10)
    fig.set_figwidth(15)
    plt.show()
```

```
def plot_short_term(T_700_flat, T_700_tre, T_850_flat, T_850_tre):
    #Plotting both simulated and measured temperature data for inner and outer layers, for both
    #The following plots are for short-term charging.
    fig, ax = plt.subplots(2,2)
    ax[0,0].set_title("Flat, inner and outer, 700 A")
    ax[0,0].plot(data_700.index/60, T_700_flat[:, 0], 'r', label="simulated T_inner")
    ax[0,0].plot(data_700.index/60, T_700_flat[:, 1], 'b', label="simulated T_outer")
    ax[0,0].plot(data_700.index/60, np.array(data_700['mean_inner_flat']), 'r--', label="measur
    ax[0,0].plot(data_700.index/60, np.array(data_700['mean_outer_flat']), 'b--', label="measur
    ax[0,0].legend()
    ax[0,0].grid()
    ax[0,0].set_xlabel("Time [min]")
    ax[0,0].set_ylabel("T [deg C]")
    ax[0,0].set_xlim(0,111)
    ax[0,0].set_xticks(np.arange(0,111,10))
    ax[0,0].set_yticks(np.arange(20,86,5))

    ax[0,1].set_title("Flat, inner and outer, 850 A")
    ax[0,1].plot(data_850.index/60, T_850_flat[:, 0], 'r', label="simulated T_inner")
    ax[0,1].plot(data_850.index/60, T_850_flat[:, 1], 'b', label="simulated T_outer")
    ax[0,1].plot(data_850.index/60, np.array(data_850['mean_inner_flat']), 'r--', label="measur
    ax[0,1].plot(data_850.index/60, np.array(data_850['mean_outer_flat']), 'b--', label="measur
    ax[0,1].legend()
    ax[0,1].grid()
    ax[0,1].set_xlabel("Time [min]")
    ax[0,1].set_ylabel("T [deg C]")
    ax[0,1].set_xlim(0,111)
    ax[0,1].set_xticks(np.arange(0,111,10))
    ax[0,1].set_yticks(np.arange(20,121,5))

    ax[1,0].set_title("Trefoil, inner and outer, 700 A")
    ax[1,0].plot(data_700.index/60, T_700_tre[:, 0], 'r', label="simulated T_inner")
    ax[1,0].plot(data_700.index/60, T_700_tre[:, 1], 'b', label="simulated T_outer")
    ax[1,0].plot(data_700.index/60, np.array(data_700['mean_inner_tre']), 'r--', label="measure
    ax[1,0].plot(data_700.index/60, np.array(data_700['mean_outer_tre']), 'b--', label="measure
    ax[1,0].legend()
    ax[1,0].grid()
    ax[1,0].set_xlabel("Time [min]")
    ax[1,0].set_ylabel("T [deg C]")
    ax[1,0].set_xlim(0,111)
    ax[1,0].set_xticks(np.arange(0,111,10))
    ax[1,0].set_yticks(np.arange(20,86,5))

    ax[1,1].set_title("Trefoil, inner and outer, 850 A")
    ax[1,1].plot(data_850.index/60, T_850_tre[:, 0], 'r', label="simulated T_inner")
    ax[1,1].plot(data_850.index/60, T_850_tre[:, 1], 'b', label="simulated T_outer")
    ax[1,1].plot(data_850.index/60, np.array(data_850['mean_inner_tre']), 'r--', label="measure
    ax[1,1].plot(data_850.index/60, np.array(data_850['mean_outer_tre']), 'b--', label="measure
    ax[1,1].legend()
    ax[1,1].grid()
    ax[1,1].set_xlabel("Time [min]")
    ax[1,1].set_ylabel("T [deg C]")
    ax[1,1].set_xlim(0,111)
    ax[1,1].set_xticks(np.arange(0,111,10))
    ax[1,1].set_yticks(np.arange(20,121,5))

    fig.set_figheight(10)
    fig.set_figwidth(14)
    plt.show()
```

Simulating non-optimized parameters

In [3]:

```
#Defining the model parameters from the steady-state calculations.
C_al = 583 #J/K.m
C_ins = 1890 #J/K.m
h_inner = 92.707
h_outer = 10.010
A_al2ins_flat = 0.055 #flat
A_ins2a_flat = 0.120 #flat
A_al2ins_tre = 0.032
A_ins2a_tre = 0.098
R_cold = 0.134e-3 #Ohm/m

#Collecting model parameters into numpy arrays, and formating to float32 datatype.
theta_flat = np.array([C_al, C_ins, h_inner*A_al2ins_flat, h_outer*A_ins2a_flat, R_cold], dtype
theta_tre = np.array([C_al, C_ins, h_inner*A_al2ins_tre, h_outer*A_ins2a_tre, R_cold], dtype=np

#Creating instances of the cable thermal models for both flat and trefoil formation.
dt = 60
cable_flat = ThermalModel(theta_flat, dt)
cable_tre = ThermalModel(theta_tre, dt)
```

In [4]:

```
#Importing lab test data from excel
filename = "Data_full.xlsx"
data_CL = import_data_excel(filename, 'LT_CL')
data_465 = import_data_excel(filename, 'LT465')
data_520 = import_data_excel(filename, 'LT520')
data_700 = import_data_excel(filename, 'ST700')
data_850 = import_data_excel(filename, 'ST850')

u_CL, x0_CL_flat, x0_CL_tre = prepare_data(data_CL)
u_465, x0_465_flat, x0_465_tre = prepare_data(data_465)
u_520, x0_520_flat, x0_520_tre = prepare_data(data_520)
u_700, x0_700_flat, x0_700_tre = prepare_data(data_700)
u_850, x0_850_flat, x0_850_tre = prepare_data(data_850)

#Simulating all scenarios from the lab testing.
T_CL_flat = cable_flat.sim(x0_CL_flat, u_CL)
T_CL_tre = cable_tre.sim(x0_CL_tre, u_CL)

T_465_flat = cable_flat.sim(x0_465_flat, u_465)
T_465_tre  = cable_tre.sim( x0_465_tre,  u_465)

T_520_flat = cable_flat.sim(x0_520_flat, u_520)
T_520_tre  = cable_tre.sim( x0_520_tre,  u_520)

T_700_flat = cable_flat.sim(x0_700_flat, u_700)
T_700_tre  = cable_tre.sim( x0_700_tre,  u_700)

T_850_flat = cable_flat.sim(x0_850_flat, u_850)
T_850_tre  = cable_tre.sim( x0_850_tre,  u_850)
```

In [5]:

```
#Plotting both simulated and measured temperature data for inner and outer layers, for both for
#The following plots are for long-term charging.
plot_long_term(T_CL_flat, T_CL_tre, T_465_flat, T_465_tre, T_520_flat, T_520_tre)
```

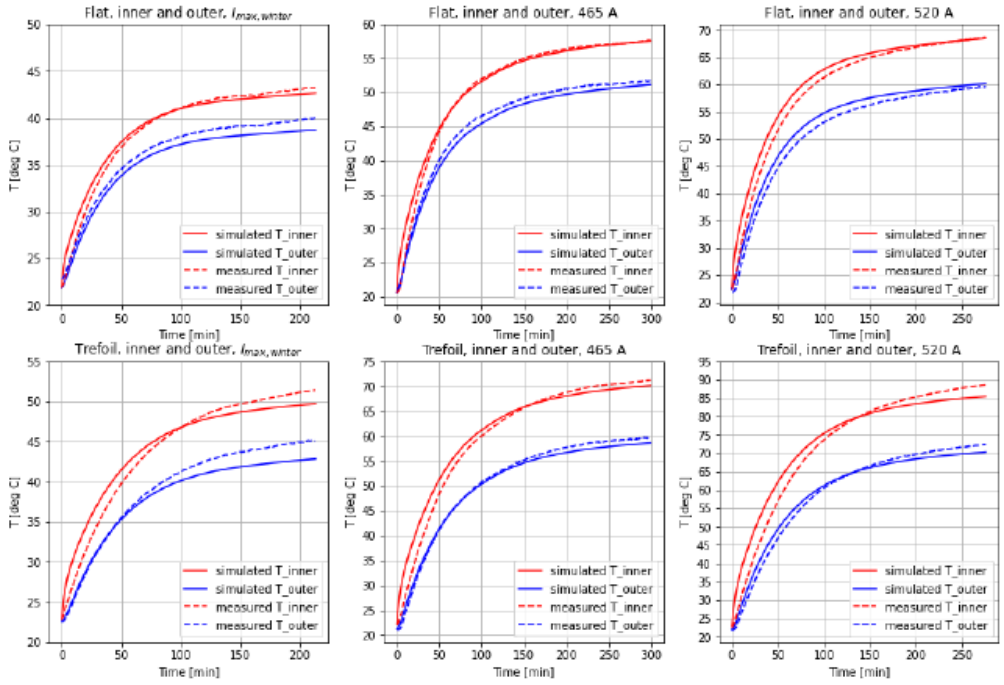

In [6]:

```
#Plotting both simulated and measured temperature data for inner and outer layers, for both for
#The following plots are for short-term charging.
plot_short_term(T_700_flat, T_700_tre, T_850_flat, T_850_tre)
```

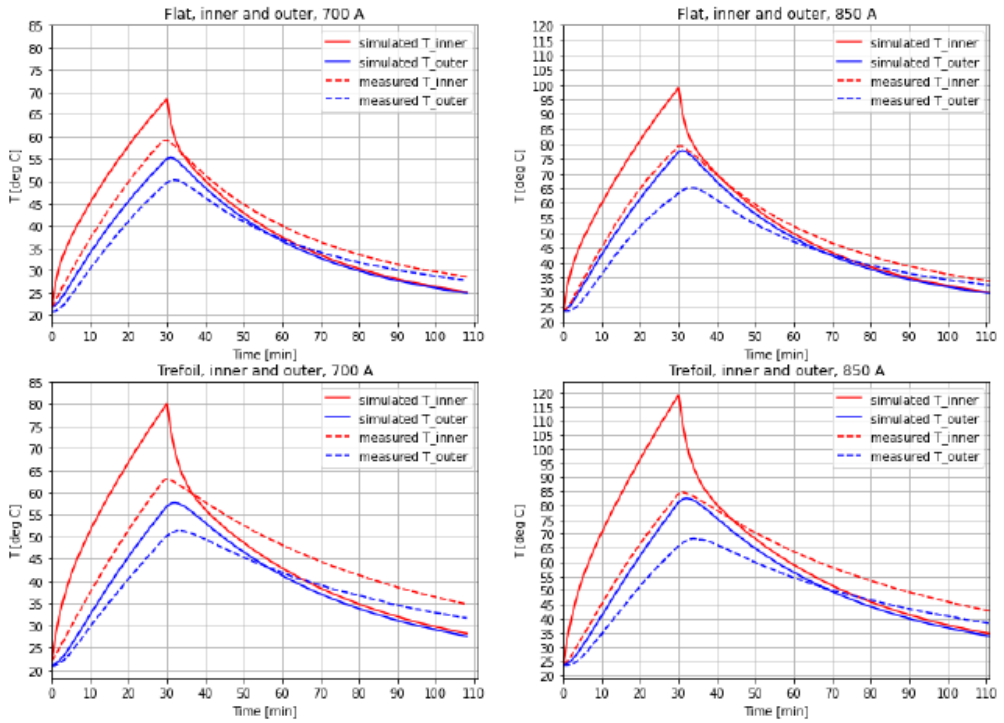

Simulation with large-bound optimized parameters

In [7]:

```
#Defining the optimized parameters found in the Prameter Optimization notebook.
adj_flat = np.array([9.99993215, 1.71286402, 3.09675702, 3.1980199,  3.28429336], dtype=np.floa
adj_tre = np.array( [7.27844226, 0.79451982, 1.97047804, 1.96049627, 2.13605855], dtype=np.floa

theta_flat_opt = theta_flat*adj_flat
theta_tre_opt = theta_tre*adj_tre

#Creating instances of the cable thermal models for both flat and trefoil formation.
dt = 60
cable_flat = ThermalModel(theta_flat_opt, dt)
cable_tre = ThermalModel(theta_tre_opt, dt)
```

In [8]:

```
#Simulating all scenarios from the lab testing with optimized parameters.
T_CL_flat = cable_flat.sim(x0_CL_flat, u_CL)
T_CL_tre = cable_tre.sim(x0_CL_tre, u_CL)

T_465_flat = cable_flat.sim(x0_465_flat, u_465)
T_465_tre  = cable_tre.sim( x0_465_tre,  u_465)

T_520_flat = cable_flat.sim(x0_520_flat, u_520)
T_520_tre  = cable_tre.sim( x0_520_tre,  u_520)

T_700_flat = cable_flat.sim(x0_700_flat, u_700)
T_700_tre  = cable_tre.sim( x0_700_tre,  u_700)

T_850_flat = cable_flat.sim(x0_850_flat, u_850)
T_850_tre  = cable_tre.sim( x0_850_tre,  u_850)
```

In [9]:

```
#Plotting both simulated and measured temperature data for inner and outer layers, for both for
#The following plots are for long-term charging.
plot_long_term(T_CL_flat, T_CL_tre, T_465_flat, T_465_tre, T_520_flat, T_520_tre)
```

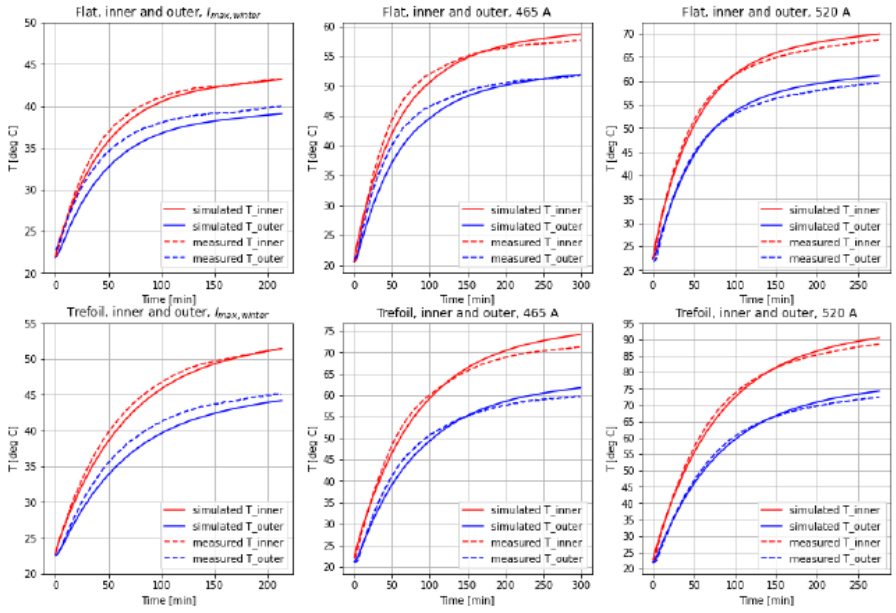

In [10]:

```
#Plotting both simulated and measured temperature data for inner and outer layers, for both for
#The following plots are for short-term charging.
plot_short_term(T_700_flat, T_700_tre, T_850_flat, T_850_tre)
```

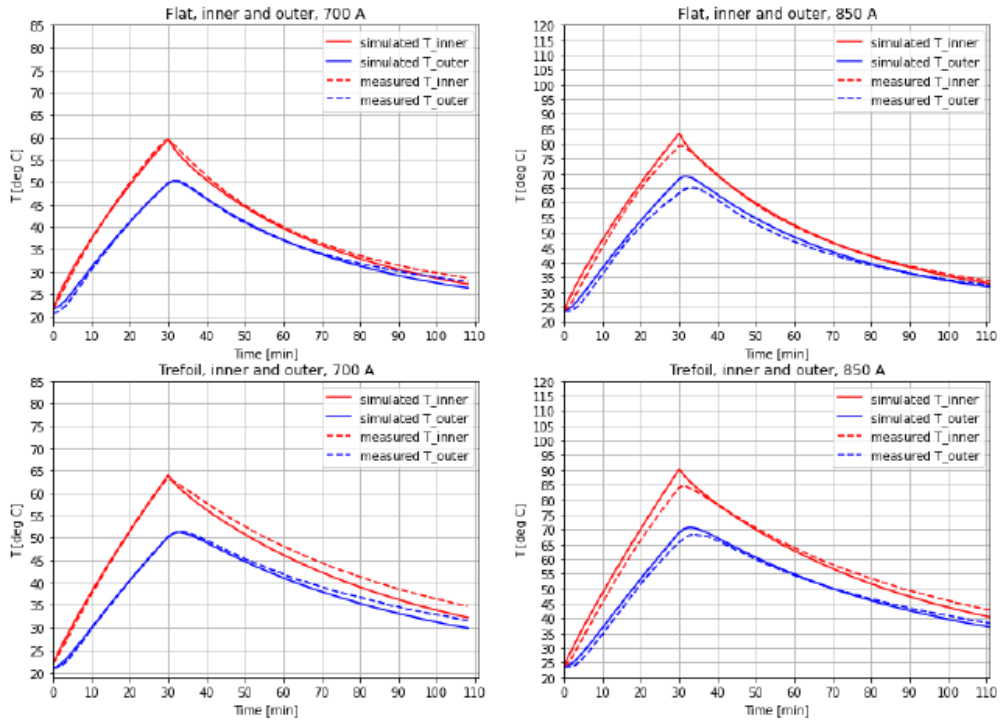

Simulation with small bounded optimized parameters

In [11]:

```
#Defining the optimized parameters found in the Prameter Optimization notebook.
adj_flat = np.array([1.49898723, 0.5, 0.61660843, 0.60746084, 0.62580462], dtype=np.float32)
adj_tre = np.array( [1.49992286, 0.71452468, 0.77748906, 0.69020832, 0.75452057], dtype=np.floa

theta_flat_opt = theta_flat*adj_flat
theta_tre_opt = theta_tre*adj_tre

#Creating instances of the cable thermal models for both flat and trefoil formation.
dt = 60
cable_flat = ThermalModel(theta_flat_opt, dt)
cable_tre = ThermalModel(theta_tre_opt, dt)
```

In [12]:

```
#Simulating all scenarios from the lab testing with optimized parameters.
T_CL_flat = cable_flat.sim(x0_CL_flat, u_CL)
T_CL_tre = cable_tre.sim(x0_CL_tre, u_CL)

T_465_flat = cable_flat.sim(x0_465_flat, u_465)
T_465_tre  = cable_tre.sim( x0_465_tre,  u_465)

T_520_flat = cable_flat.sim(x0_520_flat, u_520)
T_520_tre  = cable_tre.sim( x0_520_tre,  u_520)

T_700_flat = cable_flat.sim(x0_700_flat, u_700)
T_700_tre  = cable_tre.sim( x0_700_tre,  u_700)

T_850_flat = cable_flat.sim(x0_850_flat, u_850)
T_850_tre  = cable_tre.sim( x0_850_tre,  u_850)
```

In [13]:

```
#Plotting both simulated and measured temperature data for inner and outer layers, for both for
#The following plots are for long-term charging.
plot_long_term(T_CL_flat, T_CL_tre, T_465_flat, T_465_tre, T_520_flat, T_520_tre)
```

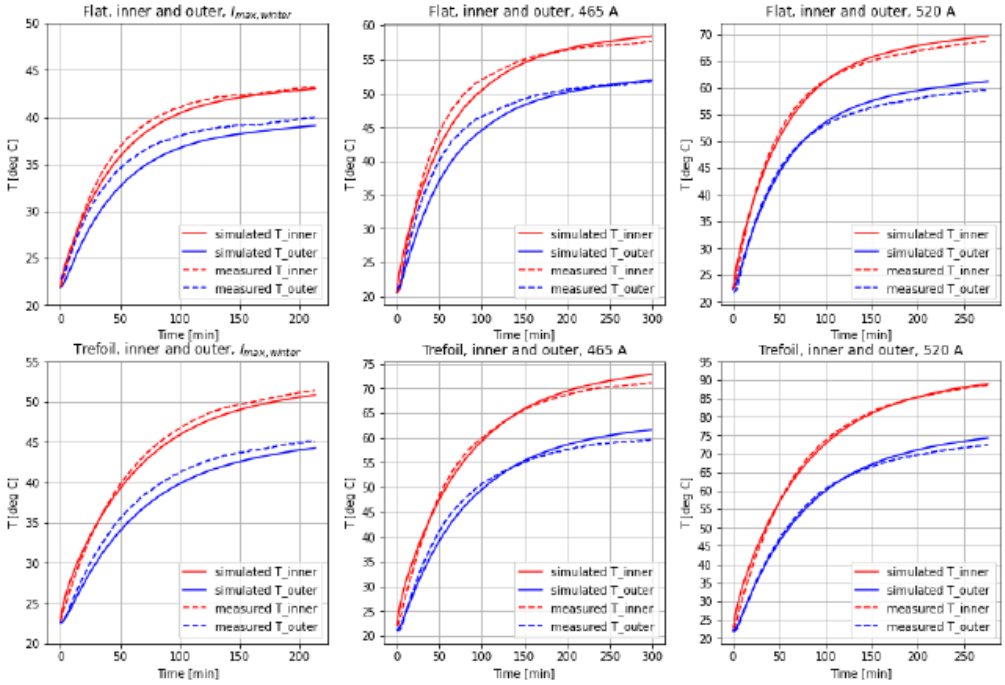

In [14]:

```
#Plotting both simulated and measured temperature data for inner and outer layers, for both for
#The following plots are for short-term charging.
plot_short_term(T_700_flat, T_700_tre, T_850_flat, T_850_tre)
```

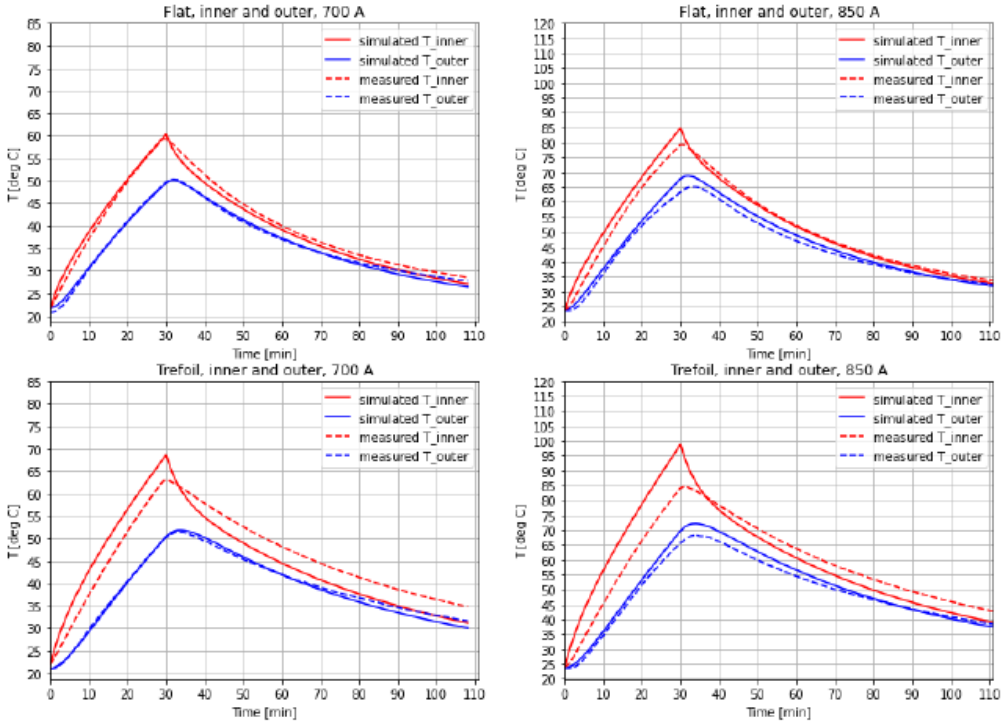

Maximum temperature for different currents simulations

Note that the simulation is done with the closely bounded optimized parameters

In [15]:

```
#Creating instances of the cable thermal models for both flat and trefoil formation.
dt = 60
cable_flat = ThermalModel(theta_flat_opt, dt)
cable_tre = ThermalModel(theta_tre_opt, dt)

T_env = 20
x0 = np.array([T_env, T_env], dtype=np.float32)
T = 30

u_shape = np.ones((T, 2), dtype=np.float32)

T_max_flat_inner = []
T_max_flat_outer = []
T_max_tre_inner = []
T_max_tre_outer = []


```

```
I_test = np.linspace(100, 1200, 100)
for I_el in I_test:
    for i in range(T):
        u = u_shape
        u[:, 0] = I_el
        u[:, 1] = T_env
        T_flat = cable_flat.sim(x0, u)
        T_tre = cable_tre.sim(x0, u)
    T_max_flat_inner.append(np.max(T_flat[:,0]))
    T_max_flat_outer.append(np.max(T_flat[:,1]))
    T_max_tre_inner.append(np.max(T_tre[:,0]))
    T_max_tre_outer.append(np.max(T_tre[:,1]))

T_max_flat_inner = np.array(T_max_flat_inner)
T_max_flat_outer = np.array(T_max_flat_outer)
T_max_tre_inner =  np.array(T_max_tre_inner)
T_max_tre_outer =  np.array(T_max_tre_outer)
```

In [16]:

```
#Defining data from lab-tests:
data_700_inner_flat = (700, np.max(data_700['mean_inner_flat'])-data_700.iloc[-1]['env'])
data_700_outer_flat = (700, np.max(data_700['mean_outer_flat'])-data_700.iloc[-1]['env'])
data_700_inner_tre =  (700, np.max(data_700['mean_inner_tre'])- data_700.iloc[-1]['env'])
data_700_outer_tre =  (700, np.max(data_700['mean_outer_tre'])- data_700.iloc[-1]['env'])

data_850_inner_flat = (850, np.max(data_850['mean_inner_flat'])-data_850.iloc[-1]['env'])
data_850_outer_flat = (850, np.max(data_850['mean_outer_flat'])-data_850.iloc[-1]['env'])
data_850_inner_tre =  (850, np.max(data_850['mean_inner_tre'])- data_850.iloc[-1]['env'])
data_850_outer_tre =  (850, np.max(data_850['mean_outer_tre'])- data_850.iloc[-1]['env'])

#Plotting results
fig, ax = plt.subplots(2,1)
fontsize = 13

T_ticks_tre = np.arange(0, T_max_tre_inner[-1]+1-T_env, 10)
T_ticks_flat = np.arange(0, T_max_flat_inner[-1]+1-T_env, 10)
I_ticks = np.arange(I_test[0], I_test[-1]+1, 50)

t = np.linspace(0, T, len(T_max_flat_inner))

ax[0].set_title("Temperature difference after 30 minutes, Flat formation", fontsize=fontsize)
ax[0].plot(I_test, T_max_flat_inner-T_env, label="T_max flat, inner", color='r')
ax[0].plot(I_test, T_max_flat_outer-T_env, label="T_max flat, outer", color='b')
ax[0].set_xlabel("Current [A]", fontsize=fontsize)
ax[0].set_ylabel("$₩Delta T = T - T_{env}$", fontsize=fontsize)
ax[0].set_xticks(I_ticks)
ax[0].set_yticks(T_ticks_flat)
ax[0].legend()
ax[0].grid()

ax[1].set_title("Temperature difference after 30 minutes, Trefoil formation", fontsize=fontsize
ax[1].plot(I_test, T_max_tre_inner-T_env, label="T_max tre, inner", color='r')
ax[1].plot(I_test, T_max_tre_outer-T_env, label="T_max tre, outer", color='b')
ax[1].set_xlabel("Current [A]", fontsize=fontsize)
ax[1].set_ylabel("$₩Delta T = T - T_{env}$", fontsize=fontsize)
ax[1].set_xticks(I_ticks)
ax[1].set_yticks(T_ticks_tre)
ax[1].legend()
ax[1].grid()

```

```
#Inserting lab measurements
ax[0].scatter(data_700_inner_flat[0], data_700_inner_flat[1], marker='o', color='r', s=70)
ax[0].scatter(data_850_inner_flat[0], data_850_inner_flat[1], marker='o', color='r', s=70)
ax[0].scatter(data_700_outer_flat[0], data_700_outer_flat[1], marker='o', color='b', s=70)
ax[0].scatter(data_850_outer_flat[0], data_850_outer_flat[1], marker='o', color='b', s=70)

ax[1].scatter(data_700_inner_tre[0], data_700_inner_tre[1], marker='o', color='r', s=70)
ax[1].scatter(data_850_inner_tre[0], data_850_inner_tre[1], marker='o', color='r', s=70)
ax[1].scatter(data_700_outer_tre[0], data_700_outer_tre[1], marker='o', color='b', s=70)
ax[1].scatter(data_850_outer_tre[0], data_850_outer_tre[1], marker='o', color='b', s=70)

fig.set_figheight(8)
fig.set_figwidth(12)
fig.tight_layout()
plt.show()
```

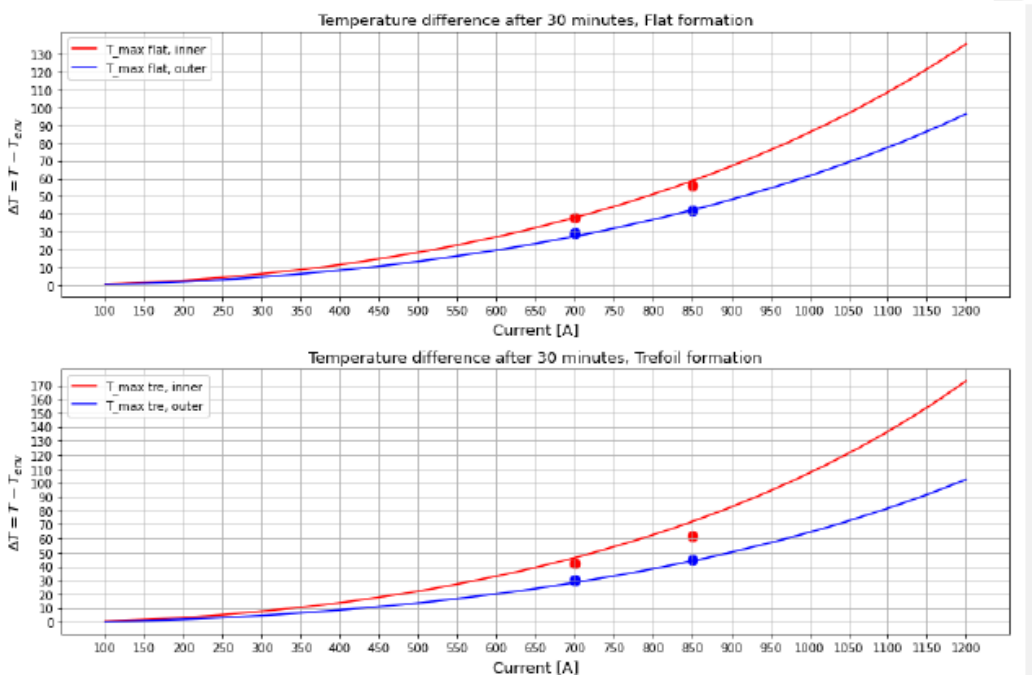

Conductor temperatures for different currents and environment temperatures

In [17]:

```
#Creating instances of the cable thermal models for both flat and trefoil formation.
dt = 60 #sec
cable_flat = ThermalModel(theta_flat_opt, dt)
cable_tre = ThermalModel(theta_tre_opt, dt)

T_env_array = np.linspace(-10, 40, 100)
I_array = np.linspace(100, 1000, 100)

x0 = np.array([20, 20], dtype=np.float32)
T = 60 * 7  #5 hours

u_shape = np.ones((T, 2), dtype=np.float32)

T_ss_flat = []
T_ss_tre = []
```

```
16
17 #Finds the steady-state temperatures for flat
18 for T_env in T_env_array:
19     for I in I_array:
20         u = u_shape
21         u[:, 0] = I
22         u[:, 1] = T_env
23         T_flat = cable_flat.sim(x0, u)
24         T_ss_flat.append(T_flat[-1, 0]) #Obtains the inner conductor temperature
25
26 #Finds the steady-state temperatures for trefoil
27 for T_env in T_env_array:
28     for I in I_array:
29         u = u_shape
30         u[:, 0] = I
31         u[:, 1] = T_env
32         T_tre = cable_tre.sim(x0, u)
33         T_ss_tre.append(T_tre[-1, 0]) #Obtains the inner conductor temperature
34
35 T_ss_flat = np.array(T_ss_flat).reshape((len(T_env_array), len(I_array)))
36 T_ss_tre = np.array(T_ss_tre).reshape((len(T_env_array), len(I_array)))
```

In [18]:

```
1  #Defining data from lab-tests:
2  data_465_flat = (data_465.iloc[-1]['env'], 465)
3  data_465_tre = (data_465.iloc[-1]['env'], 465)
4
5  data_520_flat = (data_520.iloc[-1]['env'], 520)
6  data_520_tre = (data_520.iloc[-1]['env'], 520)
7
8  #Plotting the contour plot for the steady state tempertures, flat formation
9  #Code inspiration from: https://matplotlib.org/stable/gallery/images_contours_and_fields/contou
10 delta = 0.025
11 x = T_env_array
12 y = I_array
13
14 X, Y = np.meshgrid(x, y)
15
16 fig, ax = plt.subplots(1, 2)
17
18 #Plotting Flat
19 Z = np.array(T_ss_flat, dtype=np.int16).T
20 levels = np.array([0, 10, 20, 30, 40, 50, 60, 70, 80, 90, 100, 120, 140])
21
22 CS = ax[0].contour(X, Y, Z, colors=['k'], levels=levels)
23 ax[0].clabel(CS, inline=True, fontsize=12, fmt='%1.1d')
24 ax[0].set_xlabel("$T_{env}$ $[^{#odot}C]$", fontsize=13)
25 ax[0].set_ylabel("Current [A]", fontsize=13)
26 ax[0].set_xticks(np.arange(T_env_array[0], T_env_array[-1]+5, 5))
27 ax[0].set_yticks(np.arange(I_array[0], I_array[-1]+5, 50))
28 ax[0].set_xlim(T_env_array[0], T_env_array[-1])
29 ax[0].set_ylim(I_array[0], 800)
30
31 ax[0].scatter(data_465_flat[0], data_465_flat[1], marker='o', s=100)
32 ax[0].scatter(data_520_flat[0], data_520_flat[1], marker='o', s=100)
33 ax[0].grid()
34 ax[0].set_title('Steady-state temperatures for flat formation', fontsize=13)
35
```

```
#Plotting Trefoil
Z = np.array(T_ss_tre, dtype=np.int16).T
levels = np.array([0, 10, 20, 30, 40, 50, 60, 70, 80, 90, 100, 120, 140, 160, 180])

CS = ax[1].contour(X, Y, Z, colors=['k'], levels=levels)
ax[1].clabel(CS, inline=True, fontsize=12, fmt='%1.1d')
ax[1].set_xlabel("$T_{env}$ $[^{\circ}C]$", fontsize=13)
ax[1].set_ylabel("Current [A]", fontsize=13)
ax[1].set_xticks(np.arange(T_env_array[0], T_env_array[-1]+5, 5))
ax[1].set_yticks(np.arange(I_array[0], I_array[-1]+5, 50))
ax[1].set_xlim(T_env_array[0], T_env_array[-1])
ax[1].set_ylim(I_array[0], 800)

ax[1].scatter(data_465_tre[0], data_465_tre[1], marker='o', s=100)
ax[1].scatter(data_520_tre[0], data_520_tre[1], marker='o', s=100)
ax[1].grid()
ax[1].set_title('Steady-state temperatures for trefoil formation', fontsize=13)

fig.set_figheight(7)
fig.set_figwidth(15)
```

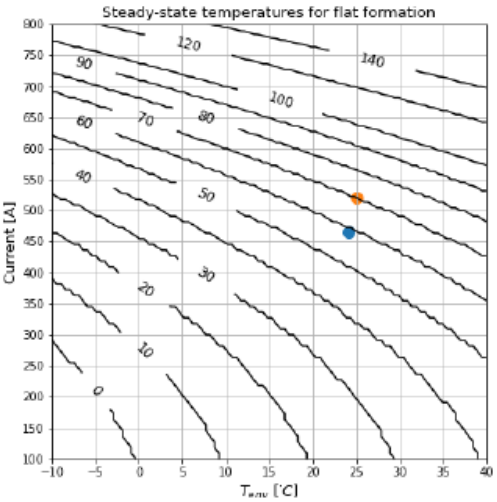

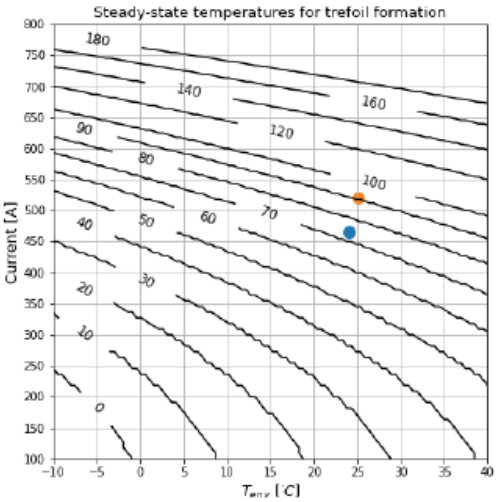

Appendix F

Periodic loading with same currents

In this notebook, periodic loading profiles with the same currents and the same durations is simulated, and lab experiments are presented and compared with simulations.

In [1]:

```
#Importing the relevant modules
import numpy as np
from Thermal_models import ThermalModel
from numba import njit, float32, int32
import pandas as pd

import matplotlib
import matplotlib.cm as cm
import matplotlib.pyplot as plt
import matplotlib.collections as collections

#Used to import measurement data from Excel to a pandas dataframe,
#and doing some preprocessing of the data.
def import_data_excel(filename, sheet_name):
    #Created an excel-file with only the data points
    data = pd.read_excel(filename, sheet_name=sheet_name, index_col="time")
    data["mean_inner_flat"] = data[sensor_id_flat_inner].mean(axis=1)
    data["mean_outer_flat"] = data[sensor_id_flat_outer].mean(axis=1)
    data["mean_inner_tre"] = data[sensor_id_tre_inner].mean(axis=1)
    data["mean_outer_tre"] = data[sensor_id_tre_outer].mean(axis=1)
    data.drop(columns=["Nr1", "Nr2", "Nr3", "Nr4", "Nr5",
                       "Nr6", "Nr7", "Nr8", "Nr9", "Nr10"], inplace=True)
    data.drop(columns=["Nr11", "Nr12", "Nr13",
                       "Nr14", "Nr15", "Nr16"], inplace=True)
    return data

#Preparing initial conditions and the model inputs for simulation.
def prepare_data(data):
    I = np.array(data["current"])
    T_env = np.array(data['env'])
    u = np.array([I, T_env], dtype=np.float32).T
    x0_flat = np.array([data["mean_inner_flat"].iloc[0],
                        data["mean_inner_flat"].iloc[0]],
                        dtype=np.float32)
    x0_tre = np.array([data["mean_inner_tre"].iloc[0],
                       data["mean_outer_tre"].iloc[0]],
                       dtype=np.float32)
    return u, x0_flat, x0_tre

#Defining which sensor numbers that are included in the average temperature measuremen
sensor_id_flat_inner = ['Nr1', 'Nr3', 'Nr5']
sensor_id_flat_outer = ['Nr2', 'Nr4', 'Nr6']
sensor_id_tre_inner = ['Nr11', 'Nr13', 'Nr15']
sensor_id_tre_outer = ['Nr12', 'Nr14', 'Nr16']
```

In [2]:

```
#This is a helper function for calculating the input array for a simulation,
#given T_on and T_off times.
@njit
def calc_input_array(T_on, T_off, n_periods, I_in, T_env, dt):
    #Current input
    T_tot = T_on + T_off
    n_on = int(T_on/dt)-1
    n_off = int(T_off/dt)-1
    I_array = I_in*np.ones(n_on, dtype=np.float32)
    I_array = np.append(I_array, np.zeros(n_off))
    I = I_array.copy()

    for i in range(n_periods-1):
        I = np.append(I, I_array)

    x0 = np.array([T_env, T_env], dtype=np.float32)

    #T_env input
    T_env = T_env*np.ones_like(I, dtype=np.float32)
    u = np.zeros((2, len(I)), dtype=np.float32)
    u[0] = I
    u[1] = T_env
    return u.T

#Simulates a range of different scenarios, where T_on and T_off changes.
#The output is a grid of the maximum currents given the T_on and T_off values.
def sim_temp_cycle(x0, T_on_array, T_off_array, I_test, n_periods, T_env, theta, dt):
    T_max = np.zeros((len(T_on_array), len(T_off_array)))
    I_max = np.zeros_like(T_max)
    cable = ThermalModel(theta, dt)
    for j, T_on in enumerate(T_on_array):
        for i, T_off in enumerate(T_off_array):
            for I_el in I_test:
                u = calc_input_array(T_on, T_off, n_periods, I_el, T_env, dt)
                T_temps = cable.sim(x0, u)
                T_max_el = np.max(T_temps)
                if T_max_el > 90:
                    T_max[i, j] = T_max_el
                    I_max[i, j] = I_el
                    break
                else:
                    T_max[i, j] = T_max_el
                    I_max[i, j] = I_el
    return T_max, I_max
```

In [3]:

```
#Defining the model parameters from the steady-state calculations.
C_al = 583 #J/K.m
C_ins = 1890 #J/K.m
h_inner = 92.707
h_outer = 10.010
A_al2ins_flat = 0.055 #flat
A_ins2a_flat = 0.120 #flat
A_al2ins_tre = 0.032
A_ins2a_tre = 0.098
R_cold = 0.134e-3 #Ohm/m

adj_flat = np.array([1.49898723, 0.5, 0.61660843, 0.60746084, 0.62580462], dtype=np.flo
adj_tre = np.array( [1.49992286, 0.71452468, 0.77748906, 0.69020832, 0.75452057], dtype

#Collecting model parameters into numpy arrays, and formating to float32 datatype.
theta_flat = np.array([C_al, C_ins, h_inner*A_al2ins_flat, h_outer*A_ins2a_flat, R_colo
                       dtype=np.float32)*adj_flat
theta_tre = np.array([C_al, C_ins, h_inner*A_al2ins_tre, h_outer*A_ins2a_tre, R_cold],
                     dtype=np.float32)*adj_tre

#Creating instances of the cable thermal models for both flat and trefoil formation.
dt = 60
cable_flat = ThermalModel(theta_flat, dt)
cable_tre = ThermalModel(theta_tre, dt)
```

In [4]:

```
T_env = 22
dt = 20
n_periods = 2 #Defines how many charging cycles to be simulated
n_points_T_on = 200 #Number of data points for T_on
n_points_T_off = 200 #Number of data points for T_off
n_points_I = 200 #Number of data points for the current values

T_on_lim = (10, 60) #The range of tested T_on values
T_off_lim = (10, 60) #The range of tested T_off values
I_lim = (500, 1800) #The range of tested current values

I_test = np.linspace(I_lim[0], I_lim[1], n_points_I)
T_on_array = np.linspace(T_on_lim[0]*60, T_on_lim[1]*60, n_points_T_on)
T_off_array = np.linspace(T_off_lim[0]*60, T_off_lim[1]*60, n_points_T_off)
x0 = np.array([T_env, T_env], dtype=np.float32)

#Obtain the maximum current values for a range of different T_on and T_off vales.
T_max, I_max = sim_temp_cycle(x0, T_on_array, T_off_array, I_test, n_periods, T_env, th
```

In [5]:

```
#Plotting the contour plot for the I_max values.
#Code inspiration from: https://matplotlib.org/stable/gallery/images_contours_and_fiel
delta = 0.025
x = T_on_array/60 #Gets time in minutes
y = T_off_array/60

X, Y = np.meshgrid(x, y)
Z = np.array(I_max, dtype=np.int16)

fig, ax = plt.subplots()
ax.set_title('Maximum current with periodic charging, simulated 2 periods', fontsize=1
ax.grid()
levels = np.array([600, 610, 620, 630, 640, 650, 660, 670, 680, 700,
                   725, 750, 775, 800, 850, 900, 950, 1000], dtype=np.int16)
CS = ax.contour(X, Y, Z, colors=['k'], levels=levels)
ax.clabel(CS, inline=True, fontsize=10.5, fmt='%1.1d')

ax.set_xlabel("$T_{on}$  [min]", fontsize=13)
ax.set_ylabel("$T_{off}$ [min]", fontsize=13)
ax.set_xlim(T_on_lim[0], T_on_lim[1])
ax.set_ylim(T_off_lim[0], T_off_lim[1])
ax.set_xticks(np.arange(T_on_lim[0], T_on_lim[1]+5, 5))
ax.set_yticks(np.arange(T_off_lim[0], T_off_lim[1]+5, 5))

ax.axvspan(0, T_on_lim[0], facecolor='#929591', alpha=0.1, hatch="x")
ax.axhspan(0, T_off_lim[0], facecolor='#929591', alpha=0.1, hatch="x")

fig.set_figheight(7)
fig.set_figwidth(9)
```

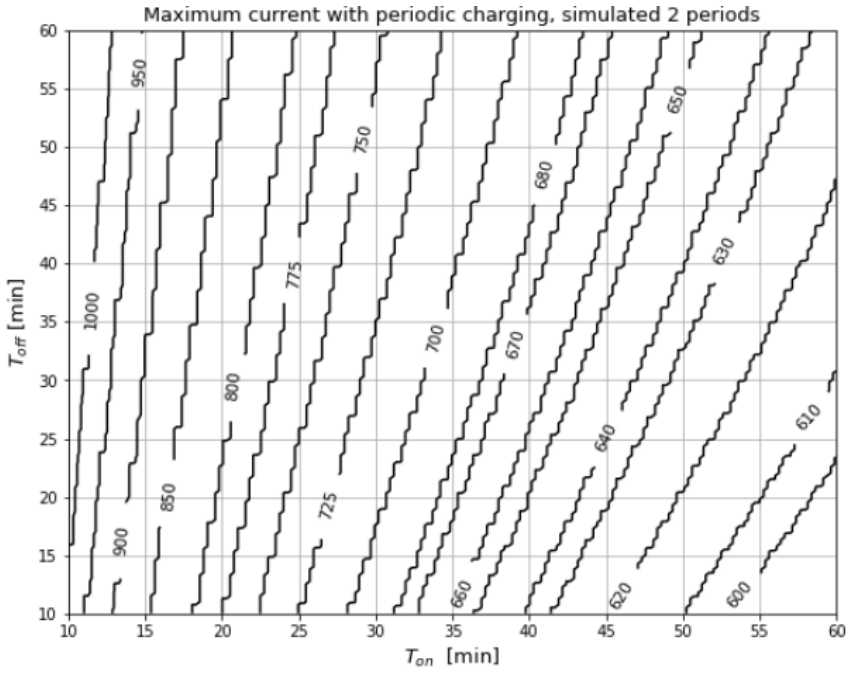

Making the table for maxmum current values

In [6]:

```
#Defining the indices that will be printed
idx = np.arange(0, 201, 20)
idx[-1] -= 1

#Creating a Pandas DataFrame with the current values, and fixing the index and column r
data = pd.DataFrame(I_max)
data.index = np.round(T_off_array/60, 0)
data = data.iloc[idx].T
data.index = np.round(T_on_array/60, 0)
data = data.iloc[idx].T
data = data.round(decimals=0)

data.to_excel("Current_data_periodic_charging.xlsx")
```

Simulation vs Lab-measurements of periodic charging same currents

In [7]:

```
#Importing lab test data from excel
filename = "Data_full.xlsx"
data_640 = import_data_excel(filename, 'SC640').iloc[:180]
data_675 = import_data_excel(filename, 'SC675')
data_725 = import_data_excel(filename, 'SC725').iloc[:180]

u_640, x0_640_flat, x0_640_tre = prepare_data(data_640)
u_675, x0_675_flat, x0_675_tre = prepare_data(data_675)
u_725, x0_725_flat, x0_725_tre = prepare_data(data_725)

#Simulating all scenarios from the lab testing.
T_640_flat = cable_flat.sim(x0_640_flat, u_640)
T_640_tre = cable_tre.sim(  x0_640_tre,  u_640)

T_675_flat = cable_flat.sim(x0_675_flat, u_675)
T_675_tre  = cable_tre.sim( x0_675_tre,  u_675)

T_725_flat = cable_flat.sim(x0_725_flat, u_725)
T_725_tre  = cable_tre.sim( x0_725_tre,  u_725)
```

In [8]:

```
#Plotting both simulated and measured temperature data for inner and outer layers, for
fig, ax = plt.subplots(2,3)
ax[0,0].set_title("Flat, inner and outer, 640 A")
ax[0,0].plot(data_640.index/60, T_640_flat[:, 0], 'r', label="simulated T_inner")
ax[0,0].plot(data_640.index/60, T_640_flat[:, 1], 'b', label="simulated T_outer")
ax[0,0].plot(data_640.index/60, np.array(data_640['mean_inner_flat']), 'r--', label="me
ax[0,0].plot(data_640.index/60, np.array(data_640['mean_outer_flat']), 'b--', label="me
ax[0,0].legend()
ax[0,0].grid()
ax[0,0].set_xlabel("Time [min]")
ax[0,0].set_ylabel("T [deg C]")
ax[0,0].set_xticks(np.arange(0, 181, 20))
ax[0,0].set_yticks(np.arange(20, 81, 5))

ax[0,1].set_title("Flat, inner and outer, 675 A")
ax[0,1].plot(data_675.index/60, T_675_flat[:, 0], 'r', label="simulated T_inner")
ax[0,1].plot(data_675.index/60, T_675_flat[:, 1], 'b', label="simulated T_outer")
ax[0,1].plot(data_675.index/60, np.array(data_675['mean_inner_flat']), 'r--', label="me
ax[0,1].plot(data_675.index/60, np.array(data_675['mean_outer_flat']), 'b--', label="me
ax[0,1].legend()
ax[0,1].grid()
ax[0,1].set_xlabel("Time [min]")
ax[0,1].set_ylabel("T [deg C]")
ax[0,1].set_xticks(np.arange(0, 121, 20))
ax[0,1].set_yticks(np.arange(20, 81, 5))

ax[0,2].set_title("Flat, inner and outer, 725 A")
ax[0,2].plot(data_725.index/60, T_725_flat[:, 0], 'r', label="simulated T_inner")
ax[0,2].plot(data_725.index/60, T_725_flat[:, 1], 'b', label="simulated T_outer")
ax[0,2].plot(data_725.index/60, np.array(data_725['mean_inner_flat']), 'r--', label="me
ax[0,2].plot(data_725.index/60, np.array(data_725['mean_outer_flat']), 'b--', label="me
ax[0,2].legend()
ax[0,2].grid()
ax[0,2].set_xlabel("Time [min]")
ax[0,2].set_ylabel("T [deg C]")
ax[0,2].set_xticks(np.arange(0, 181, 20))
ax[0,2].set_yticks(np.arange(20, 81, 5))

ax[1,0].set_title("Trefoil, inner and outer, 640 A")
ax[1,0].plot(data_640.index/60, T_640_tre[:, 0], 'r', label="simulated T_inner")
ax[1,0].plot(data_640.index/60, T_640_tre[:, 1], 'b', label="simulated T_outer")
ax[1,0].plot(data_640.index/60, np.array(data_640['mean_inner_tre']), 'r--', label="mea
ax[1,0].plot(data_640.index/60, np.array(data_640['mean_outer_tre']), 'b--', label="mea
ax[1,0].legend()
ax[1,0].grid()
ax[1,0].set_xlabel("Time [min]")
ax[1,0].set_ylabel("T [deg C]")
ax[1,0].set_xticks(np.arange(0, 181, 20))
ax[1,0].set_yticks(np.arange(20, 96, 5))

ax[1,1].set_title("Trefoil, inner and outer, 675 A")
ax[1,1].plot(data_675.index/60, T_675_tre[:, 0], 'r', label="simulated T_inner")
ax[1,1].plot(data_675.index/60, T_675_tre[:, 1], 'b', label="simulated T_outer")
ax[1,1].plot(data_675.index/60, np.array(data_675['mean_inner_tre']), 'r--', label="mea
ax[1,1].plot(data_675.index/60, np.array(data_675['mean_outer_tre']), 'b--', label="mea
ax[1,1].legend()
ax[1,1].grid()
ax[1,1].set_xlabel("Time [min]")
ax[1,1].set_ylabel("T [deg C]")
```

```
ax[1,1].set_xticks(np.arange(0, 121, 20))
ax[1,1].set_yticks(np.arange(20, 96, 5))

ax[1,2].set_title("Trefoil, inner and outer, 725 A")
ax[1,2].plot(data_725.index/60, T_725_tre[:, 0], 'r', label="simulated T_inner")
ax[1,2].plot(data_725.index/60, T_725_tre[:, 1], 'b', label="simulated T_outer")
ax[1,2].plot(data_725.index/60, np.array(data_725['mean_inner_tre']), 'r--', label="mea
ax[1,2].plot(data_725.index/60, np.array(data_725['mean_outer_tre']), 'b--', label="mea
ax[1,2].legend()
ax[1,2].grid()
ax[1,2].set_xlabel("Time [min]")
ax[1,2].set_ylabel("T [deg C]")
ax[1,2].set_xticks(np.arange(0, 181, 20))
ax[1,2].set_yticks(np.arange(20, 96, 5))

fig.set_figheight(10)
fig.set_figwidth(15)
plt.show()
```

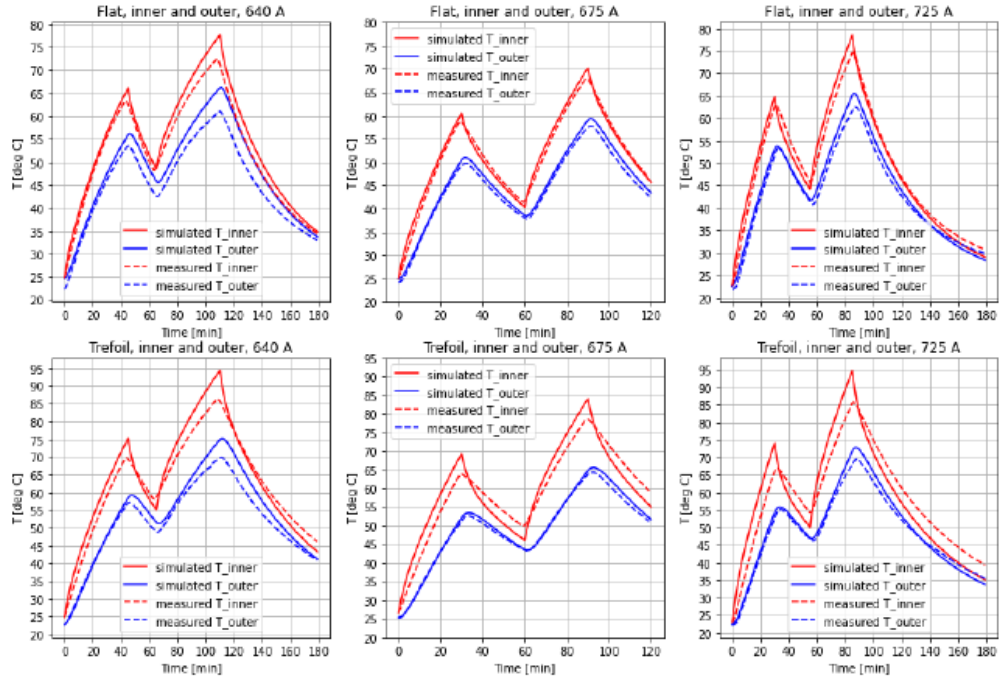

Appendix G

Periodic loading with different currents

In this notebook, periodic loading profiles with different currents is simulated, and lab experiments are presented and compared with simulations.

In [1]:

```
#Importing the relevant modules
import numpy as np
from Thermal_models import ThermalModel
from numba import njit, float32, int32
import time
import pandas as pd

import matplotlib
import numpy as np
import matplotlib.cm as cm
import matplotlib.pyplot as plt
import matplotlib.collections as collections

#Used to import measurement data from Excel to a pandas dataframe,
#and doing some preprocessing of the data.
def import_data_excel(filename, sheet_name):
    #Created an excel-file with only the data points
    data = pd.read_excel(filename, sheet_name=sheet_name, index_col="time")
    data["mean_inner_flat"] = data[sensor_id_flat_inner].mean(axis=1)
    data["mean_outer_flat"] = data[sensor_id_flat_outer].mean(axis=1)
    data["mean_inner_tre"] = data[sensor_id_tre_inner].mean(axis=1)
    data["mean_outer_tre"] = data[sensor_id_tre_outer].mean(axis=1)
    data.drop(columns=["Nr1", "Nr2", "Nr3", "Nr4", "Nr5",
                       "Nr6", "Nr7", "Nr8", "Nr9", "Nr10"], inplace=True)
    data.drop(columns=["Nr11", "Nr12", "Nr13",
                       "Nr14", "Nr15", "Nr16"], inplace=True)
    return data

#Preparing initial conditions and the model inputs for simulation.
def prepare_data(data):
    I = np.array(data["current"])
    T_env = np.array(data['env'])
    u = np.array([I, T_env], dtype=np.float32).T
    x0_flat = np.array([data["mean_inner_flat"].iloc[0],
                        data["mean_inner_flat"].iloc[0]],
                        dtype=np.float32)
    x0_tre = np.array([data["mean_inner_tre"].iloc[0],
                       data["mean_outer_tre"].iloc[0]],
                       dtype=np.float32)
    return u, x0_flat, x0_tre

#Defining which sensor numbers that are included in the average temperature measurement
sensor_id_flat_inner = ['Nr1', 'Nr3', 'Nr5']
sensor_id_flat_outer = ['Nr2', 'Nr4', 'Nr6']
sensor_id_tre_inner = ['Nr11', 'Nr13', 'Nr15']
sensor_id_tre_outer = ['Nr12', 'Nr14', 'Nr16']
```

In [2]:

```
@njit
def calc_input_array(T_on, T_off, I1, I2, T_env, dt):
    #Current input
    T_tot = T_on + T_off
    n_on = int(T_on/dt)
    n_off = int(T_off/dt)

    I1_array = I1*np.ones(n_on)
    I2_array = I2*np.ones(n_on)
    I_array = np.concatenate((I1_array, np.zeros(n_off), I2_array))
    T_env = T_env*np.ones_like(I_array)

    u = np.zeros((2, len(I_array)), dtype=np.float32)
    u[0] = I_array
    u[1] = T_env
    return u.T

def sim_temp_cycle(I1_array, I2_array, T_off_test, x0, T_env, theta_tre, dt, T_on):
    T_off_min = np.zeros((len(I1_array), len(I2_array)))
    cable = ThermalModel(theta_tre, dt)
    for j, I1 in enumerate(I1_array):
        for i, I2 in enumerate(I2_array): #Starts with the longest T_off
            for T_off in T_off_test[::-1]:
                u = calc_input_array(T_on, T_off, I1, I2, T_env, dt)
                T_temps = cable.sim(x0, u)
                T_max_el = np.max(T_temps)
                if T_max_el > 90:
                    T_off_min[i, j] = T_off
                    break
                else:
                    T_off_min[i, j] = T_off
    return T_off_min
```

In [3]:

```
#Defining the model parameters from the steady-state calculations.
C_al = 583 #J/K.m
C_ins = 1890 #J/K.m
h_inner = 92.707
h_outer = 10.010
A_al2ins_flat = 0.055 #flat
A_ins2a_flat = 0.120 #flat
A_al2ins_tre = 0.032
A_ins2a_tre = 0.098
R_cold = 0.134e-3 #Ohm/m

adj_flat = np.array([1.49898723, 0.5, 0.61660843, 0.60746084, 0.62580462], dtype=np.flo
adj_tre = np.array( [1.49992286, 0.71452468, 0.77748906, 0.69020832, 0.75452057], dtype

#Collecting model parameters into numpy arrays, and formating to float32 datatype.
theta_flat = np.array([C_al, C_ins, h_inner*A_al2ins_flat, h_outer*A_ins2a_flat, R_colo
                       dtype=np.float32)*adj_flat
theta_tre = np.array([C_al, C_ins, h_inner*A_al2ins_tre, h_outer*A_ins2a_tre, R_cold],
                     dtype=np.float32)*adj_tre

#Creating instances of the cable thermal models for both flat and trefoil formation.
dt = 60
cable_flat = ThermalModel(theta_flat, dt)
cable_tre = ThermalModel(theta_tre, dt)
```

30 Min on-time

In [4]:

```
t1 = time.time() #For timing the code execution

#Defining the periodic simulation parameters and arrays
T_env = 22
dt = 40
T_on = 30*30

n_points_I1 = 200
n_points_I2 = 200
n_points_T_off = 200

T_off_lim = (0, 240) #min
I1_lim = (200, 1200)
I2_lim = (500, 1200)

T_off_test = np.linspace(T_off_lim[0]*60, T_off_lim[1]*60, n_points_T_off)
I1_array = np.linspace(I1_lim[0], I1_lim[1], n_points_I1)
I2_array = np.linspace(I2_lim[0], I2_lim[1], n_points_I2)

x0 = np.array([T_env, T_env], dtype=np.float32)

#Simulating the minimum T_off values for a range of different currents
T_off = sim_temp_cycle(I1_array, I2_array, T_off_test, x0, T_env, theta_tre, dt, T_on)
print("Time for command completion: ", time.time()-t1)
```

```
Time for command completion:  1464.9170048236847
```

In [5]:

```
#Plotting the contour plot for the T_off values.
#Code inspiration from: https://matplotlib.org/stable/gallery/images_contours_and_field
delta = 0.025
x = I1_array
y = I2_array

X, Y = np.meshgrid(x, y)
Z = np.array(T_off/60, dtype=np.int16)

fig, ax = plt.subplots()
ax.set_title('Minimum $T_{off}$  time with two 30 min charging periods', fontsize=14)
ax.grid()
levels = np.array([0, 15, 30, 45, 60, 90, 120, 180])
CS = ax.contour(X, Y, Z, colors=['k'], levels=levels)
# ax.clabel(CS, inline=True, fontsize=11, inline_spacing=-4)

ax.set_xlabel("$I_{1}$ [A]", fontsize=14)
ax.set_ylabel("$I_{2}$ [A]", fontsize=14)
ax.set_xlim(200, 1000)
ax.set_ylim(650, 1000)

ax.set_xticks(np.arange(200, 1100+5, 50))
ax.set_yticks(np.arange(600, 1100+5, 25))
Z = Z == 0

z = np.ma.masked_where(Z <= 0, Z)
cs = ax.contourf(X, Y, z, locator=matplotlib.ticker.LogLocator(), cmap=cm.get_cmap('bir
fig.set_figheight(10)
fig.set_figwidth(10)
plt.show()
```

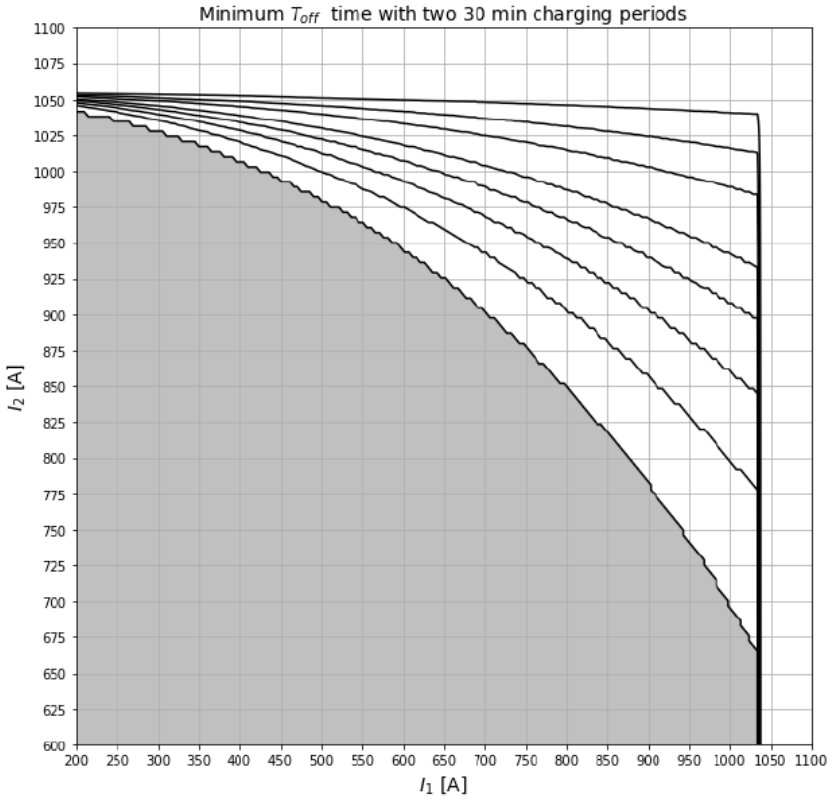

60 min on-time

In [6]:

```
t1 = time.time()
T_env = 22
dt = 40
T_on = 30*60

#Defining the periodic simulation parameters and arrays
n_points_I1 = 200
n_points_I2 = 200
n_points_T_off = 200

T_off_lim2 = (0, 180) #min
I1_lim2 = (200, 900)
I2_lim2 = (200, 900)

T_off_test2 = np.linspace(T_off_lim2[0]*60, T_off_lim2[1]*60, n_points_T_off)
I1_array2 = np.linspace(I1_lim2[0], I1_lim2[1], n_points_I1)
I2_array2 = np.linspace(I2_lim2[0], I2_lim2[1], n_points_I2)

x0 = np.array([T_env, T_env], dtype=np.float32)

#Simulating the minimum T_off values for a range of different currents
T_off2 = sim_temp_cycle(I1_array2, I2_array2, T_off_test2, x0, T_env, theta_tre, dt, T_
print("Time for command completion: ", time.time()-t1)
```

```
Time for command completion:  1612.5845727920532
```

In [7]:

```
#Plotting the contour plot for the T_off values.
#Code inspiration from: https://matplotlib.org/stable/gallery/images_contours_and_fiel
delta = 0.025
x = I1_array2
y = I2_array2

X, Y = np.meshgrid(x, y)
Z = T_off2/60

fig, ax = plt.subplots()
ax.set_title('Minimum $T_{off}$  time with two 60 min charging periods', fontsize=14)
ax.grid()
levels = np.array([0, 15, 30, 45, 60, 90, 120, 180])
CS = ax.contour(X, Y, Z, colors=['k'], levels=levels)
# ax.clabel(CS, inline=True, fontsize=12, inline_spacing=5)

ax.set_xlabel("$I_{1}$ [A]", fontsize=14)
ax.set_ylabel("$I_{2}$ [A]", fontsize=14)
ax.set_xlim(350, 800)
ax.set_ylim(500, 800)

ax.set_xticks(np.arange(350, 850+5, 50))
ax.set_yticks(np.arange(600, 850+5, 50))
Z = Z == 0

z = np.ma.masked_where(Z <= 0, Z)
cs = ax.contourf(X, Y, z, locator=matplotlib.ticker.LogLocator(), cmap=cm.get_cmap('bi

fig.set_figheight(10)
fig.set_figwidth(10)
plt.show()
```

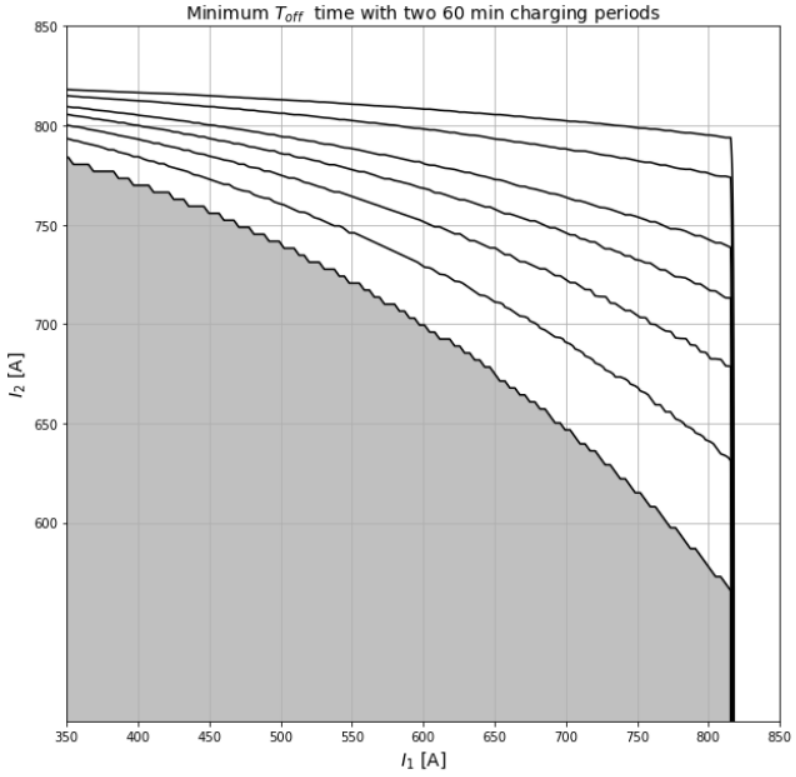

Simulation vs Lab-measurements of periodic charging different currents

In [8]:

```
#Importing lab test data from excel
filename = "Data_full.xlsx"
data_800_660 = import_data_excel(filename, 'DC800-660').iloc[:180]
data_500_825 = import_data_excel(filename, 'DC500-825').iloc[:180]

u_800_660, x0_800_660_flat, x0_800_660_tre = prepare_data(data_800_660)
u_500_825, x0_500_825_flat, x0_500_825_tre = prepare_data(data_500_825)

#Simulating all scenarios from the lab testing.
T_800_660_flat = cable_flat.sim(x0_800_660_flat, u_800_660)
T_800_660_tre = cable_tre.sim(  x0_800_660_tre,  u_800_660)

T_500_825_flat = cable_flat.sim(x0_500_825_flat, u_500_825)
T_500_825_tre  = cable_tre.sim( x0_500_825_tre,  u_500_825)
```

In [9]:

```
#Plotting both simulated and measured temperature data for inner and outer layers, for
fig, ax = plt.subplots(2,2)
ax[0,0].set_title("Flat, inner and outer, 800 - 660 A")
ax[0,0].plot(data_800_660.index/60, T_800_660_flat[:, 0], 'r', label="simulated T_inner
ax[0,0].plot(data_800_660.index/60, T_800_660_flat[:, 1], 'b', label="simulated T_outer
ax[0,0].plot(data_800_660.index/60, np.array(data_800_660['mean_inner_flat']), 'r--', l
ax[0,0].plot(data_800_660.index/60, np.array(data_800_660['mean_outer_flat']), 'b--', l
ax[0,0].legend()
ax[0,0].grid()
ax[0,0].set_xlabel("min")
ax[0,0].set_ylabel("T [deg C]")
ax[0,0].set_xticks(np.arange(0, 181, 15))
ax[0,0].set_yticks(np.arange(20, 86, 5))

ax[0,1].set_title("Flat, inner and outer, 500 - 825 A")
ax[0,1].plot(data_500_825.index/60, T_500_825_flat[:, 0], 'r', label="simulated T_inner
ax[0,1].plot(data_500_825.index/60, T_500_825_flat[:, 1], 'b', label="simulated T_outer
ax[0,1].plot(data_500_825.index/60, np.array(data_500_825['mean_inner_flat']), 'r--', l
ax[0,1].plot(data_500_825.index/60, np.array(data_500_825['mean_outer_flat']), 'b--', l
ax[0,1].legend()
ax[0,1].grid()
ax[0,1].set_xlabel("min")
ax[0,1].set_ylabel("T [deg C]")
ax[0,1].set_xticks(np.arange(0, 181, 15))
ax[0,1].set_yticks(np.arange(20, 86, 5))

ax[1,0].set_title("Trefoil, inner and outer, 800 - 660 A")
ax[1,0].plot(data_800_660.index/60, T_800_660_tre[:, 0], 'r', label="simulated T_inner"
ax[1,0].plot(data_800_660.index/60, T_800_660_tre[:, 1], 'b', label="simulated T_outer"
ax[1,0].plot(data_800_660.index/60, np.array(data_800_660['mean_inner_tre']), 'r--', la
ax[1,0].plot(data_800_660.index/60, np.array(data_800_660['mean_outer_tre']), 'b--', la
ax[1,0].legend()
ax[1,0].grid()
ax[1,0].set_xlabel("min")
ax[1,0].set_ylabel("T [deg C]")
ax[1,0].set_xticks(np.arange(0, 181, 15))
ax[1,0].set_yticks(np.arange(20, 101, 5))

```

```
39 ax[1,1].set_title("Trefoil, inner and outer, 500 - 825 A")
40 ax[1,1].plot(data_500_825.index/60, T_500_825_tre[:, 0], 'r', label="simulated T_inner'
41 ax[1,1].plot(data_500_825.index/60, T_500_825_tre[:, 1], 'b', label="simulated T_outer'
42 ax[1,1].plot(data_500_825.index/60, np.array(data_500_825['mean_inner_tre']), 'r--', la
43 ax[1,1].plot(data_500_825.index/60, np.array(data_500_825['mean_outer_tre']), 'b--', la
44 ax[1,1].legend()
45 ax[1,1].grid()
46 ax[1,1].set_xlabel("min")
47 ax[1,1].set_ylabel("T [deg C]")
48 ax[1,1].set_xticks(np.arange(0, 181, 15))
49 ax[1,1].set_yticks(np.arange(20, 101, 5))
50
51 fig.set_figheight(10)
52 fig.set_figwidth(15)
53 plt.show()
```